

**FIELD EVALUATION OF IN-SITU TEST TECHNOLOGY FOR  $Q_C/Q_A$  DURING  
CONSTRUCTION OF PAVEMENT LAYERS AND EMBANKMENTS**

A Thesis

Submitted to the Graduate Faculty of the  
Louisiana State University and  
Agricultural and Mechanical College  
in partial fulfillment of the  
requirements for the degree of  
Master of Science in Civil Engineering

In

The Department of Civil and Environmental Engineering

By

Munir D. Nazzal

B.Sc., Birzeit University, Birzeit, West Bank, 2002

December, 2003

## DEDICATION

*To*

*The memory of my father*

*My mother*

*My fiancée, Inas*

*Uncle Bassam & Aunt Shirley*

*Uncle Nadeem*

*My family*

*&*

*All the people who helped me*

## ACKNOWLEDGEMENTS

I want to express my deep gratitude to my advisors, Dr. Murad Abu-Farsakh and Dr. Khalid Alshibli, for their guidance throughout this study. Dr. Murad provided me with all the knowledge, experience and support that I needed to accomplish this thesis. It was a great pleasure for me to have him as my advisor. His help and support are really appreciated. I am also grateful for Dr. Khalid for the help and support he provided during my study. Special thanks should also be given to Dr. Mehmet Tumay and Dr. Louay Mohammad for serving as my committee members and for providing me with all the information I needed during my thesis work.

This research project was funded by the Louisiana Transportation Research Center (LTRC Project No. 02-1GT) and Louisiana Department of Transportation and Development (State Project No. 736-02-9995). Thanks should also be given to Louisiana Transportation Research Center Pavement & Geotechnical Research staff, especially Melba Bounds, Paul Brady, William Tierney, and Gary Keel for their help through out my work. I want also to thank my colleague Ekram Seyman for his cooperation in this study. Finally, I would like to extend my acknowledgements to all the student workers, especially Waleed, who worked with me in this project.

## TABLE OF CONTENTS

DEDICATION .....	ii
ACKNOWLEDGEMENTS .....	iii
LIST OF TABLES .....	vii
LIST OF FIGURES .....	ix
ABSTRACT .....	xii
CHAPTER ONE : INTRODUCTION.....	1
1.1 Background.....	1
1.2 Objectives.....	2
1.3 Thesis Outline.....	3
CHAPTER TWO: LITERATURE REVIEW.....	4
2.1 Geogauge.....	4
2.1.1 Geogauge Principle Of Operation.....	4
2.1.2 GeoGauge Soil Stiffness and Moduli Calculation.....	7
2.1.3 Geogauge Stiffness Modulus Correlation with Moduli of Other In-situ Tests .....	9
2.2 Dynamic Cone Penetrometer (DCP).....	10
2.2.1 Existing Correlations Between DCP And California Bearing Ratio (CBR).....	12
2.2.2 Existing Correlations Between DCP And Different Moduli .....	14
2.2.3 Soil Classification Based on DCP Results.....	16
2.2.4 Current Application of DCP in Pavement Assessment .....	17
2.3 Light Falling Weight Deflectometer (LFWD).....	18
2.3.1 Existing Correlation between LFWD Moduli and Other In-Situ Test Moduli.....	20
2.4 Falling Weight Deflectometer (FWD).....	22
2.4.1 FWD Moduli Backcalculation .....	24
2.4.2 Application of FWD .....	25
2.5 Static Plate Load Test (PLT).....	27
2.5.1 PLT Moduli .....	28
2.6 California Bearing Ratio (CBR).....	30
CHAPTER THREE: METHODOLOGY .....	33
3.1 Field Testing .....	33
3.1.1 US Highway 190.....	33
3.1.2 Louisiana State Highway 182 .....	34
3.1.3 US Highway 61.....	38
3.1.4 Test Sections at LA-DOTD Accelerated Load facility (ALF).....	39
3.1.4.1 ALF Clayey Silt Soil Section.....	41
3.1.4.2 Cement-Soil Section (1) .....	43
3.1.4.3 Cement-Soil Section (2) .....	43
3.1.4.4 Lime Treated Soil Section .....	46

3.1.4.5 Crushed Lime stone .....	47
3.1.4.6 Calcium Sulfate Hemihydrate (Florolite) Section .....	49
3.1.4.7 Trench Sections.....	50
3.2 CBR Tests .....	56
CHAPTER FOUR: ANALYSIS OF TEST RESULTS AT THE ALF SITE.....	58
4.1 ALF Test Sections.....	58
4.2 Trench Sections .....	63
CHAPTER FIVE: PARAMETRIC STUDY .....	71
5.1 Experiment Setup.....	71
5.2 Test Procedure .....	71
5.3 Test Materials .....	73
5.4 Test Results .....	73
CHAPTER SIX: EVALUATION OF GEOGAUGE, DCP, AND LFWD IN-SITU MEASUREMENTS .....	77
6.1.1 Repeatability .....	77
6.1.1 Geogauge Stiffness Device .....	77
6.1.2 LFWD .....	79
6.2 Moduli from Plate Load Test.....	80
6.3 Modulus and Zone of Influence of Different Devices .....	80
6.3.1 Burmister Solution for Two Layer Systems .....	82
6.3.2 Odmarks Method .....	83
6.4 Regression Analysis.....	85
6.4.1 Geogauge Modulus Correlations .....	88
6.4.1.1 Geogauge versus FWD .....	88
6.4.1.2 Geogauge versus PLT .....	89
6.4.1.3 Geogauge versus CBR .....	89
6.4.2 LFWD Modulus Correlations .....	91
6.4.2.1 LFWD versus FWD .....	91
6.4.2.2 LFWD versus PLT .....	93
6.4.2.3 LFWD versus CBR .....	93
6.4.3 DCP Correlations .....	93
6.4.3.1 DCP versus FWD.....	95
6.4.3.2 DCP versus PLT .....	96
6.4.3.3 DCP versus CBR.....	98
CHAPTER SEVEN: CONCLUSIONS AND RECOMMENDATIONS .....	100
7.1 Conclusions .....	100
7.2 Recommendations.....	102
REFERENCES .....	103
APPENDIX A GEOGAUGE OPERATION PROCEDURE .....	108

APPENDIX B SAS OUPUT .....	111
VITA .....	112

## LIST OF TABLES

Table 2.1	Poisson Ratios for Different materials (Haung, 1993) .....	8
Table 2.2	Geogauge and FWD suggested values to characterize base layer .....	9
Table 2.3	Values of B (Chua, 1988) .....	16
Table 2.4	Suggested classification for granular soil using DCP (Huntley 1990) .....	17
Table 2.5	Suggested classification for cohesive soil using DCP (Huntley 1990) .....	17
Table 2.6	Specification for different types of LFWD (Fleming 2001).....	19
Table 3.1	Summary of results for base course sections at highway US 190 .....	35
Table 3.2	Dry density and moisture content measurement at highway US 190.....	37
Table 3.3	Summary of Geogauge, LFWD, and DCP test results for highway LA 182.....	38
Table 3.4	Dry density and moisture content measurements at highway LA 182 .....	38
Table 3.5	Summary of results for subbase section at the US highway 61 .....	38
Table 3.6	Geogauge, LFWD, and nuclear gauge test results for ALF clayey silt section .....	43
Table 3.7	Summary of DCP result for three layers after 6 passes .....	43
Table 3.8	Geogauge, LFWD, and nuclear gauge test results with number of passes for cement-soil section (1).....	44
Table 3.9	Geogauge and LFWD test results with time for cement-soil section (1).....	44
Table 3.10	DCP Test results with number of passes for cement-soil section (1).....	45
Table 3.11	DCP test results with time for cement-soil section (1) .....	45
Table 3.12	Test results with number of passes for cement-soil section (2).....	45
Table 3.13	DCP test results with number of passes for cement-soil section (2) .....	45
Table 3.14	Geogauge and LFWD test results with time for cement-soil section (2).....	46
Table 3.15	DCP test results with time for cement-soil section (2) .....	46

Table 3.16	DCP test results with number of passes for lime treated soil section .....	46
Table 3.17	Test Geogauge, LFWD, and nuclear gauge test results with number of passes for lime treated soil section.....	47
Table 3.18	Geogauge, LFWD test results with time for lime treated soil section.....	47
Table 3.19	DCP test results with time for lime treated soil section.....	47
Table 3.20	Summary of test results for crushed lime stone section.....	48
Table 3.21	DCP results after construction of crushed lime stone section .....	48
Table 3.22	DCP test results with number of passes for Florolite section .....	49
Table 3.23	Summary of test results with number of passes for Florolite section .....	50
Table 3.24	Test results with time for Florolite section .....	50
Table 3.25	DCP test results with time for Florolite section.....	50
Table 3.26	Test results for crushed lime stone trench .....	55
Table 3.27	Test results for sand trench .....	56
Table 3.28	Test results for RAP trench.....	56
Table 6.1	Summary for all Test Results.....	86
Table 6.2	Summary of CBR test results.....	87

## LIST OF FIGURES

Figure 2.1	Geogauge.....	5
Figure 2.2	Schematic of the Geogauge (Humboldt, 1998).....	7
Figure 2.3	Dynamic Cone Penetrometer (DCP).....	12
Figure 2.4	Prima 100, Light Falling Weight Deflectometer.....	21
Figure 2.5	Screen of Prima 100 software.....	21
Figure 2.6	Dynatest model 8000 (FWD) (LTRC 2000).....	24
Figure 2.7	Typical curve for plate load tests on soils.....	30
Figure 3.1	Layout of field test measurements.....	34
Figure 3.2	Gradation for the crushed lime stone tested at highway US 190.....	35
Figure 3.3	Layout and profile for sections at highway US 190.....	35
Figure 3.4	Layout and profile for sections at highway LA 182.....	36
Figure 3.5	Layout and profile for sections constructed at ALF site.....	40
Figure 3.6	Proctor curve for ALF clayey silt soil.....	41
Figure 3.7	Different sections constructed at ALF Site.....	42
Figure 3.8	Conducting tests on cement-soil and crushed lime stone sections at ALF site.....	42
Figure 3.9	Construction of ALF sections.....	44
Figure 3.10	Gradation of tested material at the crushed limestone section.....	48
Figure 3.11	Gradation of Florolite.....	49
Figure 3.12	Construction of trenches at ALF site.....	51
Figure 3.13	Typical cross-section for constructed trenches.....	52
Figure 3.14	Compaction of trenches at ALF site.....	53
Figure 3.15	Testing RAP and sand trenches at ALF site.....	53

Figure 3.16	Gradation of crushed lime stone.....	54
Figure 3.17	Gradation of sand .....	54
Figure 3.18	Gradation of RAP .....	55
Figure 3.19	United machine used to conduct CBR tests .....	57
Figure 4.1	Geogauge modulus variation with number of passes .....	59
Figure 4.2	Geogauge modulus variation with number of passes .....	59
Figure 4.3	Geogauge modulus variation with time.....	60
Figure 4.4	Rainfall record during tesing period (Louisiana Office of State Climatology, 2003) .....	60
Figure 4.5	LFWD modulus variation with number of passes.....	62
Figure 4.6	LFWD modulus variation with time.....	62
Figure 4.7	DCP-PR with time for cement soil section (1).....	64
Figure 4.8	DCP-PR with time for cement soil section (2).....	64
Figure 4.9	DCP-PR with time for lime treated soil section .....	65
Figure 4.10	DCP-PR with time for Florolite section .....	65
Figure 4.11	Trench test measurements with respect to Standard Proctor curves .....	66
Figure 4.12	Geogauge modulus versus dry unit weight for different trenches.....	66
Figure 4.13	LFWD modulus versus dry unit weight for different trenches.....	67
Figure 4.14	DCP-PR profiles for crushed lime stone trench sections .....	68
Figure 4.15	DCP-PR profiles For RAP trench sections.....	69
Figure 4.16	DCP-PR profiles For sand trench sections .....	69
Figure 5.1	Test box in which the experiments were conducted.....	72
Figure 5.2	The constructed mold within soil in test box.....	72
Figure 5.3	Geogauge stiffness modulus curve for Florolite layer vs. thickness .....	74

Figure 5.4	LFWD stiffness modulus curve for Florolite layer vs. thickness.....	74
Figure 5.5	Geogauge stiffness modulus curve for sand layer vs. thickness .....	75
Figure 5.6	Geogauge stiffness modulus curve for clay layer vs. thickness .....	76
Figure 5.7	LFWD stiffness modulus curve for clay layer vs. thickness.....	76
Figure 6.1	Layout of Geogauge measurements for seating-validation test .....	78
Figure 6.2	$C_v$ variation with LFWD stiffness .....	79
Figure 6.3	Definition of modulus from PLT.....	81
Figure 6.4	$M_{FWD}$ vs. $E_G$ .....	89
Figure 6.5	$E_{PLT(i)}$ vs. $E_G$ .....	90
Figure 6.6	$E_{PLT(v2)}$ vs. $E_G$ .....	90
Figure 6.7	CBR vs $E_G$ .....	91
Figure 6.8	$M_{FWD}$ vs. $E_{LFWD}$ .....	92
Figure 6.9	$M_{FWD}$ vs. $E_{LFWD}$ correlation, comparison to Fleming (2000).....	92
Figure 6.10	$E_{PLT(i)}$ vs. $E_{LFWD}$ .....	94
Figure 6.11	$E_{PLT(v2)}$ vs. $E_{LFWD}$ .....	94
Figure 6.12	CBR vs. $E_{LFWD}$ .....	95
Figure 6.13	$M_{FWD}$ vs. DCP-PR.....	96
Figure 6.14	$E_{PLT(i)}$ vs. DCP-PR .....	97
Figure 6.15	$E_{PLT(2)}$ vs. DCP-PR.....	98
Figure 6.16	CBR vs DCP-PR.....	99

## ABSTRACT

With the coming changes from an empirical to mechanistic-empirical pavement design, it becomes essential to move towards changing the quality control/quality assurance ( $Q_C/Q_A$ ) procedures of compacted materials from a unit weight-based criterion to a stiffness/strength based criterion. The non-destructive in-situ tests such as Geogauge, Dynamic Cone Penetrometer (DCP), and Light Falling Weight Deflectometer (LFWD) can be used as effective tools in the assessment of subsurface conditions and in evaluating the stiffness of pavement materials and embankment. This thesis evaluates the potential use of these three devices to reliably measure the stiffness characteristics of highway materials for possible application in the  $Q_C/Q_A$  procedures during and after the construction of pavement layers and embankments. To achieve this, field tests were conducted on highway sections selected from different projects in Louisiana State. In addition, six test sections and three trench sections were constructed and tested at the LTRC Accelerated Load Facility (ALF) site for testing. The field tests included conducting Geogauge, LFWD, DCP tests and standard tests such as the Plate Load Test (PLT) and Falling Weight Deflectometer (FWD) test. The California Bearing Ratio (CBR) laboratory tests were also conducted on samples collected during field tests. Statistical analysis was conducted to correlate the measurements obtained from the three investigated devices and those obtained from the standard tests. Good correlations were obtained between the measurements of the investigated devices and the standard tests. Laboratory tests were also conducted to evaluate the influence depth of the Geogauge and LFWD devices. The results of laboratory tests indicated that the average influence depth for the Geogauge and LFWD devices are about 200 mm and 280 mm, respectively.

# CHAPTER ONE

## INTRODUCTION

### 1.1 Background

Soil compaction is one of the most critical components in the construction of roads, airfields, embankments, and foundations. The durability and stability of a structure are related to achieving a proper soil compaction. Consequently, the compaction control of different soils used in the construction of highways and embankments is needed for enhancing their engineering properties. The current methods for assessing the quality control for construction of highways is based on determining the field unit weight measurements and comparing that to the maximum dry unit weight obtained in the standard or modified Proctor tests that are conducted in the laboratory. The field dry unit weight measurement is determined using either destructive tests, which include the sand cone, the rubber balloon, and the core cutter methods; or other non-destructive tests such as the nuclear density gauge.

The current unit weight based quality control methods are considered slow, hazardous, labor intensive, of uncertain accuracy, and can be unpractical in situation where there is a variation in site materials along any tested section (Fiedler et al. 1998, Livneh and Goldberg 2001). Lenk et al. (2003) indicated that the main reason for the adoption of such quality control methods is their simplicity and relatively low cost if compared to other stiffness based methods.

The purpose of soil compaction is to improve its engineering properties not only their dry unit weight and moisture content (Holtz and Kovacs, 1981). Pinard (1998) stated that quality control specifications suffer from a number of problems since the used

unit weight criteria do not reflect the engineering properties of soils in roadway conditions. Fleming (1998) also reached to similar conclusions. In addition, the key functional property of a base and subbase layers is their stiffness modulus, which is considered to be a measure of the quality of support which they provide to the overlaying asphalt or concrete layers (Fleming et al. 2001). Finally, the design method of pavements is based on engineering parameters of materials such as their stiffness and /or strength, which results in a missing link between the design process and construction quality control.

As a result, the quality control/ quality assurance procedures of construction should be based on a criterion that closely correlates to the performance parameters used in the design. A fundamental performance parameter for constructed highway layers is the elastic stiffness modulus of the materials. Different non-destructive test devices are reported to measure the in-situ elastic stiffness modulus of highway materials; these test devices include the Dynamic Cone Penetrometer (DCP), Light Falling Weight Deflectometer (LFWD), and Geogauge.

## **1.2 Objectives**

There are three main objectives for this thesis. The first objective is to evaluate the feasibility of using Geogauge, LFWD, and DCP devices to measure in-situ stiffness modulus of constructed highway layers and embankments. This is achieved by conducting field tests on constructed pavement layers using the three investigated devices (Geogauge, LFWD, and DCP) along with other standard in-situ test devices (FWD and PLT) and CBR laboratory tests. The second objective is to conduct laboratory tests to determine the influence zone of the Geogauge and LFWD. The third objective is to

conduct a comprehensive regression analysis on the collected field test results to develop the best correlations between the PLT and FWD moduli and CBR value and moduli obtained from Geogauge, LFWD, and DCP measurements.

### **1.3 Thesis Outline**

This thesis is divided into seven Chapters. A description of the devices to be evaluated as well as the standard test devices that are used is presented in the second chapter. Chapter two also includes a detailed review of previous research that was conducted for the purpose of evaluating these devices and the different existing correlations between the moduli measured using these devices and those measured using other standard devices. A description of all field tests and the properties of tested material are presented in Chapter three. Chapter four presents the analysis of tests conducted at the ALF site. The laboratory tests that were conducted to evaluate the influence depth of both the Geogauge and LFWD devices are presented in the fifth chapter. Chapter six presents an evaluation to the Geogauge, LFWD, and DCP test device. This includes the statistical analysis that was performed to develop a correlation between the stiffness measurements using these devices and the reference tests. Finally, the conclusions and recommendations of this thesis are summarized in the last chapter.

## **CHAPTER TWO**

### **LITERATURE REVIEW**

This chapter presents a review of all test devices that were used in the investigation. This summary includes existing correlations for soil measurement acquired by test devices under evaluation (i.e. Geogauge, LFWD, and DCP).

#### **2.1 Geogauge**

The stiffness gauge technology was originally developed by the defense industry for detecting land mines. The collaboration between Bolts, Beranek and Newman of Cambridge, MA, CNA consulting Engineers of Minneapolis, MN and Humboldt (FHWA research program) resulted in introducing the Humboldt Stiffness Gauge known as Geogauge (Figure 1), to the transportation industry (Fiedler et al. 1998). Geogauge measures the in-place stiffness of compacted soil at the rate of about one test per 1.5 minutes. It weighs about 10 kilograms (22 lbs), is 280 mm (11 inch) in diameter and 254 mm (10 inch) tall, and rests on the soil surface via a ring-shaped foot (Fiedler et al. 1998). It has an annular ring which contacts the soil with an outside diameter of 114 mm (4.50 inch), an inside diameter of 89 mm (3.50 inch), and a thickness of 13 mm (0.50 inch) (Lenke et al., 2003). It is expected that future Geogauge models will include on-board moisture measurement instruments and a global positioning system (Fiedler et al., 1998).

##### **2.1.1 Geogauge Principle of Operation**

The principle of operation of the Geogauge is to generate a very small dynamic force at frequencies of 100 to 196 Hz. In a laboratory study, Sawangsuriya et al. (2001)

estimated the force generated by the Geogauge to be 9 N. The Geogauge operation includes generating a very small displacement to the soil, which is less than  $1.27 \times 10^{-6}$  m (0.0005 in.), at 25 steady state frequencies between 100 and 196 Hz. The stiffness is determined at each frequency and the average is displayed. The entire process takes about one and half minutes. The Geogauge is powered by a set of 6 D-cell batteries, and it is designed such that the deflection produced from equipment operating nearby will not affect its measurement, since the frequency generated by traffic (at highway speed) is approximately 30 Hz, which is below the Geogauge operating frequency (Humboldt Mfg. Co. 1999, Geogauge guide).



Figure 2.1 Geogauge

The force applied by the shaker and transferred to the ground is measured by differential displacement across the flexible plate by two velocity sensors (Figure 2.2).

This can be expressed as follows

$$F_{dr} = K_{flex}(X_2 - X_1) = K_{flex}(V_2 - V_1) \quad (2.1)$$

Where:

$F_{dr}$  = force applied by shaker

$K_{flex}$  = stiffness of the flexible plane

$X_1$  = displacement at rigid plate

$X_2$  = displacement at flexible plate

$V_1$  = velocity at rigid plate

$V_2$  = velocity at flexible plate

At frequencies of operation, the ground-input impedance will be dominantly stiffness controlled:

$$K_{soil} = \frac{F_{dr}}{X_1} \quad (2.2)$$

Where

$K_{soil}$  = stiffness of soil

Thus the soil stiffness can be calculated as:

$$\overline{K_{soil}} = K_{flex} \sum_1^n \left( \frac{(X_2 - X_1)}{X_1} \right) = K_{flex} \sum_1^n \left( \frac{(V_2 - V_1)}{V_1} \right) \quad (2.3)$$

Where  $n$  is the number of test frequencies.

Using velocity measurements eliminates the need for a non-moving reference for the soil displacement and permits accurate measurement of small displacements. It is assumed that the Geogauge response is dominated by the stiffness of the underlying soil. The operation procedure for Geogauge as suggested by Humboldt is provided in Appendix A.

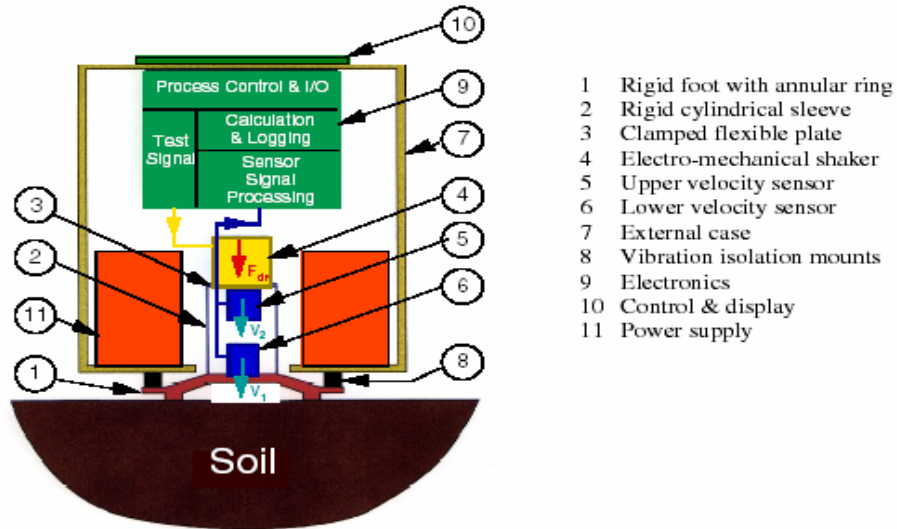


Figure 2.2 Schematic of the Geogauge (Humboldt, 1998)

### 2.1.2 Geogauge Soil Stiffness and Moduli Calculations

The measured soil stiffness from the Geogauge can be used to calculate the soil elastic modulus. The static stiffness,  $K$ , of a rigid annular ring on a linear elastic, homogeneous, and isotropic half space has the following functional form (Egorov 1965):

$$K = \frac{ER}{(1 - \nu^2)\omega(n)} \quad (2.4)$$

Where

$E$  = modulus of elasticity

$\nu$  = Poisson's ratio of the elastic medium

$R$  = the outside radius of the annular ring

$\omega(n)$  = a function of the ratio of the inside diameter and the outside diameter of the annular ring. For the ring geometry of the Geogauge, the parameter  $\omega(n)$  is equal to 0.565, hence,

$$K = \frac{1.77ER}{(1 - \nu^2)} \quad (2.5)$$

Based on Equation 2.5 the Geogauge stiffness could be converted to an elastic stiffness modulus using the equation proposed by CA Consulting Engineers as follows:

$$E_G = H_{SG} \frac{(1 - \nu^2)}{1.77R} \quad (2.6)$$

Where

$E_G$ = the elastic stiffness modulus in MPa

$H_{SG}$ = the Geogauge stiffness reading in MN/m

$R$ = the radius of the Geogauge foot [57.15 mm =2.25 inches]

In this study, Poisson's ratio was selected from the values shown in Table 2.1 to calculate Geogauge stiffness modulus for the tested soils. For a Poisson's ratio of 0.35, a factor of approximately 8.67 can be used to convert the Geogauge stiffness (in MN/m) to a stiffness modulus (in MPa). The Geogauge manufacturer (Humboldt) recommends that it should be used only up to 23 MN/m; the reason is that the Geogauge may lose accuracy when measuring stiffness greater than 23 MN/m (Chen et al., 2000).

Table 2.1 Poisson Ratios for Different materials (Haung, 1993)

Material	Range	Typical value
Portland cement concrete	0.15-0.2	0.15
Untreated granular materials	0.3-0.4	0.35
Cement treated granular materials	0.1-0.2	0.15
Cement treated fine-grained soils	0.15-0.35	0.25
Lime stabilized materials	0.1-0.25	0.2
Lime-flyash mixtures	0.1-0.15	0.15
Dense Sand	0.2-0.4	0.35
Fine-grained soils	0.3-0.45	0.4
Saturated soft soils	0.4-0.5	0.45

Lenke et al. (2003) have indicated that the equations used in calculating the Geogauge is based on the assumption of infinite elastic half space, which is violated

when considering the fact that pavement sections consist of layers with finite thickness that are made up of material with different strength properties.

### 2.1.3 Geogauge Stiffness Modulus Correlation with Moduli of Other In-situ Tests

In his study, Chen et al. (1999) reported that the base moduli measured with the FWD are higher than those measured with the Geogauge. Chen et al. (2000) suggested a general relationship between the Geogauge stiffness and the FWD back-calculated modulus,  $M_{FWD}$  as follows

$$M_{FWD} = 37.65 H_{SG} - 261.96 \quad (2.8)$$

Where:

$M_{FWD}$  is expressed in MPa

$H_{SG}$  is the Geogauge stiffness reading expressed in MN/m

They also suggested that the quality of base layers can be classified by FWD or Geogauge results as listed in Table 2.2. A Dirt-Seismic Pavement Analyzer (D-SPA) was also used by Chen et al. (2000) to measure the corresponding shear wave velocities ( $V_s$ ) for different quality bases as shown in Table 2.2.

Table 2.2 Geogauge and FWD suggested values to characterize base layer

Base Quality	$E_G$ (MPa)	$V_s$ (m/sec)	$M_{FWD}$ (MPa)
Weak	<87	<250	<140
Good	156-209	300-350	310-450
Excellent	>261	>400	>700

To the best knowledge of the author there were no published studies correlating Geogauge measurements to those from the plate load test; except by the CNA Consulting Engineers study, in which a number of field tests were conducted to compare the modulus from the Quasi-Static Plate Load Test (QSPLT) to the Geogauge stiffness

modulus. The results of this study are presented in equations 2.9 through 2.11. It can be noticed that these results suggest that values of the reloading elastic modulus obtained from (QSPLT) are similar in magnitude to the Geogauge stiffness modulus. On the contrary, the Geogauge modulus is nearly 7 times higher than the initial loading modulus. In addition, the results indicate that Geogauge stiffness modulus correlates better with initial modulus than with the other two moduli (Petersen et al., 2002).

$$E_{(QPLT)R} = 0.8962(E_G) + 25.9 \quad \text{with} \quad R^2 = 0.23 \quad (2.9)$$

$$E_{(QPLT)u} = 0.6158(E_G) + 10.3 \quad \text{with} \quad R^2 = 0.27 \quad (2.10)$$

$$E_{(QPLT)i} = 0.3388(E_G) + 84.7 \quad \text{with} \quad R^2 = 0.66 \quad (2.11)$$

Where  $E_{(QPLT)R}$ ,  $E_{(QPLT)u}$ , and  $E_{(QPLT)i}$  are the reloading, unloading, and initial elastic moduli, respectively, in MPa obtained from quasi-static plate load test.

## 2.2 Dynamic Cone Penetrometer (DCP)

The Dynamic Cone Penetrometer (DCP) was initially developed in South Africa for in-situ evaluation of pavement (Kleyn, 1975). Since then, it has been used in South Africa, United Kingdom, Australia, New Zealand, and several states in the U.S.A, such as California, Florida, Illinois, Minnesota, Kansas, Mississippi and Texas for site characterization of pavement layers and subgrades. The U.S Corps of Engineers also used the DCP as well. The DCP has proven to be an effective tool in the assessment of in-situ strength of pavement and subgrade, and can be used for  $(Q_C/Q_A)$  in highway construction.

The DCP is simple, economical, require minimum maintenance, easy to access sites, and provides continuous measurements of the in-situ strength of pavement section and the underlying subgrade layers without the need for digging the existing pavement as in the California Bearing Ratio test (Chen et al., 2001). The DCP consist of an upper

fixed 575 mm travel rod with 8 kg falling weigh, a lower rod containing an anvil, and a replaceable cone with apex angle of  $60^\circ$  or  $30^\circ$  and having diameter of 20 mm (Figure 2.3). The test is conducted by dropping the weight from 575 mm height and recording the number of blows versus depth. Then the penetration rate, PR (sometimes referred as DCP ratio, or penetration index PI) is calculated. The DCP ratio is defined by the slope of the curve relating the number of blows to the depth of penetration (in mm/blow) at a given linear depth segment.

DCP tests are designed to estimate the structural capacity of pavement layers and embankments. The DCP has the ability to verify both the level and uniformity of compaction, which makes it an excellent tool for quality control of pavement construction. In addition, it can also be used to determine the tested layer thickness (Chen et al., 2001). Livneh et al. (1989) demonstrated that the results from penetration tests correlate well with the in-situ CBR values. In addition, they indicated that the layer thickness obtained from DCP tests matches that obtained in the test pits, and concluded that the DCP tests are a reliable alternative for pavement evaluation. Harrison (1986) also found that there is a strong correlation between CBR and DCP penetration ratio in log-to-log form. He reported that CBR-DCP relationship is not affected by changes in moisture content and dry density.

Chen et al. (2001) also indicated that the DCP can be useful when the Falling Weight Deflectometer (FWD) back-calculated resilient moduli is not accurate, such as when the asphalt concrete layer thickness is less than 75mm or when bedrock is shallow.

During the past decade, the DCP test has been correlated to many engineering properties such as the CBR, shear strength of granular materials, and most recently, the

subgrade Resilient modulus ( $M_R$ ) Elastic Modulus ( $E_s$ ) and soil classification. In addition, MnDOT conducted many studies attempting to determine whether there is a reasonable correlation between the DCP penetration rate (PR) and in-place compaction density. Most results of DCP testing on cohesive and selected granular materials showed too much variability to practically apply a correlation. However these studies demonstrated that properly compacted granular base materials exhibit very uniform PR values.

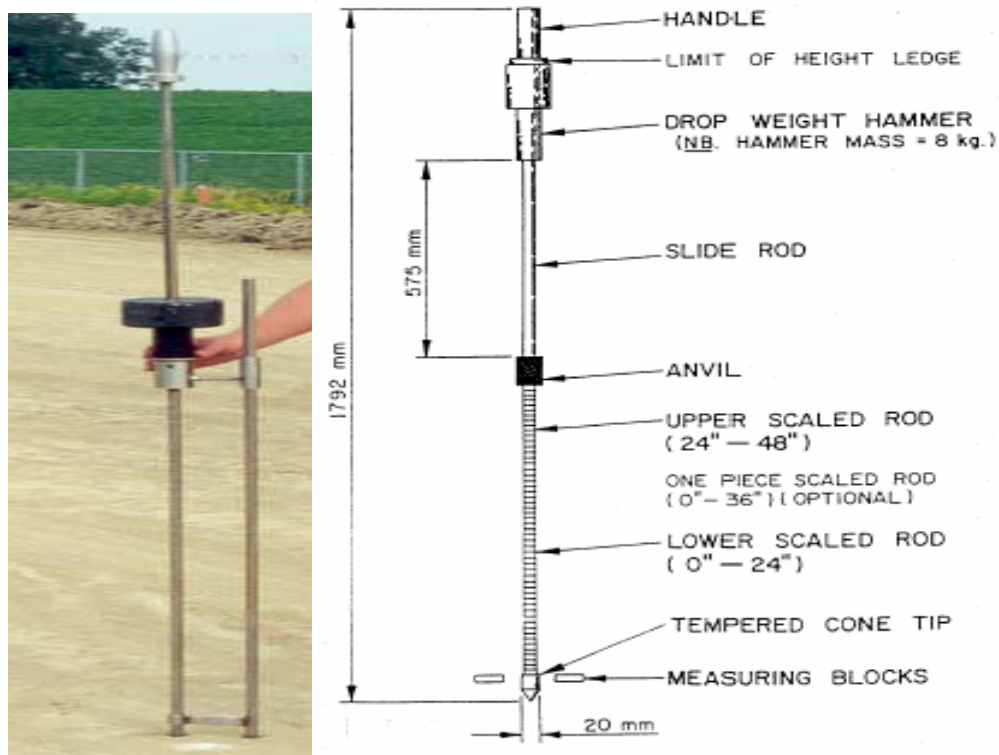


Figure 2.3 Dynamic Cone Penetrometer (DCP)

### 2.2.1. Existing Correlations between DCP and California Bearing Ratio (CBR)

In order to assess the structural properties of the pavement subgrade, the DCP values are usually correlated with the CBR of the pavement subgrade (Kleyn 1975, Livneh 1987). Different correlations were suggested between the PR in (mm/blow) and CBR value. Kelyn (1975) conducted DCP tests on 2000 samples of pavement materials in

standard molds directly following CBR determination. Based on his results the following correlation was recommended

$$\text{Log CBR} = 2.62 - 1.27 \log \text{PR} \quad (2.9)$$

Based on a field study, Smith and Pratt (1983) suggested the following correlation:

$$\text{Log CBR} = 2.56 - 1.15 \log \text{PR} \quad (2.10)$$

Riley et al. (1984) also suggested the Equation 2.10.

Livneh and Ishia (1987) conducted a correlative study between the DCP values and the in-situ CBR values. During this study, both CBR and DCP tests were done on a wide range of undisturbed and compacted fine-grained soil samples, with and without saturation in the laboratory. Compacted granular soils were tested in flexible molds with variable controlled lateral pressures. Field tests were performed on natural and compacted layers representing a wide range of potential pavement and subgrade materials. The research resulted in the following quantitative relationship between the CBR of the material and its DCP-PR value:

$$\text{Log CBR} = 2.2 - 0.71 (\log \text{PR})^{1.5} \quad (2.11)$$

In another study Livneh (1991) conducted 76 tests to revalidate the CBR-DCP relation suggested by Livneh and Ishia (1987); his results indicated that the relationship is “appropriate”. Harison (1989) also suggested the following correlation for different soils:

$$\text{Log CBR} = 2.56 - 1.16 \log \text{PR} \quad \text{for clayey-like soil of PR} > 10 \text{ (mm/blow)} \quad (2.12)$$

$$\text{Log CBR} = 2.70 - 1.12 \log \text{PR} \quad \text{for granular soil of PR} < 10 \text{ (mm/blow)} \quad (2.13)$$

For a wide range of granular and cohesive materials, the US Army Corps of Engineers found a relationship described in Equation 2.14 (Webster et al., 1992); this

equation has been adopted by many researchers (Livneh, 1995; Webster et al., 1992; Siekmeier et al, 2000; Chen et al., 2001).

$$\text{Log CBR} = 2.465 - 1.12 (\log \text{PR}) \quad \text{or} \quad \text{CBR} = 292/\text{PR}^{1.12} \quad (2.14)$$

MnDOTD also adopted Equation 2.14. They also found that the effects of soil moisture content and dry density influence both CBR and DCP values in a similar way; therefore, they are considered negligible for the correlation.

### **2.2.2 Existing Correlations between DCP and Different Moduli**

The subgrade resilient modulus, which is used in design methods based on structural analysis, can be determined either indirectly from relation between subgrade modulus ( $E_s$ ) and CBR or can be predicted directly from the DCP results. The 1993 AASHTO Guide for Design of Pavement Structures has adopted Equation 2.15 for calculating subgrade resilient modulus ( $M_R$ ), which was proposed by Huekelom and Klomp (1962):

$$M_R (\text{psi}) = 1500 * \text{CBR} \quad \text{or} \quad M_R (\text{MPa}) = 10.34 * \text{CBR} \quad (2.15)$$

The resilient moduli from which this correlation was developed ranged from 750 to 3000 times the CBR. Also, the formula is limited to fine-grained soils with a soaked CBR of 10 or less (Chen et al., 2001).

Chen et al. (2001) indicated that using Equation 2.14 to compute CBR and then using Equation 2.15 to compute modulus values from DCP tests yielded comparable results with those from FWD. Powell et al. (1984) suggested another relationship between subgrade resilient modulus and CBR as shown in Equation 2.16. Other Equations related the DCP Penetration Ratio (PR) with the subgrade modulus directly. Pen (1990) suggested the two relationships between the subgrade's elastic modulus ( $E_s$ ) in (MPa) and PR in (mm/blow) as defined in Equations 2.17 and 2.18.

$$M_R (\text{psi}) = 2550 \times \text{CBR}^{0.64} \quad \text{or} \quad M_R (\text{Mpa}) = 17.58 \times \text{CBR}^{0.64} \quad (2.16)$$

$$\text{Log} (E_s) = 3.25 - 0.89 \text{ Log} (\text{PR}) \quad (2.17)$$

$$\text{Log} (E_s) = 3.652 - 1.17 \text{ Log} (\text{PR}) \quad (2.18)$$

Chua (1988) presented a new theoretical approach to modeling and interpreting results using DCP with cone apex angle of 60. A one-dimensional model for penetration analysis of a rigid projectile into ideally locking material was used to back calculate the elastic modulus of the target medium. The model assumed that the soil medium was penetrated by one blow of horizontal disc and upon penetration, the projectile displaces the soil and the radial plastic shock wave propagates in the disc and plastic deformation take place. The equations of the above interaction were taken from Yankelevsky and Adin (1980). These equations finally led to the required theoretical relationship. In these relationships the DCP values are a function of the principal stress differences at failure ( $2\tau_0$ ).

The mathematical formulation of Chua's curve is as follow:

$$\text{Log} (E_s) = B - 0.4 \log (\text{PR}) \quad (2.19)$$

Where

$E_s$ : the elastic modulus of soil in MPa

B: a constant value depending on the value of  $2\tau_0$  and given in Table 2.3.

Results of regression analysis conducted by Chen et al. (1999) between the FWD back-calculated resilient modulus ( $M_{\text{FWD}}$ ) and the DCP-PR resulted in the following prediction model:

$$M_{\text{FWD}} = 338 (\text{PR})^{-0.39} \quad (\text{for } 10 \text{ mm/blow} < \text{PR} < 60 \text{ mm/blow}) \quad (2.20)$$

Where  $M_{\text{FWD}}$  is in MPa.

Table 2.3 Values of B (Chua, 1988)

Soil Type	$2 \tau_0$	B
Plastic clay	25	2.22
Clayey soil	50	2.44
Silty soil	75	2.53
Sandy soil	150	2.63

De Beer (1990) also proposed a correlation between the elastic modulus ( $E_s$ ) and DCP-PR, which has a form similar to CBR relation, and is shown in the following equation:

$$\text{Log}(E_s) = 3.05 - 1.07 \text{Log}(\text{PR}) \quad (2.21)$$

Based on a regression analysis, Konard and Lachance (2000) suggested a relationship between the penetration rate (PR) of a large DCP with 51 mm diameter cone and the elastic modulus of unbound aggregates and natural granular soils back-calculated from plate load tests ( $E_{\text{PLT}}$ ), and it is as follows:

$$\text{Log}(E_{\text{PLT}}) = (-0.88405) \text{Log}(\text{PR}) + 2.90625 \quad (2.22)$$

Where  $E_{\text{PLT}}$  is expressed in MPa.

### 2.2.3 Soil Classification Based on DCP Results

From an investigation of a series of case histories in Herfordshire, U.K., in which the DCP has been used, Huntley (1990) suggested a tentative classification system of soil based on penetration resistance; n in blows per 100 mm as illustrated in Tables 2.4 and 2.5. However he recommended the use of classification tables with considerable caution until a better understanding of the mechanics of skin friction on the upper drive rod is established.

Table 2.4 Suggested classification for granular soils using DCP (Huntley, 1990)

Classification	n Value Range		
		Sand	Gravelly sand
Very loose	<1	<1	<3
Loose	1-2	2-3	3-7
Medium dense	3-7	4-10	8-20
Dense	8-11	11-17	21-33
Very Dense	>11	>17	>33

Table 2.5 Suggested classification for cohesive soils using DCP (Huntley, 1990)

Classification	n Value Range
Very soft	<1
Soft	1-2
Firm	3-4
Stiff	5-8
Very stiff to hard	>8

#### 2.2.4 Current Application of DCP in Pavement Assessment

Now more than a dozen DOTs and federal agencies are using the DCP to assess the strength and uniformity of highway structures (Siekmeier et al, 2000). The MnDOT was one of the first states that have been using the DCP. MnDOT has been conducting research on the DCP since 1991. Currently the MnDOT specifies two different applications of DCP testing in its pavement assessment procedures. One application involves using the DCP as a quality control device during the backfill compaction of pavement edge drain trenches. This application was proven to be reliable and effective in improving the compaction levels of these trenches. The second application of DCP testing, specified by MnDOT, involves its use in the quality control of granular base layer compaction. Other non specified applications of the DCP by MnDOT have included investigations of soft subcut areas, determination of the condition of the base and

subgrade materials under full depth bituminous cracks and monitoring the effectiveness of subgrade flyash stabilization (Burnham, 1996). For example, the MnDOT specified that the in-situ subgrade CBR based on DCP tests should be at least 6 to minimize rutting damage to the finished grade (prior to paving) and to provide adequate subgrade support for proper compaction of the base and other layers. In addition they specified that soils with PR values greater than 25 mm/blow may need remedial procedures, such as sub-cutting, drying and compaction, backfilling with granular borrow or lime treatment (Burnham, 1996).

### **2.3 Light Falling Weight Deflectometer (LFWD)**

Light Falling Weight Deflectometer (LFWD) is a portable falling weight deflectometer that has been developed in Germany as an alternative in-situ testing device to the plate load test. Different types of LFWD exist in the market. Three main types of LFWD have been used in the previous studies; they are the German Dynamic Plate (GDP), the Transport Research Laboratory (prototype) Foundation Tester (TFT), and the Prima 100 LFWD. Table 2.6 describes a comparison between the different types of LFWD. All types exhibit many similarities in their mechanics of operation although there are many differences in design and mode of operation, which lead to variations in the measured results. Generally, the LFWD consist of a loading device that produces a defined load pulse, a loading plate, and one center geophone sensor (electric deflection-data device) to measure the center surface deflection.

The Prima 100 LFWD was used in this study (Figure 2.4). Prima 100 has been recently developed and marketed by Carl Bro Pavement Consultants (previously Phønix). It weighs 26 kg (57.2 lbs) and has a 10 kg (22 lb) falling mass which impacts a spring to

produce a load pulse of 15-20 milliseconds. For safe operation, the drop weight is supported with a transportation-lock pin and guide rod with stabilizer. Prima 100 has a load range of 1-15 kN (i.e. up to 450 kPa with its 200 mm diameter loading plate). It measures both force and deflection, utilizing a velocity transducer with a deflection range of 22 mm (Fleming et al. 2000).

Table 2.6 Specification for different types of LFWD (Fleming 2001)

Model	Plate Diameter (mm)	Mass		Total load pulse (ms)	Deflection Transducer		Stress Range (kPa)
		Falling Weight (kg)	Bearing plate (kg)		Type	On plate Ground	
GDP	300	10	17	18 ± 2	Accelerometer	Plate	100
TFT	200, 300	10	20	15-25	Velocity	Ground	<120
Prima 100	200, 300	10, 20	16	15-20	Velocity	Ground	<200

During any test operation, the center deflection ( $\delta_c$ ) of the loading plate will be measured and used to estimate the LFWD elastic stiffness modulus ( $E_{LFWD}$ ) (Figure 2.5). The expression used to calculate  $E_{LFWD}$  is similar to the one used to calculate the surface modulus of a layered media assuming a uniform Poisson's ratio ( $\nu$ ), and constant loading on an elastic half space (Boussineq elastic half space). This expression is described by Equation 2.23 :

$$E_{LFWD} = \frac{2(1-\nu^2)\sigma \times R}{\delta_c} \quad (2.23)$$

Where

$\sigma$  = the applied stress

R= the plate radius

A complete analysis of the LFWD field data can provide an estimate of the linear-elastic response of the individual material making up the pavement structure and its

supporting layer. Therefore, it is well-suitable for application in the  $Q_C/Q_A$  procedures for the construction of pavement layers and other geo-materials. However, there are currently limited published data relating to its efficiency (Fleming et al. 2000).

### 2.3.1 Existing Correlation between LFWD Moduli and Other In-Situ Test Moduli

The German Code for the design of flexible pavement structures recommends Equation 2.24 to relate the stiffness moduli calculated from the plate load test, and the German Dynamic Plate test (GDP) (one type of the LFWD that was previously described) (Livneh and Goldberg, 2001).

$$E_{PLT(R2)} = 600 - \frac{300}{300 - E_{LFWD}} \quad (2.24)$$

Where  $E_{PLT(R2)}$  is the German reloading stiffness elastic modulus in MPa obtained by PLT test.

Fleming et al. (1988) demonstrated correlative ratio between the deformation moduli of the GDP and the FWD of about 0.5. However, Fleming (1998, 2001) reported that his extensive field-stiffness measurements on in-situ construction sites showed a relatively consistent correlation of 0.6 between the stiffness moduli of the GDP and FWD. Livneh and Goldberg (2001) suggested that the GDP (LFWD) stiffness moduli is about 0.3-0.4 times the conventional FWD moduli. Fleming et al. (2000) conducted field tests to correlate the moduli of three main types of LFWD (TFT, GDP, Prima 100) with that of the FWD. Their results showed that the  $M_{FWD}$  correlated well with moduli obtained from prima 100; Equation 2.25 shows an example correlation. However they found that the correlation coefficients with the other LFWD types was as follows:  $FWD = 1.05$  to  $2.22 E_{GDP}$ ,  $FWD = 0.76$  to  $1.32 E_{TFT}$ .

$$M_{FWD} = 1.031 E_{LFWD (Prima 100)} \quad (2.25)$$



Figure 2.4 Prima 100, Light Falling Weight Deflectometer

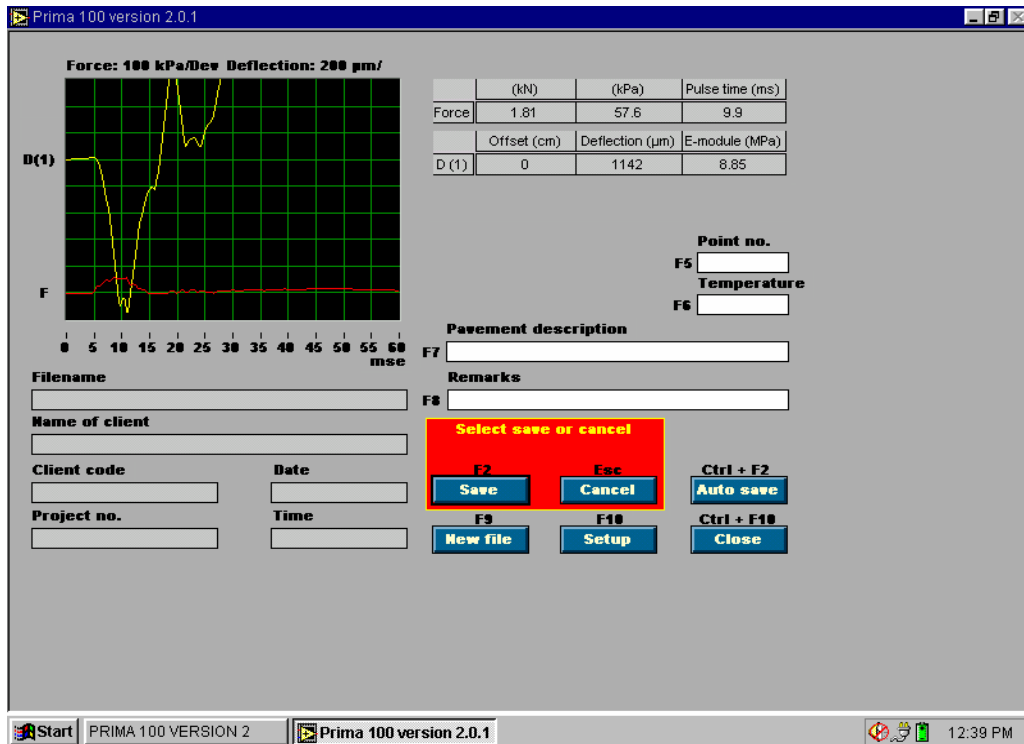


Figure 2.5 Screen of Prima 100 software

Kamiura et al. (2000) studied the relationship between LFWD (mainly Prima 100) and plate load test measurements for subgrade materials which contains volcanic soil, and silty sand, and mechanically stabilized crushed stone. They suggested the following correlation based their results:

$$\text{Log} \left( \frac{k_{\text{LFWD}}}{k_{30}} \right) = 0.0031 \log (k_{\text{LFWD}}) + 1.12 \quad (2.26)$$

Where

$k_{\text{LFWD}}$  is the ratio of stress on loading plate of the LFWD to the measured deflection at this stress.

$k_{30}$ : is the ratio of stress on plate with a diameter of 300 mm for a PLT to the measured deflection at this stress.

Kamiura et al. (2000) also indicated that the ratio of  $\frac{k_{\text{LFWD}}}{k_{30}}$  is affected by the grain size of the tested material, where this ratio increases with increasing grain size.

Fleming (2001) reported that a number of factors influence the measured stiffness of LFWD; including differences in mass, transducer type and software analysis (which records the maximum deflection as that at the time of the peak force).

#### **2.4 Falling Weight Deflectometer (FWD)**

Based on early work in France during the 1960s, the Technical University of Denmark, the Danish Road Institute and the Dynatest Group have gradually developed and employed the Falling Weight Deflectometer (FWD) for use as Non-Destructive Testing (NDT) of highway and airfield pavements. The FWD system used in this study is the Dynatest model 8000 (Figure 2.6). It consists of three main components:

- A Dynatest 8002E FWD Trailer

- A Dynatest 8600 System Processor
- A Hewlett-Packard HP-85B laptop computer.

The Dynatest 8002E FWD is a trailer mounted FWD. It consists of a drop weight mounted on a vertical shaft, and it can be towed by most conventional vehicles. The drop weight is hydraulically lifted to predetermined heights ranging from 50 to 510 mm. The weight is usually dropped onto a 300 mm or a 450 mm diameter loading plate resting on a 5.6 mm thick rubber buffer, which is usually used to improve the uniformity of loading stress distribution over the whole loading plate area (Dynatest, 1995).

The impact of the falling weight is capable of producing impact loads approximately half-sinusoidal wave, and having a loading time of between 25 and 40 ms applies impulse loading to a circular plate in contact with the pavement surface. Usually the load range from 6.7 kN to 155.7 kN depending on the magnitude of the dropping mass and the height of the drop. The applied load is recorded by a load cell. The FWD also has seven geophones. These factory calibrated geophones register the peak deflections due to an applied load. The geophones are positioned at 0, 305, 457, 610, 914, 1219, 1524 mm away from the center of the loading plate. A suitable hole is provided in the center of the loading plate such that the center deflection may also be measured. A transducer holder is also provided for each of the seven geophones. They are in movable holders along a 2.45 m raise/lower bar, for precise deflection basin measurements. The load cell and seismic deflection transducers are connected to sockets in a protective Trailer Connection Box on the trailer. The geophones and the Trailer Connection Box are connected to the 8600 System Processor (Dynatest, 1995).

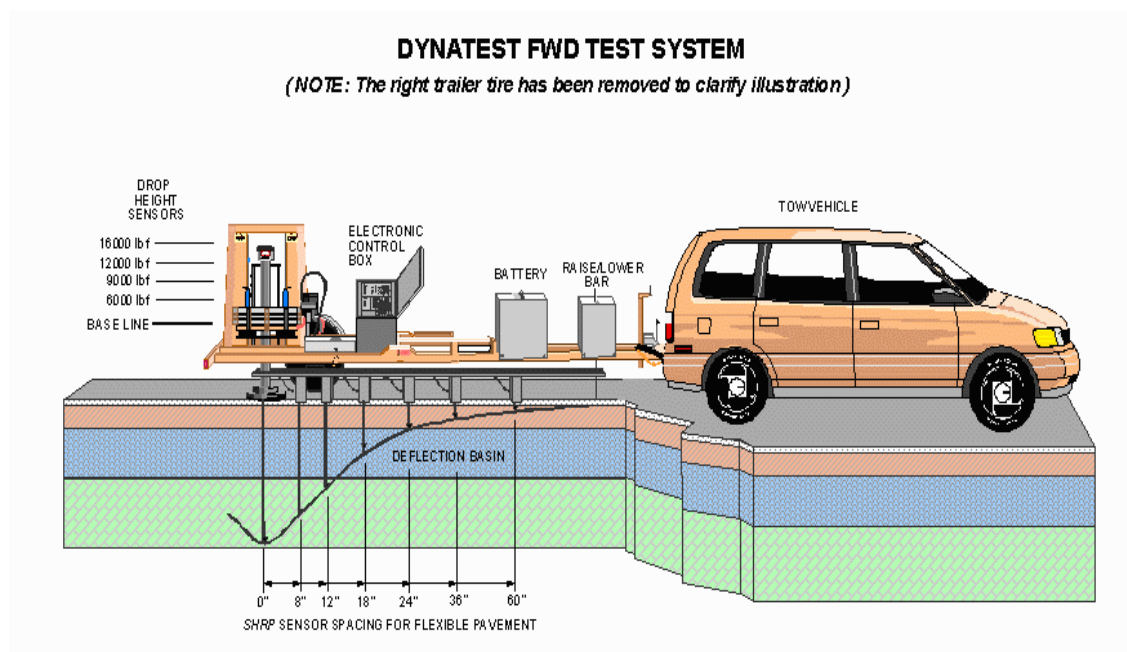


Figure 2.6 Dynatest model 8000 (FWD) (LTRC 2000)

The Dynatest 8600 System Processor is a microprocessor based control and signal processing unit that connects the FWD trailer with the computer. It controls the FWD operation, performs scanning, conditioning and further processing of the geophone signals and monitors the status of the FWD unit to ensure correct measurements. The application of the loading is remotely controlled by the operator.

#### 2.4.1 FWD Moduli Backcalculation

The analysis performed on any FWD data is aimed at determining the resilient modulus of each layer in a pavement section and the depth of the underlying bedrock layer. This analysis is usually referred to as the FWD back-calculation process. To perform the analysis, the properties such as the elastic modulus and Poisson's ratio, should be known for the materials in each pavement layer. In addition, the thickness of each pavement layer is also required in this analysis (FHWA, 1994).

The back-calculation procedure involves calculation of theoretical deflections under the applied load using assumed pavement moduli. These theoretical deflections are compared with measured deflections and the assumed moduli are then adjusted in an iterative procedure until there is no significant difference between theoretically calculated and the measured deflections. The moduli determined in this method represent the pavement response to load and can be used to calculate stresses or strains in the pavement structure. Examples of current back-calculation programs currently in use include the MODULUS, ELMOD and EVERCALC programs. ELMOD 4.0 program was used in this study.

#### **2.4.2 Application of FWD**

The FWD was used to provide periodic non-destructive evaluation of the structural capacity of different pavement sections. It has proved to be a good non-destructive test for pavement structure assessment mainly because of its speed, better simulation of traffic loading, and results that can directly be applied in structural design (Fleming et al. 2000). Now, there are more than 300 FWD worldwide in operation for routine non-destructive testing and research purposes. Most testing is performed on completed pavement structures. Less experience has been gained with the use of the FWD on road bases, subbase and subgrade (Gurp et al., 2000). Furthermore, Falling Weight Deflectometer (FWD) data may be questionable, such as when the AC thickness is less than 3 inches, or when shallow bedrock is encountered. These two situations often cause a misinterpretation of FWD data (Chen et al., 2001).

Current research on FWD, suggests that the FWD can be used in the quality control during construction of pavement layers. Zaghoul and Saeed (1996) suggested an

empirical approach to set FWD target deflections. In this approach trial sections are constructed and FWD tests are performed at locations showing acceptable density levels to determine the required target deflections. They also suggested that the  $Q_C/Q_A$  procedures include dividing pavement sections into homogenous segments, and FWD tests are conducted on each layer, then statistical tests should be conducted on measured deflections in order to evaluate the construction quality and to identify weak points.

Furthermore, Rogers et al. (2000) performed tests using FWD to determine the relation between the stiffness and the dry density of a base course layer. Their test results showed that although the stiffness increased during the initial compaction passes, adequate stiffness development took place only when the density is close to its maximum value at the optimum moisture content. Based on this result, they suggested that there is no evident correlation between dry density and the stiffness measured by FWD.

Although the FWD is classified as a suitable device for stiffness measurements, it is sometimes considered unnecessarily complicated for base and subbase testing (Fleming, 2000). In addition, the use of the FWD to evaluate the pavement structure during construction of subgrade, subbases, and base layers is faced with some problems. One of these problems lies in that pavement layers which are under construction are not as accessible to FWDs as for completed roads. Another drawback of using FWD for monitoring the load carrying capacity of a pavement structure under construction is that the uneven surface causes tilting of the deflection sensors. Tilting in excess of a certain value leads to inaccurate deflection measurement that can not be used in back calculation (Gurp et al., 2000).

## 2.5 Static Plate Load Test (PLT)

The Static Plate Load Test (PLT) has been a useful site investigation tool for many years and has been used for proof testing of pavement structure layers in many European countries. Currently it is used for both rigid and flexible pavements. The test consists of loading a circular plate that is in close contact with the layer to be tested and measuring deflections under load increments. The plates used for runways are usually 76.2 cm (30 inch) in diameter, but for roads they are usually smaller, with a diameter of 30.5 cm (12 inch). In order to prevent bending of the plate, other plates with decreasing diameters are usually placed on top of it. The load is transmitted to the plates by a hydraulic jack, acting against heavy mobile equipment as a reaction plate. The corresponding deflection is usually measured at four points on the plate surface, at right angles to one another, by means of dial gages attached to a horizontal beam with its supports placed far enough away from the plate such that it will not be affected by any applied load (Rodriguez et al. 1988).

Plate tests can be conducted using variable procedures depending on the information desired. In all cases, when a load is applied to the plate, the plate deflects according to the general relationship shown in Figure 2.7. The load must be sustained on the plate until all measured settlement has diminished; this is done to ensure that the true deflection for each load increment is obtained. The time required for settlement is determined by plotting a time-deformation curve while the test is in progress, and identifying where this curve has become essentially horizontal. Generally a load increment is applied when the rate of deformation has approached about 0.001 in/min (Holtz et al 1981).

The method of performing PLT test on soils and flexible pavement is described by ASTM D1195-93. In this method, the PLT test should continue until a peak load is reached or until the ratio of load increment to settlement increment reaches a minimum, steady magnitude.

In some PLT tests, it is desirable to determine the relative amounts of plastic and elastic deformations. To accomplish this, loads are applied and maintained until all settlement has stopped. Then, the load is removed and higher loads are applied until a curve is obtained. After the final load is applied, the load is released in the same increments to obtain the rebound cycle. This procedure can also be done to obtain cyclic-load values. Which are extremely useful to determine the elastic properties of the subgrade (Yoder and Witczak, 1975).

### **2.5.1 PLT Moduli**

Plate loading tests can be used to estimate the modulus of subgrade reaction ( $k$ ). Determination of the modulus of subgrade reaction is made in the field on the selected subgrade soil at its natural moisture content. This test is conducted by subjecting the subgrade to a known stress at a predetermined rate of speed using a loading system, and recording the resulting settlement. The modulus of subgrade reaction can be calculated using the following relation (Yoder and Witczak, 1975):

$$k = \frac{p}{\delta} \quad (2.27)$$

Where

$p$  = unit load on plate (psi)

$\delta$  : deflection of the plate (in.)

In addition the PLT can be used to determine the elastic stiffness modulus of different pavement layers. Usually, the load is often cycled several times to measure a more stable elastic stiffness (Fleming et al. 2001). The general equation used to determine the elastic static modulus for the PLT as follow (Yoder and Witczak, 1975):

$$E_{plt} = \frac{1.18pR}{\delta} \quad (2.28)$$

Where

$E_{plt}$  = plate load elastic modulus

$p$  = applied pressure

$R$  = radius of plate

$\delta$  = deflection of plate at pressure,  $p$

1.18 = factor for rigid plate

The factor of 1.18 in Equation 2.28 is based on a Poisson's ratio of 0.5. It has been noted that the materials used in roadway construction have Poisson's ratios typically ranging from 0.25 to 0.4, which might introduce some error with these types of materials (Horhota, 1996).

German Code for the design of flexible pavement structures specifies performing in-situ plate-bearing tests on constructed pavement layers. For the second cycle of the regular plate-bearing test, the German code defines a reloading stiffness modulus called  $E_{plt(R2)}$  using the following equation (Livneh and Goldberg, 2001):

$$E_{R2} = \frac{2p(1-\nu^2)}{\pi R \delta} \quad (2.29)$$

$p$  = applied load by the end of the second cycle

$\delta$  = deflection under the second loading cycle of the plate

The German code specifies a minimum static plate load reloading stiffness modulus ( $E_{PLT(R2)}$ ), of 45 MPa at the top of the subgrade. In addition, performing the plate-bearing test is also mandatory at the top of the subbase, with a minimum a value  $E_{PLT(R2)}$  of 120 MPa for light traffic and 150 MPa for heavy traffic (Livneh and Goldberg, 2001).

The static plate test is relatively slow, and it needs usually a loaded truck or a frame to jack against, which can be major a practical difficulties for using the PLT. Small-scale devices, such as like Geogauge, LFWD and DCP are faster and can also access difficult site areas more easily.

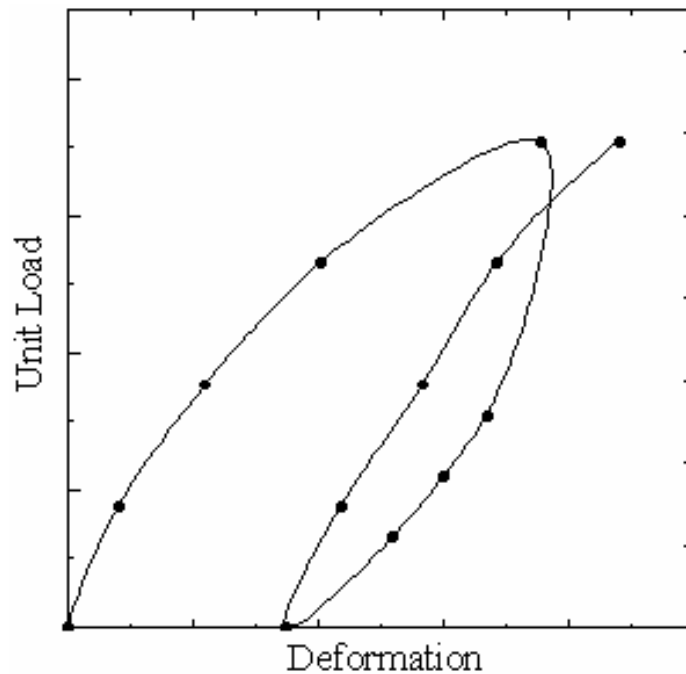


Figure 2.7 Typical curve for plate load tests on soils

## 2.6 California Bearing Ratio (CBR)

The California Bearing Ratio (CBR) test is a relatively simple test that is commonly used as an indicator of the strength of a subgrade soil, subbase, and base

course material in highways and airfield pavement systems. The test is described in ASTM D1883-99 standard.

The CBR test is used primarily to empirically determine the required thicknesses of flexible pavements. It is normally performed on remolded (compacted) specimens, although they may be conducted on undisturbed soils or on soils in the field. Remolded specimens may be compacted to their maximum unit weights at their optimum moisture contents if the CBR is desired at 100% maximum dry unit weight and optimum moisture content. CBR tests can also be performed at the desired unit weights and moisture contents. Soil specimens are tested by placing them in water for 96 hours in order to simulate very poor soil conditions. The CBR is defined as the ratio (expressed as a percentage) obtained by dividing the penetration stress required to cause a piston with a diameter of 49 mm (1.95 inch) to penetrate 0.10 in. into the soil by a standard penetration stress of 1,000 psi. This standard penetration stress is roughly what is required to cause the same piston to penetrate 0.10 in. into a mass of crushed rock. The CBR may be thought of as an indication of the strength of the soil relative to that of crushed rock. The CBR may be expressed as (Yoder and Witczak, 1975):

$$\text{CBR} = \frac{\text{penetration stress (psi) required to penetrate 0.10 in.}}{1000 \text{ psi}} \times 100\% \quad (2.30)$$

It should be noted that the 1,000 psi in the denominator is the standard penetration stress for 0.10-in. penetration. If the bearing ratio based on a penetration stress required to penetrate 0.20 in with a corresponding standard penetration stress of 1,500 psi is greater than the one for a 0.10-in penetration, the test should be repeated, and if the result is still similar, the ratio based on the, 0.20-in penetration should be reported as the CBR value.

According to the procedure described in ASTM D1883-99, if the CBR is desired at an optimum water content and some percentage of maximum dry unit weight, three specimens should be prepared and tested from soil to within  $\pm 0.5\%$  of the optimum water content and using a different compactive effort for each specimen such that the dry unit weights of these specimens vary above and below the desired value. Then the CBR for the three specimens should be plotted against their corresponding dry unit weight, and from this plot the CBR for the desired dry unit weight can be determined.

The CBR test is sensitive to the texture of the soil, its water content and the compacted density. The result of a CBR test also depends on the resistance to the penetration of the piston. Therefore, the CBR indirectly estimates the shear strength of the material being tested (Rodriguez et al. 1988).

## **CHAPTER THREE**

### **METHODOLOGY**

#### **3.1 Field Testing**

This thesis included conducting field tests on several highway sections in different projects within the State of Louisiana. In addition, nine test sections and trenches were constructed and tested at the LA-DOTD Accelerated Load facility (ALF) site. In each field test five Geogauge measurements, five LFWD measurements, and one DCP measurements were taken. The PLT and FWD tests were also conducted on each test section for use as reference measurement. The dry unit weight and moisture content were obtained using the nuclear density gauge. Figure 3.1 describes the layout of the field tests. The reason for taking five Geogauge and LFWD measurement at the same section was to estimate the average value and evaluate the reliability of these devices. In this study, only the average value and the corresponding coefficient of variation of the GoeGauge and the LFWD measurement are reported. It should be indicated that the reported DCP-PR represents the average penetration rate along the thickness of the tested layer. The following sections describe in details the tests conducted in this study.

##### **3.1.1 US Highway 190**

Tests were conducted at three different stations (12+530, 12+650, and 15+800) within the US highway 190. In all tests, a 200 mm (8 inch) thick crushed limestone base course section built on top of a 200 mm (8 inch) lime-treated subbase layer was tested. The crushed limestone has the gradation shown in Figure 3.2 and is classified as A-1-a, and GW-GC, according to the American Association of State Highway and Transportation (AASHTO) classification system, and the Unified Soil Classification System (USCS), respectively. Figure 3.3 shows the layout and profile of the tested

section. Tables 3.1 presents the summary of the test results for the Geogauge, LFWD, and DCP conducted on US 190. Table 3.2 presents the results of dry density and moisture content using the nuclear density gauge.

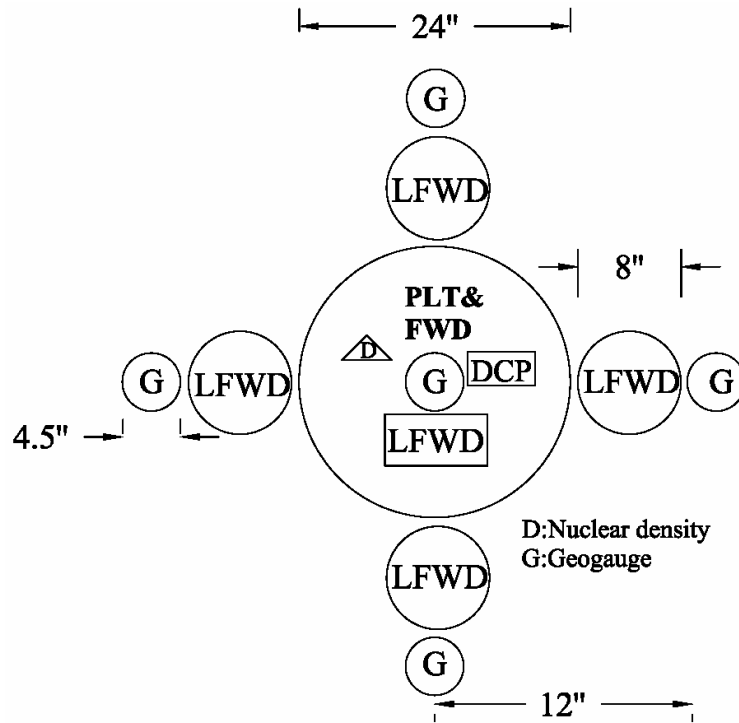


Figure 3.1 Layout of field test measurements

### 3.1.2 Louisiana State Highway 182

Louisiana State Highway 182 had a major rehabilitation project; in which the whole pavement section was reconstructed. During the construction of this project, four sections were selected and tested; including a subgrade, lime-treated and cement-stabilized sub-bases, and a cement-stabilized base sections. The layout and profile of the tested section tested is presented in Figure 3.4. In the first section, the subgrade layer located at station 47+10 was tested before and after being stabilized by mixing the soil with 10% lime by volume. The subgrade soil was classified as A6, and CL, according to the AASHTO classification system and USCS, respectively.

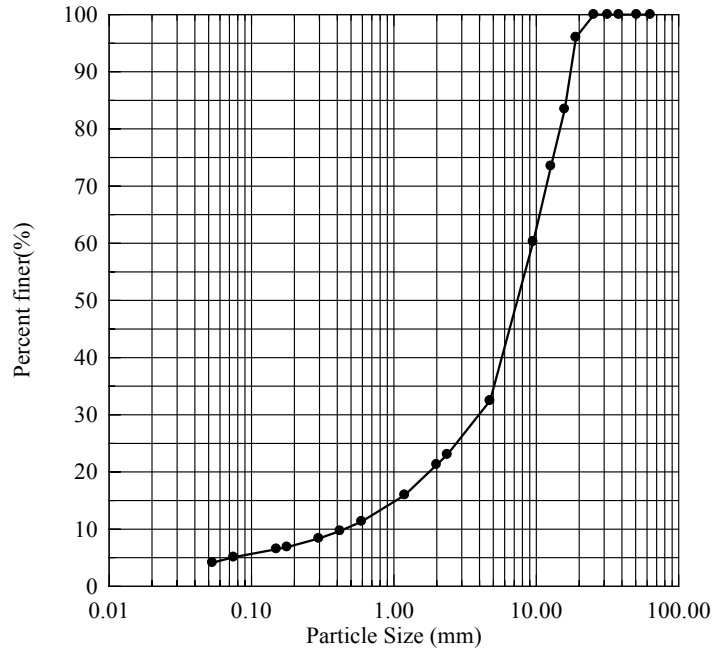


Figure 3.2 Gradation for the crushed limestone tested at highway US 190

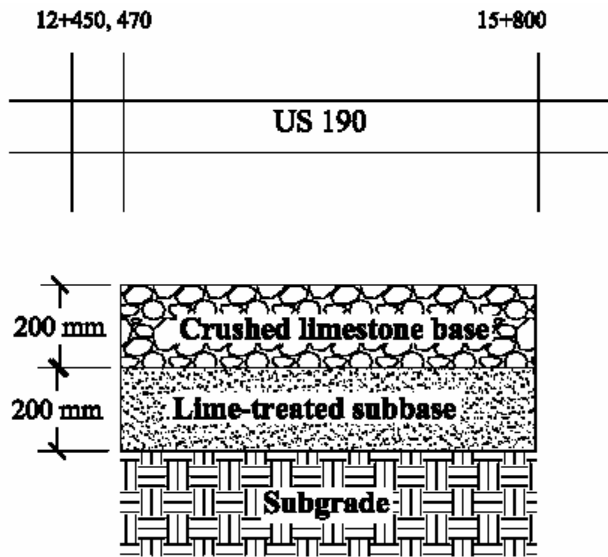


Figure 3.3 Layout and profile for sections at highway US 190

Table 3.1 Summary of results for base course sections at highway US 190

Station	$E_G$ (MPa)	$C_V$ %	$E_{LFWD}$ (MPa)	$C_V$ %*	DCP-PR (mm/blow)
15+800	155.90	3.64	240	4.75	4.80
12+530	128.5	3.24	106.13	5.61	6.85
12+650	119.6	3.64	104.70	6.13	5.70

$C_V$ %\*: coefficient of variation

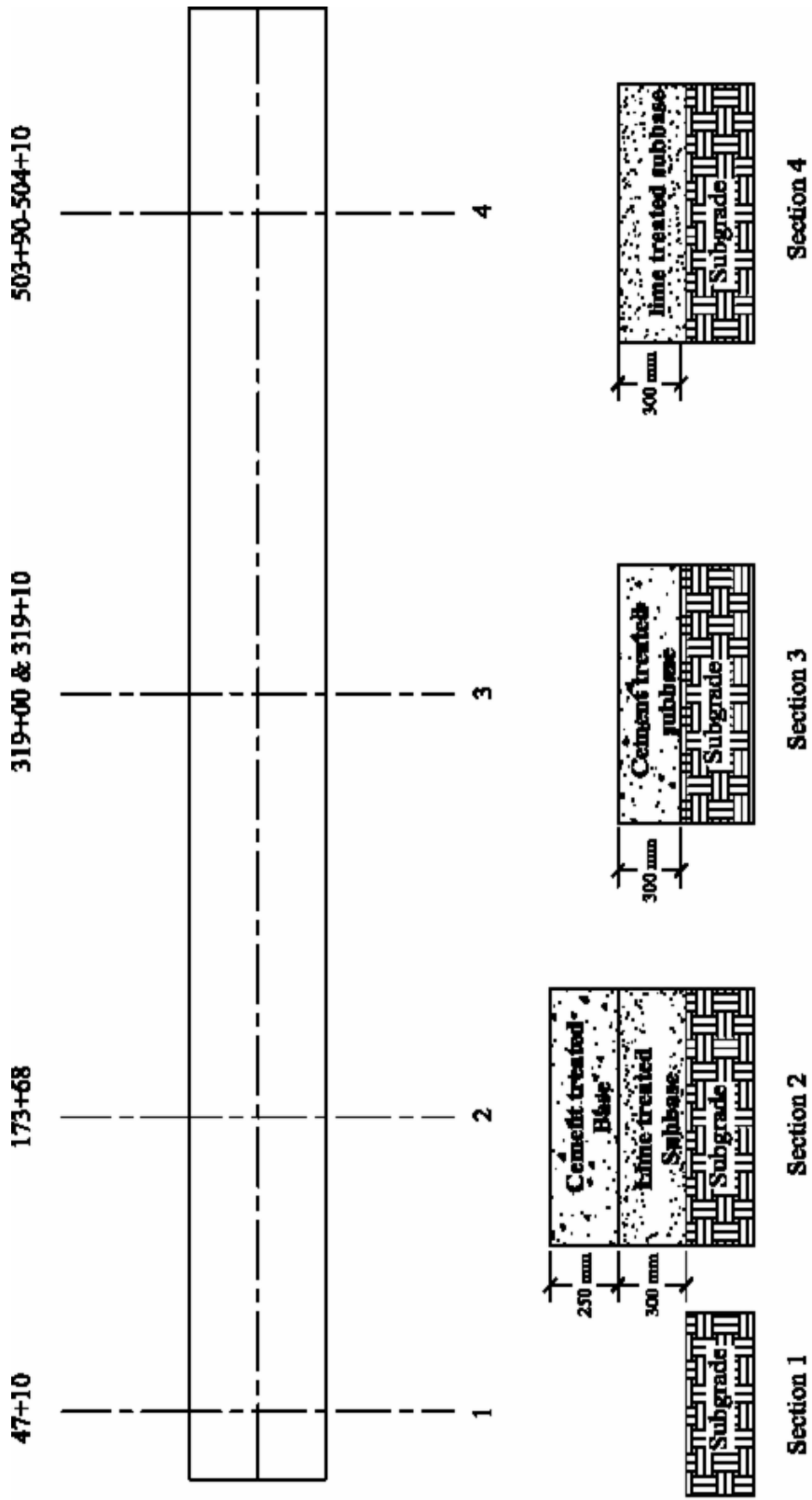


Figure 3.4 Layout and profile for sections at highway LA 182

Table 3.2 Dry density and moisture content measurement at highway US 190

Station	$\gamma_d^*$ kN/m <sup>3</sup>	mc %**
12+530	18.9	7.8
12+650	18.9	8.85

$\gamma_d^*$ : the dry unit weight

mc%\*\* : the moisture content

In addition, the optimum moisture content and the maximum dry unit weight obtained in the standard proctor test for the subgrade soil were 16.57 kN/m<sup>3</sup> (105.5 lb/ft<sup>3</sup>) and 16.4%, respectively. The second section was a 300 mm (12 inch) thick cement stabilized subbase that was tested at stations 319+00 and 319+10. This section was constructed by mixing the soil with 4% of cement by volume. The soil in this section was classified as A4 and CL-ML according to the AASHTO classification system and USCS, respectively. The soil also had an optimum moisture content of 10.7%, and a maximum dry unit weight of 19.6 kN/m<sup>3</sup> (124.8 lb/ft<sup>3</sup>), as measured in the standard proctor tests. The third section was 254 mm (10 inch) thick cement stabilized base and was tested one day after construction at station 173+68. This section was built on top of a 300 mm (12 inch) thick lime-treated subbase, and it was constructed by mixing the soil with 6% of cement by volume. In the fourth test section a 300 mm (12 inch) inch thick lime treated subbase was tested at stations 503+90, 504+00, and 504+10. This section was constructed by mixing the soil with 10% of lime by volume. The soil in this section was classified as A4 and CL, according to the AASHTO classification system and USCS, respectively. The standard proctor curve indicated that the soil had an optimum moisture content of 10.4%, and a maximum dry unit weight of 19.1 kN/m<sup>3</sup> (121.3 lb/ft<sup>3</sup>). A summary of the Geogauge, LFWD, and DCP test results as presented in Table 3.3, while the dry density and moisture content measurements are presented in Tables 3.4.

Table 3.3 Summary of Geogauge, LFWD, and DCP test results for highway LA 182

Section	Station	$E_G$ (MPa)	$C_v$ %	$E_{LFWD}$ (MPa)	$C_v$ %	DCP-PR (mm/blow)
Untreated Subgrade	47+10	54.56	2.42	37.1	20.57	53.80
Lime treated subgrade	47+10	63.90	4.0	28.04	28.04	36.00
Cement Treated base	173+68	238.15	7.08	366.9	3.22	3.27
Cement Treated subbase	319+00	113.55	6.01	56.0	11.42	12.8
	319+10	99.68	6.12	50.9	11.45	14.25
Lime Treated Subbase	503+90	105.31	6.62	70.64	8.20	12.52
	504+00	107.64	5.84	71.56	9.165	12.22
	504+10	111.33	1.2	78.17	8.38	10.00

Table 3.4 Dry density and moisture content measurements at highway LA 182

Section	Station	$\gamma_d$ (kN/m <sup>3</sup> )	mc %
Untreated Subgrade	47+10	15.9	21.20
Lime-treated subgrade	47+10	--	--
Cement-treated base course	173+68	17.8	10.70
Cement-treated subbase	319.00	16.4	12.90
	319+10	16.3	12.80
Lime-treated Subbase	503+90	17.0	9.50
	504+00	17.5	10.20
	504+10	--	--

Table 3.5 Summary of results for subbase section at the US highway 61

Section	Passes	$E_G$ (MPa)	$C_v$ %	$E_{LFWD}$ (MPa)	$C_v$ %	DCP-PR (mm/blow)
Subbase	1	69.39	6.75	46.54	17.11	14.5
	4	80.05	4.19	69.26	15.76	10.25

### 3.1.3 US Highway 61

Field tests were conducted during the compaction of a 300 mm (12 inch) thick subbase layer at US highway 61. A rubber tire roller was used in the compaction process. A test section was selected and tested after the first and fourth roller pass, using the Geogauge, LFWD, DCP and FWD. While the PLT was only conducted after the fourth pass. The tested subbase layer consisted of unstabilized soil classified as A4 and CL-LM,

according to the AASHTO classification system and USCS, respectively. The standard proctor test results indicated that the maximum dry unit weight and optimum moisture content for this soil were 17.5 kN/ m<sup>3</sup> (111.4 lb/ft<sup>3</sup>), and 17.1%, respectively. Table 3.5 present a summary for Geogauge, LFWD, and DCP test results. The dry unit weight and moisture content was measured after the fourth roller pass and it was 16 kN/ m<sup>3</sup> and 15.63%, respectively.

#### **3.1.4 Test Sections at LA-DOTD Accelerated Load facility (ALF)**

Six sections were constructed at the LA-DOTD Accelerated Load facility (ALF) site to simulate base and subbase layers in pavement sections. These sections included: one ALF clayey silt soil, two cement stabilized soil, one lime-treated soil, one Calcium Sulfate Hemihydrates (Florolite), and one crushed limestone sections. Figure 3.5 describes the layout and profile of the six test section constructed at ALF site. The subgrade on which the sections were built was weak; therefore, it was compacted well and was treated with lime at some sections. The ALF clayey silt soil, the two cement-soil, and the lime treated sections were constructed from a soil available at the ALF site. This soil had 72% silt, 19% clay and PI=6. In addition, it was classified as A4, and CL-ML, according to the AASHTO classification system and USCS, respectively. The soil also had a maximum dry unit weight of 16.3 kN/m<sup>3</sup> (104 lb/ft<sup>3</sup>) and optimum moisture content of 18.5%, measured in the standard proctor test (Figure 3.6). The moisture content of the soil was taken directly before construction, which was in average 18.9%, similar to the optimum moisture content for this soil. No water was added during the construction. All sections were approximately 3 m × 3 m (10 ft×10 ft); except for the Florolite section which was 1.8 m×3 m (6 ft ×10 ft) (see Figure 3.7). The constructed layers in each

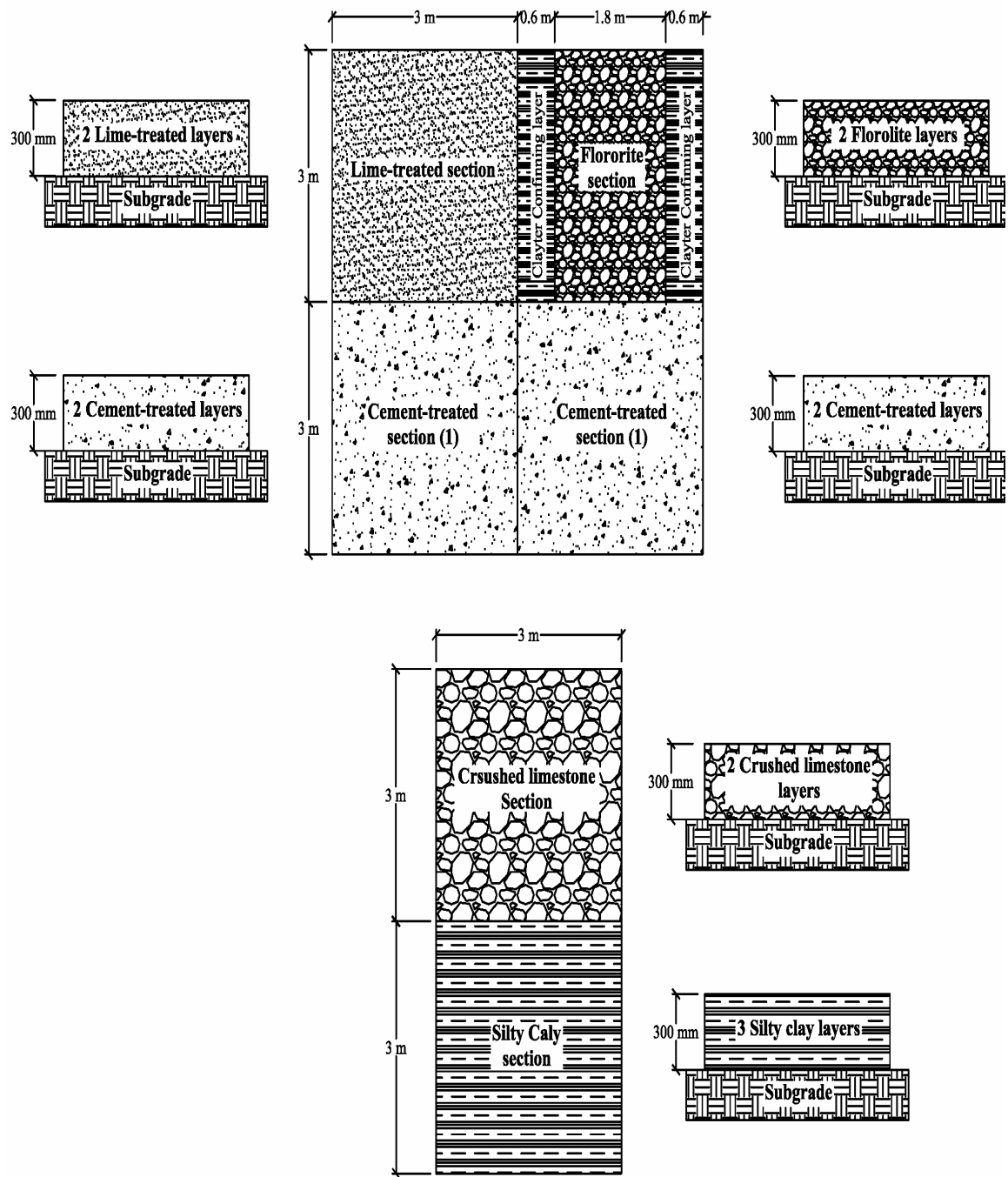


Figure 3.5 Layout and profile for sections constructed at ALF site

section had an overall thickness of 300 mm (12 inch) and were compacted using a sheet wheel roller and. The Geogauge and LFWD, DCP and dry unit weight measurements were conducted during the compaction process of each section, while FWD and PLT were conducted after the completion of compaction (Figure 3.8). In addition, all tests (except for the nuclear density gauge) were conducted with time on sections constructed from materials that gain strength with time (cement-soil, lime-treated soil, and Florolite sections). The following sections describe the tests.

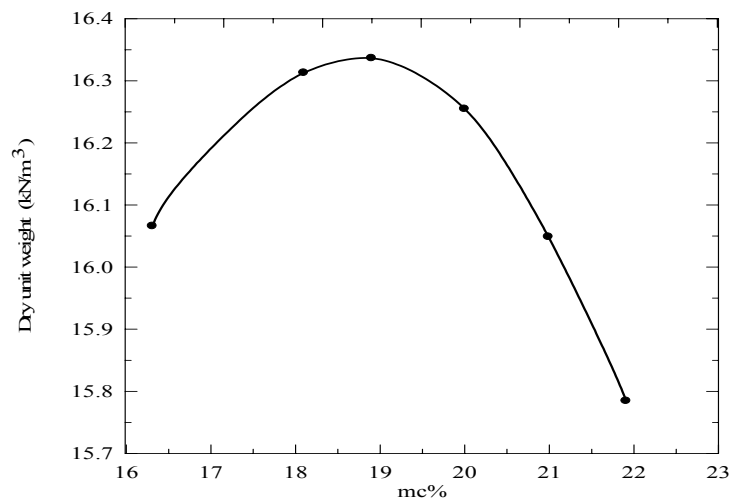


Figure 3.6 Proctor curve for ALF clayey silt soil

### 3.1.4.1 ALF Clayey Silt Soil Section

This section consisted of three sub-layers each of which had a thickness of 100 mm (4 inch). The first and second layer were compacted by four roller passes. However, the third layer was compacted by 6 roller passes. The Geogauge, LFWD and nuclear density tests were conducted at different passes during the construction, while the DCP, PLT, and FWD tests were conducted only after the sixth roller pass of the third sub-layer. Table 3.6 presents a summary of the results for the Geogauge, LFWD, and nuclear density gauge tests which were conducted both during and after constructing the section. The DCP test results are presented in Table 3.7.



Figure 3.7 Different sections constructed at ALF Site



Figure 3.8 Conducting tests on cement-soil and crushed lime stone sections at ALF site

Table 3.6 Geogauge, LFWD, and nuclear density gauge test results for ALF clayey silt section

Sub-layer	Pass No.	E <sub>G</sub> (MPa)	C <sub>V</sub> %	E <sub>LFWD</sub> (MPa)	C <sub>V</sub> %	γ <sub>d</sub> (kN/m <sup>3</sup> )	mc %
Subgrade		34.50	--	--	--	--	--
First sub-layer	1	42.87	4.81	6.892	15.1	15.0	17.7
	2	41.88	6.4	8.10	14.82	15.8	18.4
	4	48.45	8.9	6.9	13.9	15.9	18.4
Second sub-layer	1	54.81	1.69	23.64	13.3	--	--
	2	66.05	3.43	24.66	11.13	--	--
Third sub-layer	1	56.07	1.64	20.77	12.01	--	--
	4	65.44	2.64	25.76	9.04	--	--
	6	77.78	4.31	35.5	12.1	16.5	16.6

Table 3.7 Summary of DCP result for three layers after 6 passes

Layer	DCP-PR (mm/blow)
Constructed layers	29
Subgrade	12.38

#### 3.1.4.2 Cement-Soil Section (1)

This section consisted of two 150 mm (6 inch) sub-layers of cement treated soil constructed on top of the existing natural subgrade. Each layer was constructed by mixing the ALF wall soil with 5% of cement by volume using a tiller. After mixing and leveling the two sub-layers, they were compacted together for 6 passes wheel roller (see Figures 3.9). Geogauge, LFWD, and nuclear gauge test results for the different roller passes are presented in Table 3.8, while the Geogauge and LFWD test results with time are presented in Table 3.9. The DCP test results are summarized in Table 3.10 and 3.11.

#### 3.1.4.3 Cement- Soil Section (2)

This section was also constructed by the compaction of two sub-layers, 150 mm (6 inch) each. The two sub-layers were constructed in the same way and from the same material as the previous section. However, unlike the previous section the first sub-layer was compacted and tested before constructing the second sub-layer. The Geogauge,

LFWD, dry unit weight, and DCP results for tests conducted during and after compaction of this section are summarized in Tables 3.12 and 3.13. While Tables 3.14 and 3.15 summarizes results for tests conducted with time.



Figure 3.9 Construction of ALF sections

Table 3.8 Geogauge, LFWD, and nuclear gauge test results with number of passes for 3 cement-soil section (1)

Layer	Pass No.	$E_G$ (MPa)	$C_V$ %	$E_{LFWD}$ (MPa)	$C_V$ %	$\gamma_d$ (kN/m <sup>3</sup> )	mc %
Subgrade		26.52	--	--	--	--	--
Cement-soil	1	37.72	6.14	11.51	20.34	14.8	14.40
	2	56.77	7.61	15.31	15.44	15.0	15.30
	3	64.41	6.56	16.22	14.78	15.1	15.50
	4	67.14	11.39	18.11	13.97	15.6	15.70
	6	66.85	6.63	21.25	12.68	15.7	16.20

Table 3.9 Geogauge and LFWD test results with time for cement-soil section (1)

Days After Construction	$E_G$ (MPa)	$C_V$ %	$E_{LFWD}$ (MPa)	$C_V$ %
2	108.57	7.59	--	--
3	133.37	8.0	76.37	6.49
6	136.54	4.49	99.15	4.98
13	137.90	7.13	102.07	7.93
23	146.14	6.6	116.39	4.04
31	124.85	7.8	129.18	4.19
37	118.58	6.99	127.1	7.35

Table 3.10 DCP Test results with number of passes for cement-soil section (1)

Pass	Layer	DCP (mm/blow)
First	Constructed layer	43.50
	Subgrade	17.69
Sixth	Constructed layer	24.7
	Subgrade	21.64

Table 3.11 DCP test results with time for cement-soil section (1)

Days after construction	Layer	DCP (mm/blow)
2	Constructed layer	13.84
	Subgrade	17.22
6	Constructed layer	7.56
	Subgrade	21.33
13	Constructed layer	8.14
	Subgrade	14.12
23	Constructed layer	7.81
	Subgrade	13.69
31	Constructed layer	7.81
	Subgrade	16.88
37	Constructed layer	8.73
	Subgrade	13.31

Table 3.12 DCP test results with number of passes for cement-soil section (2)

Pass	Layer	DCP-PR (mm/blow)
Fifth	First layer	23.6
	Subgrade	22.17
Sixth	Second layer	15.40
	Subgrade	21.6

Table 3.13 Test results with number of passes for cement-soil section (2)

Sub-layer	Pass No.	$E_G$ (MPa)	$C_v$ %	$E_{LFWD}$ (MPa)	$C_v$ %	$\gamma_d$ ( $kN/m^3$ )	mc %
Subgrade		26.87	--	--	--	--	--
First Layer	1	44.02	2.45	--	--	--	--
	2	57.16	5.56	--	--	--	--
	4	61.65	6.06	--	--	--	--
	5	66.19	7.7	20.84	10.12	15.40	15.10
Second Layer	1	73.34	5.13	22.80	20.50	--	--
	2	79.93	3.37	30.32	15.2	--	--
	4	84.10	5.79	35.87	14.7	--	--
	6	97.23	3.91	42.09	10.37	15.20	13.500

Table 3.14 Geogauge and LFWD test results with time for cement-soil section (2)

Days After Construction	$E_G$ (MPa)	$C_V$ %	$E_{LFWD}$ (MPa)	$C_V$ %
3	194.39	6.46	228.48	2.4
10	196.70	6.43	189.1	6.1
20	186.87	6.11	184.2	5.96
28	160.09	3.86	--	--
34	150.85	6.63	169.72	5.77

Table 3.15 DCP test results with time for cement-soil section (2)

Days after construction	Layer	DCP-PR (mm/blow)
3	Constructed layer	5.69
	Subgrade	19.93
10	Constructed layer	5.42
	Subgrade	13.17
20	Constructed layer	6.00
	Subgrade	12.95
28	Constructed layer	6.1
	Subgrade	18.2
34	Constructed layer	6.89
	Subgrade	19.56

#### 3.1.4.4 Lime Treated Soil Section

This section was constructed by compacting two 150 mm (6 inch) sub-layers of lime-treated soil. In each sub-layer the ALF clayey silt soil was mixed with 8.5% lime by volume using a tiller. This section was constructed following the procedure in previous cement soil section (2). Table 3.16 and 3.17 summarizes results of test conducted during construction of this section. While results for tests conducted with time are presented in Table 3.18 and 3.19.

Table 3.16 DCP test results with number of passes for lime treated soil section

Pass No.	Layer	DCP-PR (mm/blow)
Sixth	Constructed layer	21.36
	Subgrade	17.76

Table 3.17 Test Geogauge, LFWD, and nuclear gauge test results with number of passes for lime treated soil section

Sub-layer	Pass No.	E <sub>G</sub> (MPa)	C <sub>V</sub> %	E <sub>LFWD</sub> (MPa)	C <sub>V</sub> %	γ <sub>d</sub> (kN/m <sup>3</sup> )	mc %
Subgrade		38.46	5.76	7.76	12.78	--	--
First Layer	2	72.896	4.7	--	--	--	--
	4	79.28	6.1	14.60	6.6	14.9	17.99
Second Layer	1	64.8	6.94	--	--	--	--
	2	79.66	6.08	--	--	--	--
	4	80.50	5.57	--	--	--	--
	6	83.3	4.03	30.02	12.47	15.2	16.2

Table 3.18 Geogauge, LFWD test results with time for lime treated soil section

Days After Construction	E <sub>G</sub> (MPa)	C <sub>V</sub> %	E <sub>LFWD</sub> (MPa)	C <sub>V</sub> %
3	113.86	3.33	83.15	5.83
20	82.8	0.5	42.44	10.5
28	101.87	3.0	--	--
34	99.42	5.65	54.50	14.87

Table 3.19 DCP test results with time for lime treated soil section

Days after construction	Layer	DCP-PR (mm/blow)
3	Constructed layer	15.42
	Subgrade	16.53
20	Constructed layer	17.7
	Subgrade	18.2
28	Constructed layer	16.63
	Subgrade	16.26
34	Constructed layer	16.63
	Subgrade	23.89

### 3.1.4.5 Crushed Limestone

This section consisted of two 150 mm (6 inch) sub-layers that were constructed by mixing crushed lime stone with 10% of ALF clayey silt soil by volume using a tiller to bring it within acceptable specification. The tested material had the gradation shown in Figure 3.10. The proctor test also showed that the maximum dry unit weight and the optimum moisture content for this material were 21.46 kN/m<sup>3</sup> (137.8 lb/ft<sup>3</sup>) and 5.94%, respectively. Summary of results for this section is presented in Tables 3.20 and 3.21.

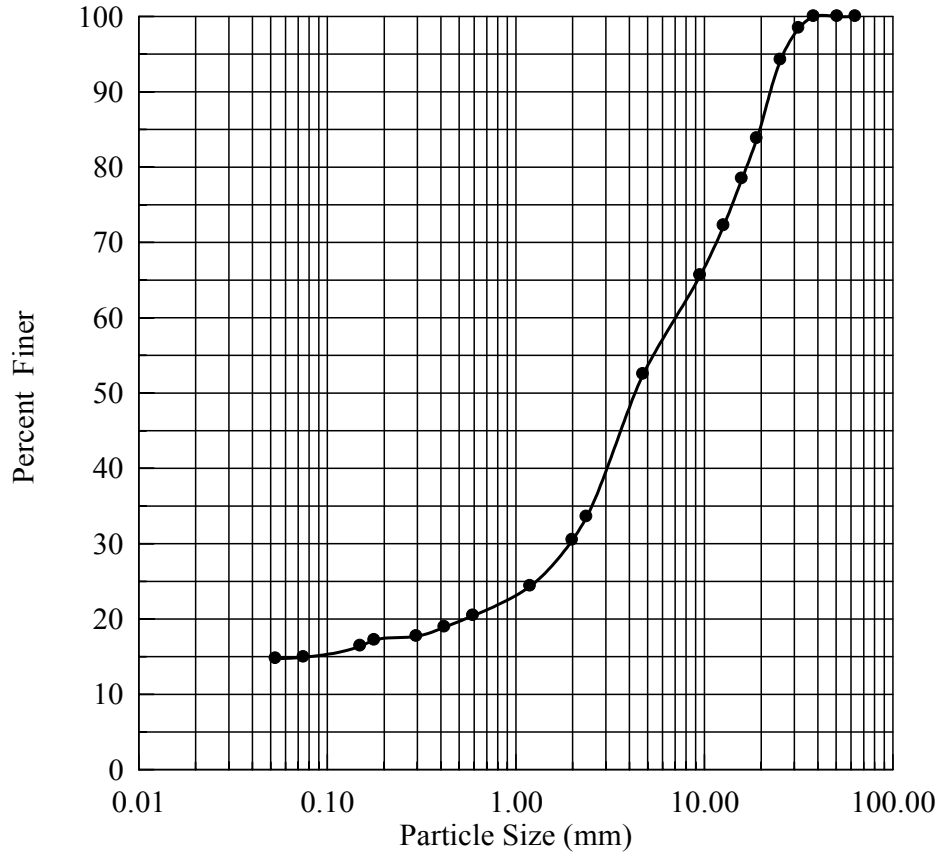


Figure 3.10 Gradation of tested material at the crushed limestone section

Table 3.20 Summary of test results for crushed limestone section

Sub-layer	Pass No.	$E_G$ (MPa)	$C_V$ %	$E_{LFWD}$ (MPa)	$C_V$ %	$\gamma_d$ ( $kN/m^3$ )	mc %
Subgrade	--	30.15	7.32	--	--	--	--
First Layer	2	57.65	1.7	23.33	12.65	--	--
	4	58.73	0.88	--	--	--	--
Second Layer	1	64.43	8.08	23.46	16.1	--	--
	2	72.11	5.47	45.35	17.21	--	--
	4	77.76	6.85	--	--	--	--
	6	91.78	3.9	81.47	10.9	19.2	7.5

Table 3.21 DCP results after construction of crushed limestone section

Layer	DCP-PR (mm/blow)
Constructed layer	12.1
Subgrade	15.13

### 3.1.4.6 Calcium Sulfate Hemihydrate (Florolite) Section

This section was also constructed by compacting two Florolite sub-layers. The Florolite is a chemical by-product of agriculture industry; it consists of 39.2 % Calcium Oxide, 51.15% Sulfur Trioxide, 0.6% Silicon dioxide, 0.75 % Phosphorous Pent oxide, 0.38 % Potassium, and 0.81 % Aluminum Oxide (Sorrento Companies Inc. DBA Louisiana Stone & Aggregates, 2003). The Florolite material used in this study has the gradation shown in Figure 3.11. The maximum dry unit weight and optimum moisture content were  $17.2 \text{ kN/m}^3$  ( $109.2 \text{ lb/ft}^3$ ) and 10.1%, respectively, as measured by the standard proctor test. This section had dimensions of  $1.8 \text{ m} \times 3 \text{ m}$  ( $6 \text{ ft} \times 10 \text{ ft}$ ).

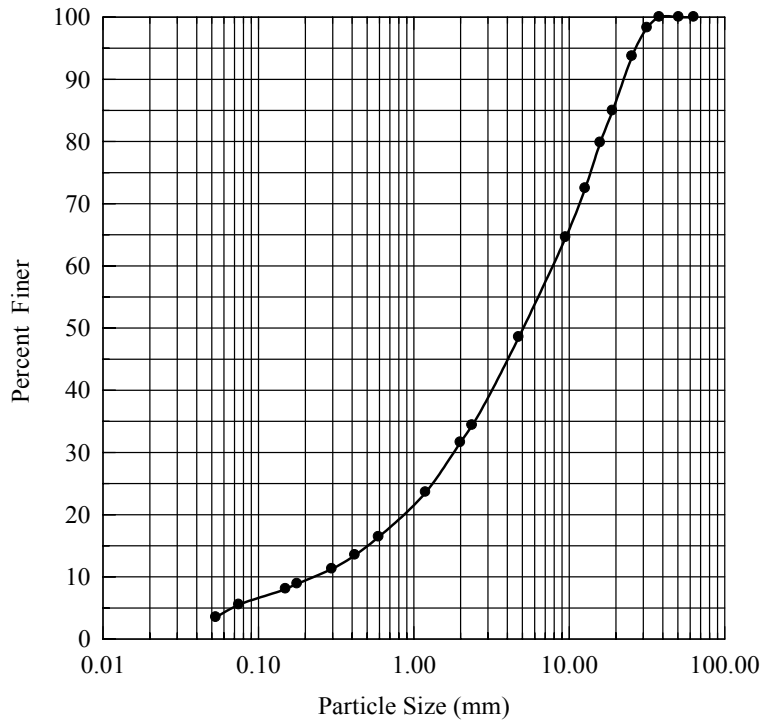


Figure 3.11 Gradation of Florolite

Table 3.22 DCP test results with number of passes for Florolite section

Pass No.	Layer	DCP-PR (mm/blow)
Sixth	Constructed layer	6.91
	Subgrade	14.3

Table 3.23 Summary of test results with number of passes for Florolite section

Sub-layer	Pass No.	E <sub>G</sub> (MPa)	C <sub>V</sub> %	E <sub>LFWD</sub> (MPa)	C <sub>V</sub> %	γ <sub>d</sub> (kN/m <sup>3</sup> )	mc %
Subgrade		36.7	--	--	--	--	--
First Layer	1	146.7	7.64	8.38	17.26	14.5	30.3
	2	150.55	.37	8.93	18.64	--	--
	4	136.92	3.73	33.01	14..71	--	--
Second Layer	1	186.69	3.03	--	--	--	--
	4	212.45	3.03	105.6	3.45	14.9	30.6

Table 3.24 Test results with time for Florolite section

Days After Construction	E <sub>G</sub> (MPa)	C <sub>V</sub> %	E <sub>LFWD</sub> (MPa)	C <sub>V</sub> %
	MPa	--	MPa	--
1	294.72	--	214.55	--
5	394.23	1.7	249.43	4.06
12	348.57	5.5	228.34	5.05
22	335.35	--	224.92	--
30	312.92	7.4	226.43	2.97
36	334.46	4.51	238.02	3.3

Table 3.25 DCP test results with time for Florolite section

Days after construction	Layer	DCP-PR (mm/blow)
5	Constructed layer	5.52
	Subgrade	10.89
12	Constructed layer	5.73
	Subgrade	10.3
22	Constructed layer	5.91
	Subgrade	10.4
29	Constructed layer	6.64
	Subgrade	11.3
36	Constructed layer	6.48
	Subgrade	11.41

### 3.1.4.7 Trench Sections

Trench sections were also built at the ALF site as a joint effort with another project for controlling trench backfill construction. For this purpose, three trenches excavated in the ground with the dimensions of 1.3×5×1 m (4×15×3 ft) (see Figure 3.12). Each trench consisted of three layers, each of which has a thickness 300 mm (12

inch). Each trench was divided into three equal sections compacted at different compaction effort: light, moderate, and heavy. The light compaction was achieved by one compaction pass using a vibratory plate compactor (Wacker Packer, Model Number WP1550 AW, 200 lb); the medium compaction was achieved by four compaction passes using the vibratory plate compactor; while the heavy compaction was achieved by four compaction passes using a Wacker Packer compactor (Model BS45Y 53 kg, 117lb) in addition to four vibratory plate compaction passes (Figure 3.14). Figure 3.13 presents the layout and profile of the tested trenches.



Figure 3.12 Construction of trenches at ALF site

After constructing each layer, Geogauge, LFWD, DCP, and dry unit weight measurements were taken for each section (see Figure 3.15). While the PLT and FWD tests were conducted only after the completions of compaction of the top layer. The first trench was constructed from crushed limestone that was classified as A1-a, and GP-GM, according to the AASHTO classification system and USCS, respectively, and had the gradation shown in Figure 3.16. The optimum moisture content and the maximum dry unit weight were 6.2% and  $21.37 \text{ kN/m}^3$  ( $135.95 \text{ lb/ft}^3$ ), respectively.

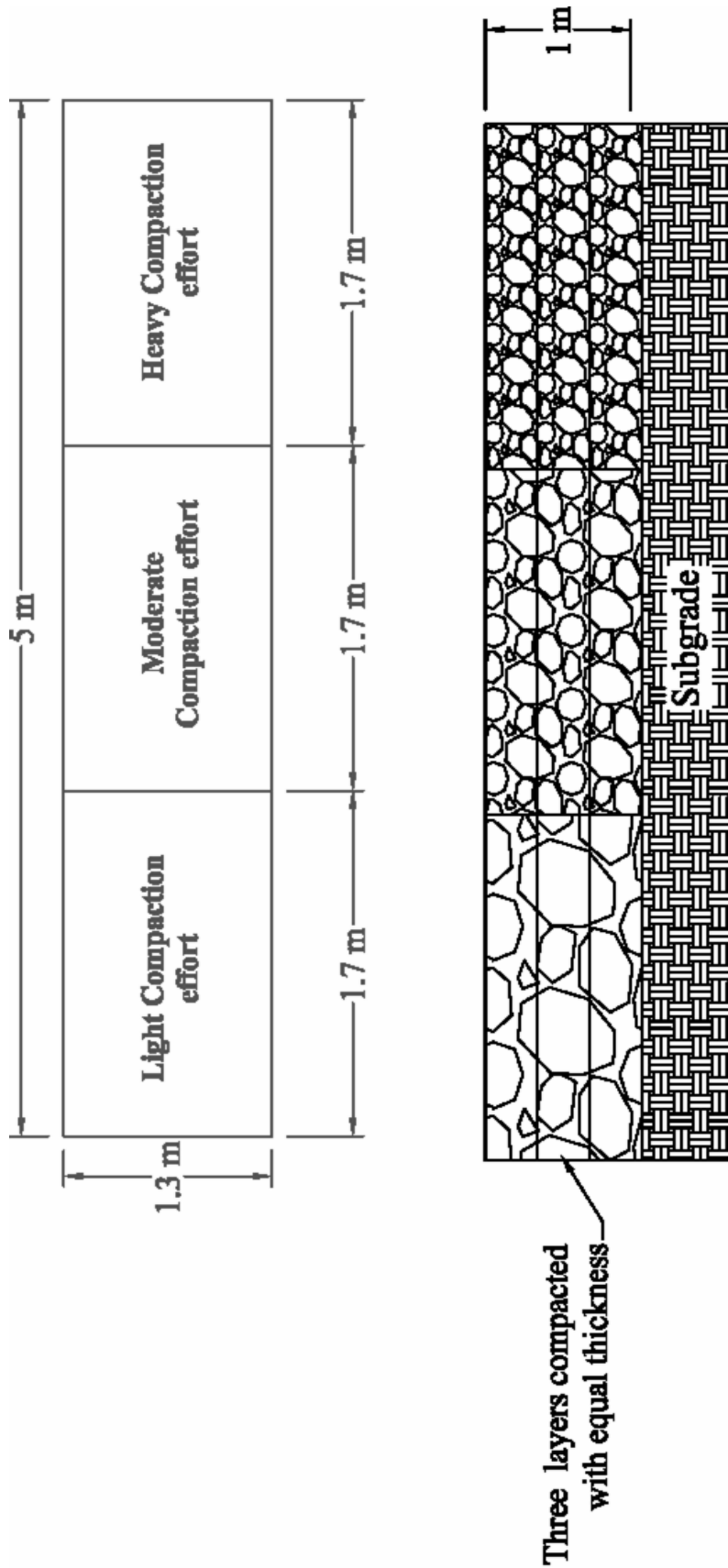


Figure 3.13 Typical cross-section for constructed trenches



Figure 3.14 Compaction of trenches at ALF site



Figure 3.15 Testing RAP and sand trenches at ALF site

The second trench was constructed from sand that was classified as A-1-b, and SP according to the AASHTO classification system and USCS, respectively, and has the gradation shown in Figure 3.17. The sand also has a maximum dry unit weight of  $16.8 \text{ kN/m}^3$  ( $107.86 \text{ lb/ft}^3$ ) and an optimum moisture content of 4.2%, measured in the standard proctor test. The third trench was constructed from Recycled Asphalt Pavement (RAP). This material is the product of milling the asphalt pavement of an existing roadway. The RAP material was classified as A-1-a, and GP, according to the AASHTO classification system and USCS, respectively. The gradation of RAP material used is shown in Figure 3.18. The RAP also has a maximum dry unit weight of  $18.41 \text{ kN/m}^3$  ( $117.1 \text{ lb/ft}^3$ ) and an optimum moisture content of 8.6% as measured in the standard

proctor test. Tables 3.26 through 3.28 present a summary for all in-situ measurements taken at each trench.

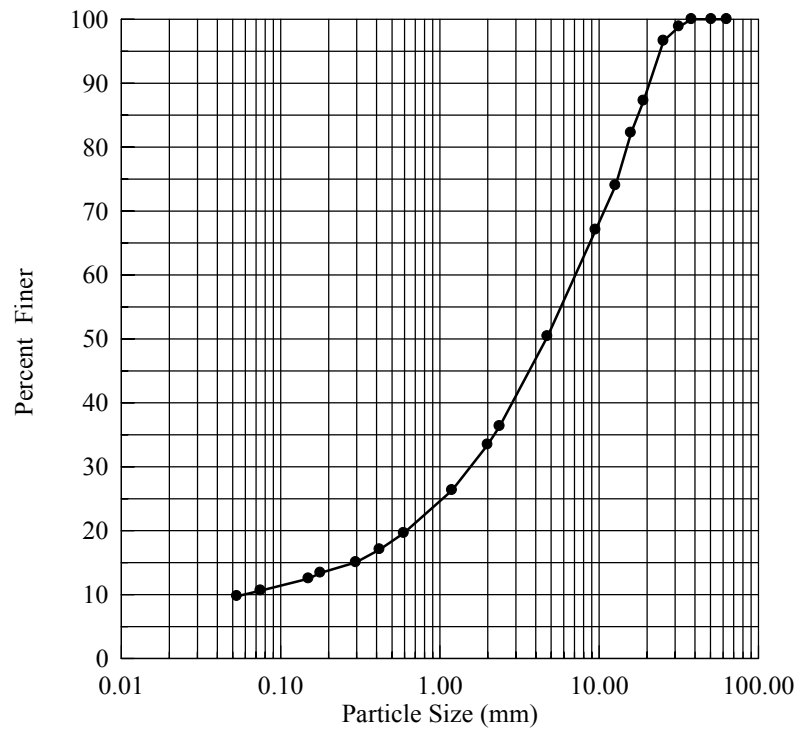


Figure 3.16 Gradation of crushed limestone

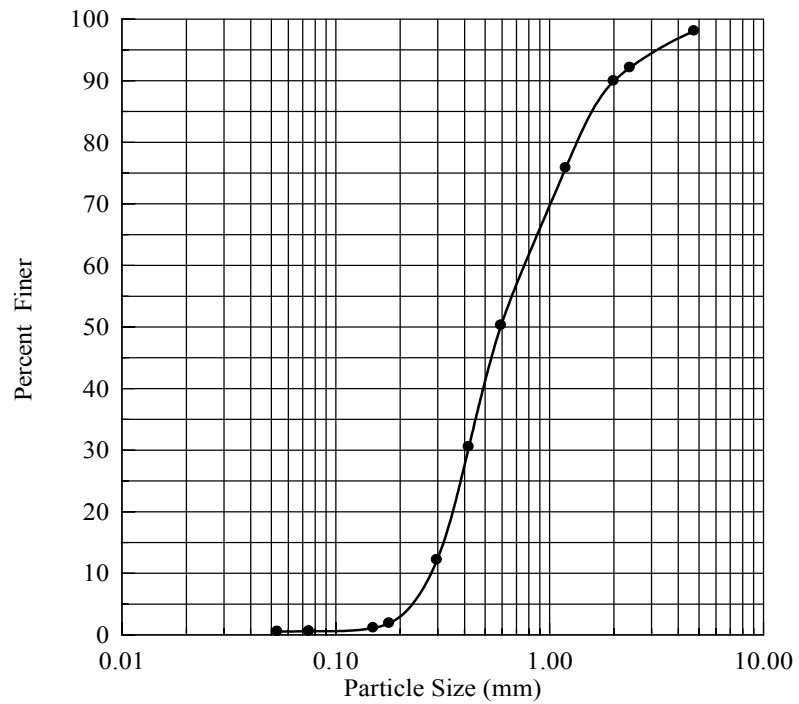


Figure 3.17 Gradation of sand

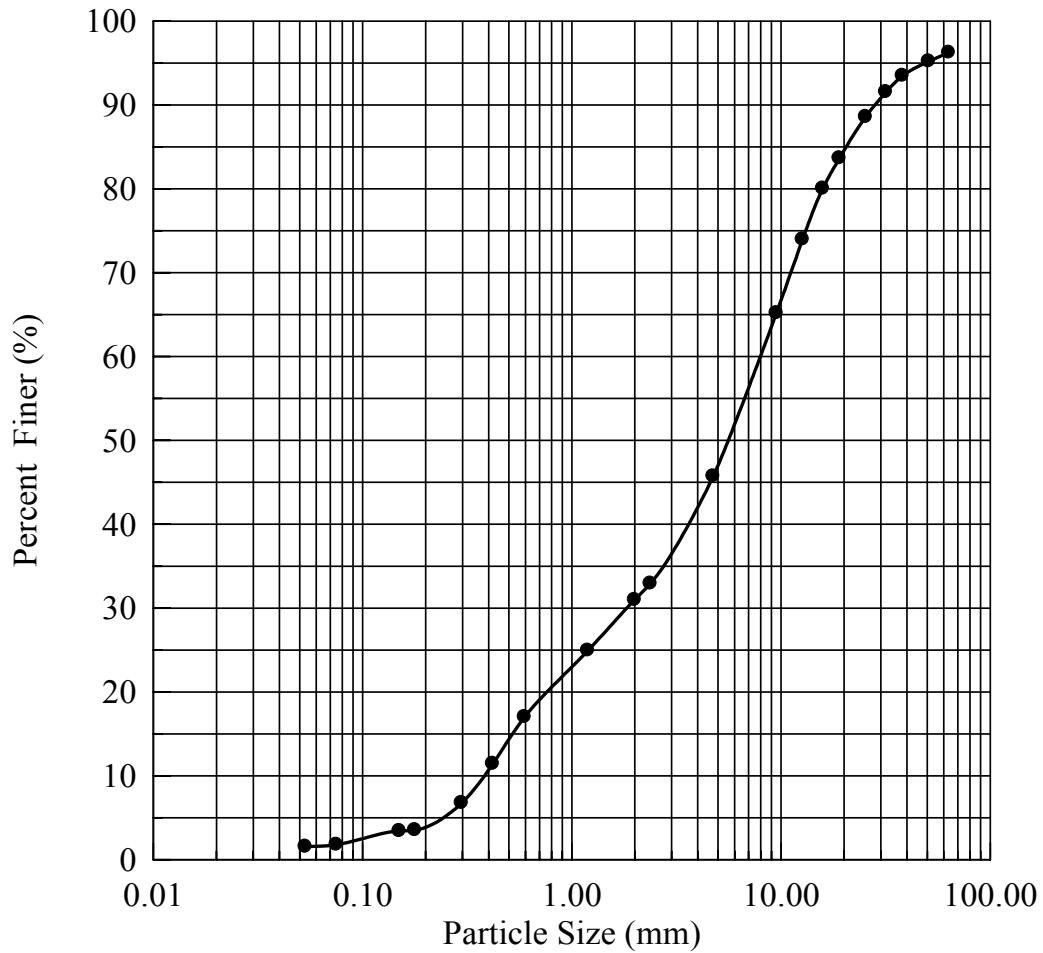


Figure 3.18 Gradation of RAP

Table 3.26 Test results for crushed lime stone trench

Layer	Compaction	$E_G$ (MPa)	$C_V$ %	$E_{LFWD}$ (MPa)	$C_V$ %	DCP-PR (mm/blow)	$\gamma_d$ (kN/m <sup>3</sup> )	mc %
First Layer	light	-	--	7.60	--	45.9	--	--
	Moderate	68.00	--	24.40	--	26.5	--	--
	Heavy	91.79	--	30.00	--	10.5	--	--
Second Layer	Light	57.4	2.75	34.5	13.5	43.8	18.7	4.80
	Moderate	72.7	4.09	49.0	12.44	23	19.0	5.10
	Heavy	99.6	4.78	79.0	2.06	9.52	21.8	5.20
Third layer	Light	51.93	2.75	30.25	13.51	37.8	18.9	4.90
	Moderate	73.06	4.04	57.28	9.26	23.1	19.1	5.20
	Heavy	95.6	3.78	82.69	3.81	9.8	21.1	5.60

Table 3.27 Test results for sand trench

Layer	Compaction	E <sub>G</sub> (MPa)	C <sub>V</sub> %	E <sub>LFWD</sub> (MPa)	C <sub>V</sub> %	DCP-PR (mm/blow)	γ <sub>d</sub> (kN/m <sup>3</sup> )	mc %
First layer	Light	67.83	--	--	--	68.5	16.4	4.00
	Moderate	77.00	--	--	--	27.2	16.6	3.20
	Heavy	66.39	--	--	--	18.1	16.0	5.50
Second Layer	Light	61.66	--	--	--	69.2	16.2	3.30
	Moderate	74.58	--	--	--	28.1	17.0	2.90
	Heavy	62.67	--	--	--	18.9	17.2	4.00
Third layer	Light	40.8	5.43	12.50	18.0	66.67	16.1	3.30
	Moderate	54.25	2.93	25.55	15.83	23.4	17.2	2.9
	Heavy	58.28	7.45	41.83	2.27	18.8	17.3	2.7

Table 3.28 Test results for RAP trench

Layer	Compaction	E <sub>G</sub> (MPa)	C <sub>V</sub> %	E <sub>LFWD</sub> (MPa)	C <sub>V</sub> %	DCP-PR (mm/blow)	γ <sub>d</sub> (kN/m <sup>3</sup> )	mc %
First layer	Light	55.8	6.08	9.2	22.7	54.2	15.2	11.9
	Moderate	86.2	--	21.0	13.88	20	15.7	13.6
	Heavy	96.0	1.3	25.2	14	14.67	16.0	14.3
Second Layer	Light	66.7	6.11	27.0	12.68	42.55	15.8	11.80
	Moderate	87.2	3.07	50.8	9.5	18.87	16.6	11.50
	Heavy	134.2	1.2	71.3	6.76	9.5	18.0	11.10
Third layer	Light	57.00	4.23	29.00	15.85	30.3	15.8	11.9
	Moderate	77.00	2.31	52.00	13.05	16.13	16.9	11.4
	Heavy	126.20	5.12	116.2	4.43	9.97	18.0	11.6

### 3.2 CBR Tests

CBR laboratory tests were also conducted on samples collected from field projects and test sections. All samples were prepared in accordance to ASTM D1883-99 without soaking them in order to correlate with the same field conditions. For unstabilized soils, all samples were prepared at the moisture content that was recorded in the field; on the other hand, for stabilized soil, samples were prepared at the moisture content at which the section was constructed. Samples of lime treated and cement stabilized soil were tested in the same sequence as they were tested in the field. Such that, if the field tests were conducted on these soil after one day of construction, then the

laboratory samples are prepared in CBR mold, placed in plastic bags (to isolate it from the surrounding environment) and then kept in LTRC humidity room for one day before testing. The United machine (Figure 3.19) of the LTRC soil lab was used to conduct the tests. This machine is fully automated with a piston that penetrates the prepared samples and has a load cell that records the resistance of the soil to penetration. The results of the CBR tests are presented in the next chapter in Table 5.2.



Figure 3.19 United machine used to conduct CBR tests

## CHAPTER FOUR

### ANALYSIS OF TEST RESULTS AT THE ALF SITE

#### 4.1 ALF Test Sections

The results of the ALF six test sections are presented in Tables 3.1 through 3.28. The variation of the Geogauge modulus with the number of passes during the construction of different test sections is shown in Figures 4.1 and 4.2. It is clear that for all tests the Geogauge stiffness modulus increases with the number of passes. For the lime treated soil and cement soil (1) sections in Figure 4.1, the Geogauge stiffness modulus approached an asymptote and hence became stable after four passes, which indicates that it reached the maximum stiffness modulus for this compactive effort. However, for the other sections in Figure 4.2 it was not clear whether the Geogauge modulus reached a peak value.

The Geogauge stiffness modulus variation with time for the four different sections is presented in Figure 4.3. It was observed that the Geogauge measurements increased with time for the first three days after construction; however, after that it decreased for all sections. The strength of these soils is expected to increase with time due to the chemical reactions that occur in cement and lime treated soils after mixing, mainly the pozzolanic reactions cement hydration and lime dehydrations, which can last for weeks after mixing. However, the two cement treated sections were covered and were not cured. Therefore, the lack of curing affected the strength gain with time for these sections since the strength gain of cement treated soil is controlled by the curing time, so if there was no curing, then the chemical reactions from which the strength is gained will not occur. In addition, the lack of curing resulted in shrinkage cracks which had affected significantly the results of the Geogauge tests and hence reduced the stiffness modulus.

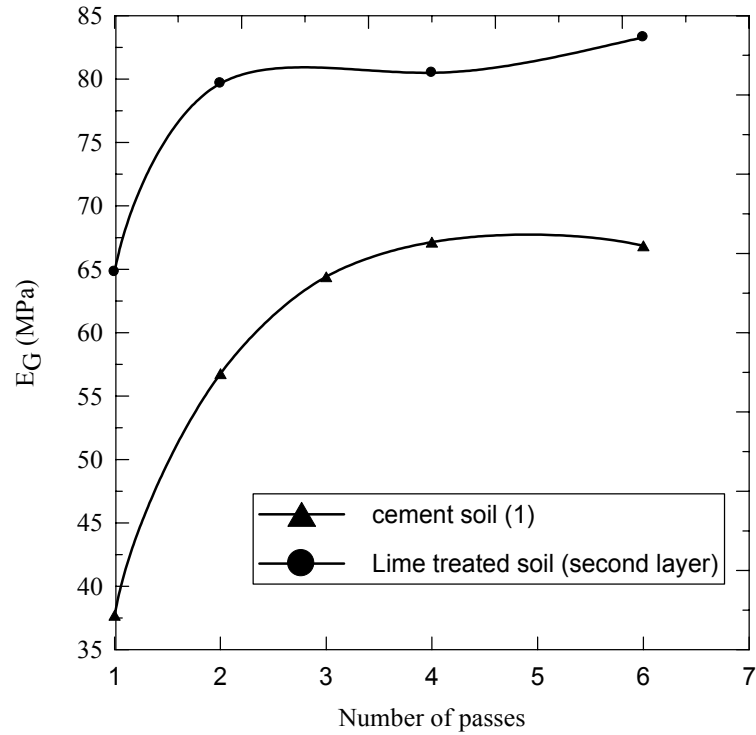


Figure 4.1 Geogauge modulus variation with number of passes

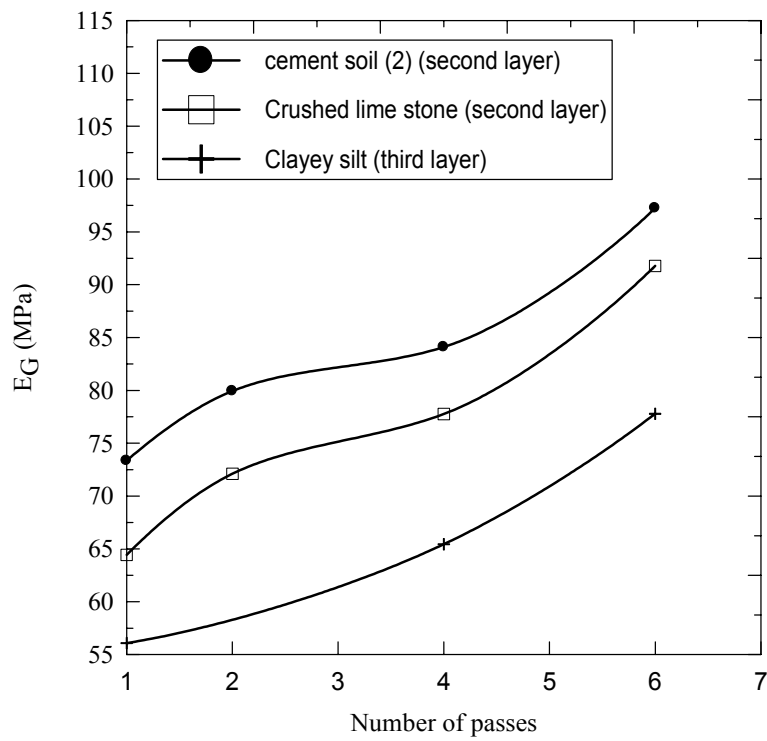


Figure 4.2 Geogauge modulus variation with number of passes

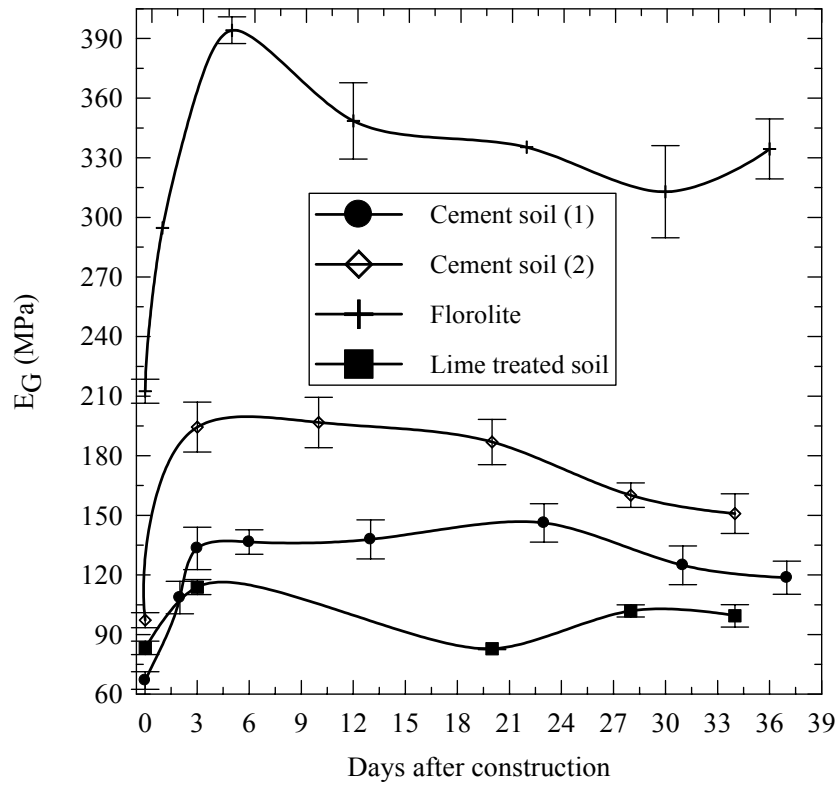


Figure 4.3 Geogauge modulus variations with time

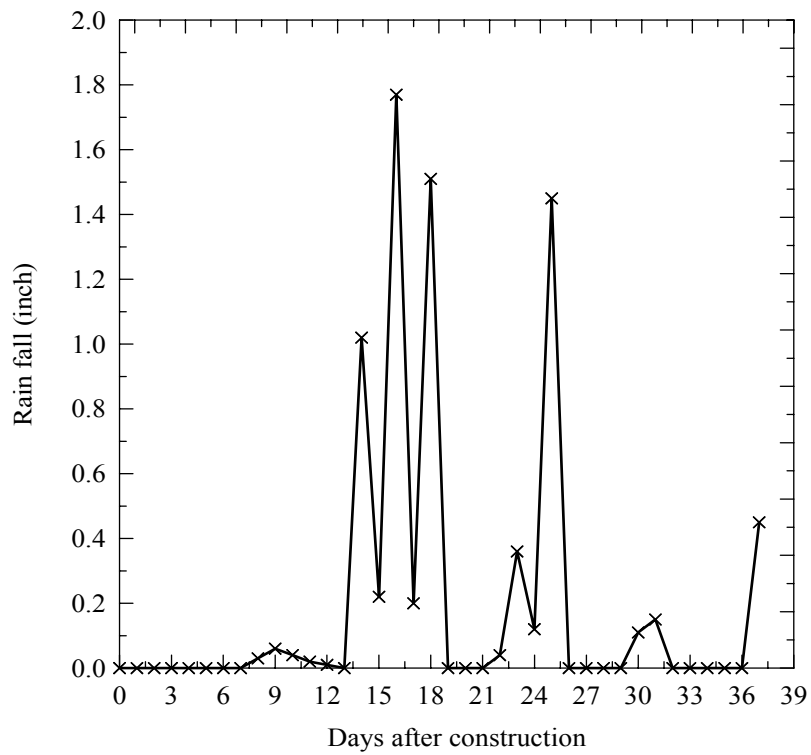


Figure 4.4 Rainfall record during testing time (Louisiana Office of State Climatology, 2003)

On the other hand, the lime treated soil and Florolite sections were not covered. Considering Figure 4.4, it can be noted that the Geogauge measurements for the lime section was influenced by the rainfall that occurred during the testing period, such that the Geogauge measurement that was taken during the rain period was significantly reduced. For the Florolite section, it was noted that this material has a high stiffness modulus and can be a strong supportive pavement layer. However, when considering Figure 4.4, it can be noticed that this material is very sensitive to moisture; such that in days that had rain the Geogauge measurement taken on Florolite section were lower than those taken on dry days. Consequently, the results suggest that the measurements on Florolite were influenced by the rain that occurred during the testing period. It should be indicated that the error in Geogauge measurement that is presented in Figure 4.3, shows that these measurements had relatively small variability, which suggests that variability of the Geogauge measurements did not significantly affect the stiffness modulus trend with time.

The variations of LFWD measurements with the number of passes for three different sections are presented in Figure 4.5 It can be noticed that the LFWD modulus increased with the number of passes. The variation of LFWD measurement with time for different sections is presented in Figure 4.6. It can be observed that for the cement soil section (1) the LFWD values increased with time until 33 days, after that it slightly decreased. However, for the other sections, shown in the same figure, the LFWD increased with the time until reaching a maximum value after three days, then it decreased. Again, the error bar for the LFWD measurements that is presented in Figure 4.6 shows that these measurements did not have much variability, which suggests that the

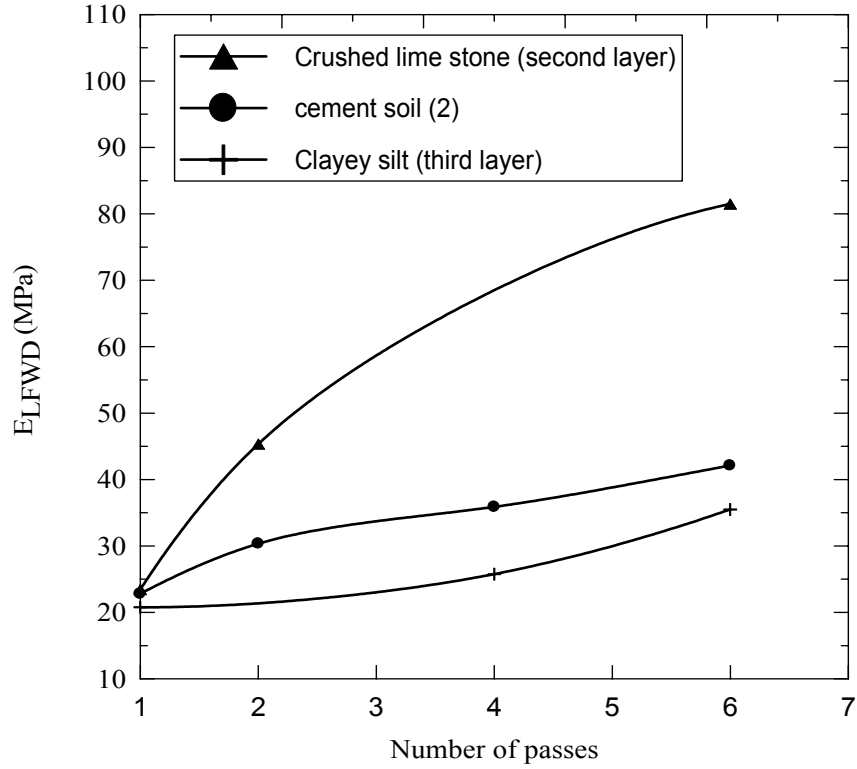


Figure 4.5 LFW modulus variation with number of passes

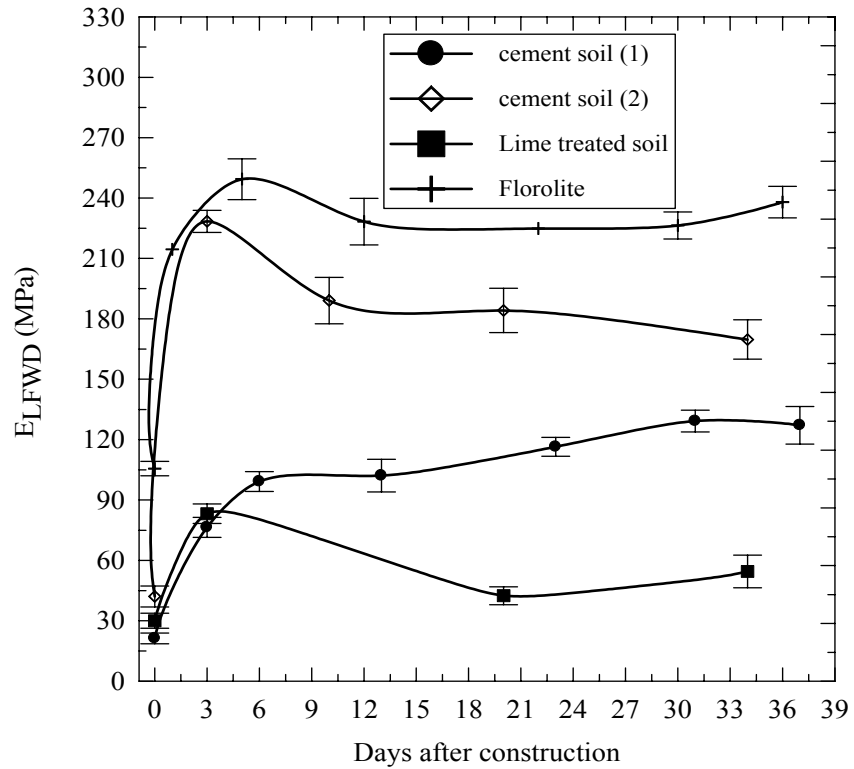


Figure 4.6 LFW modulus variation with time

variability of the test measurements did not have much influence on the stiffness modulus trend with time. By comparing the LFWD results in Figures 4.5 and 4.6 with the Geogauge results in Figures 4.1, 4.2, and 4.3 it can be seen that moduli obtained from both devices had similar trends for all test sections except for the cement treated sections, where differences were observed in the modulus trend with time. This shows that the shrinkage cracks which occurred in the cement treated sections had a more predominant effect on the Geogauge measurements than on the LFWD.

Figures 4.7 through 4.10 show the variation in DCP-PR profile with depth for four different sections immediately after construction and after about one month later. It is clear that for both cement treated soil sections, the DCP profile of the top 300 mm (12 inch) for tests conducted 37 days after construction have lower PR, compared to that for test conducted directly after construction. This indicates that both cement-soil sections have gained strength with time. On the other hand, DCP profiles for both the Florolite and lime treated sections show a slight reduction in PR between tests conducted directly after construction and those done after about one month. These results match those from the Geogauge and LFWD; therefore, the stiffness trend is same for all three test devices.

## **4.2 Trench Sections**

Figure 4.11 presents the dry unit weight and moisture content measurements for each section of the three trenches with respect to the corresponding standard Proctor curve. It can be noted that for the sand and the crushed limestone trenches, all moisture content measurements were at the dry side of the optimum moisture content obtained by the Proctor curve for each material. While for the RAP sections all moisture content measurements were wet of optimum.

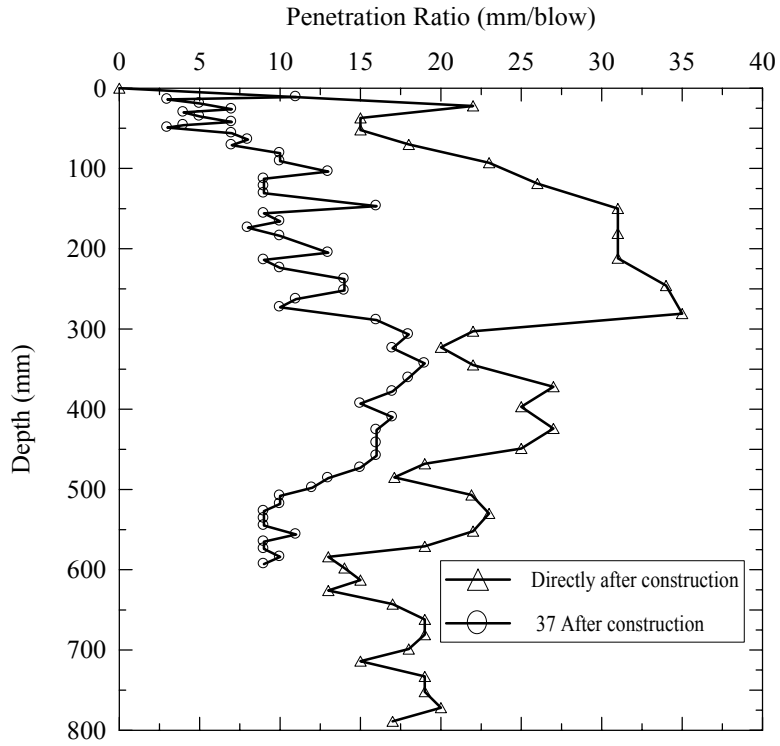


Figure 4.7 DCP-PR with time for cement soil section (1)

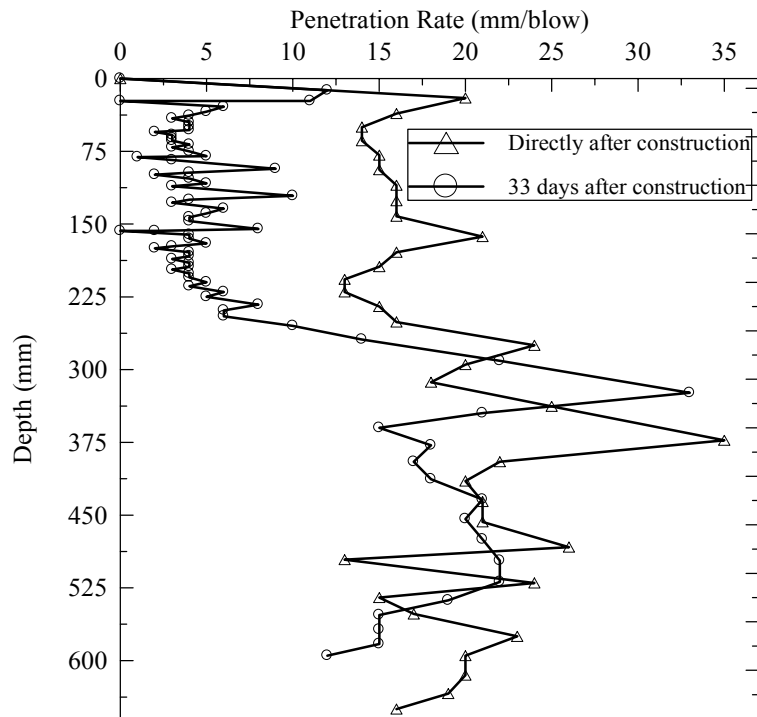


Figure 4.8 DCP-PR with time for cement soil section (2)

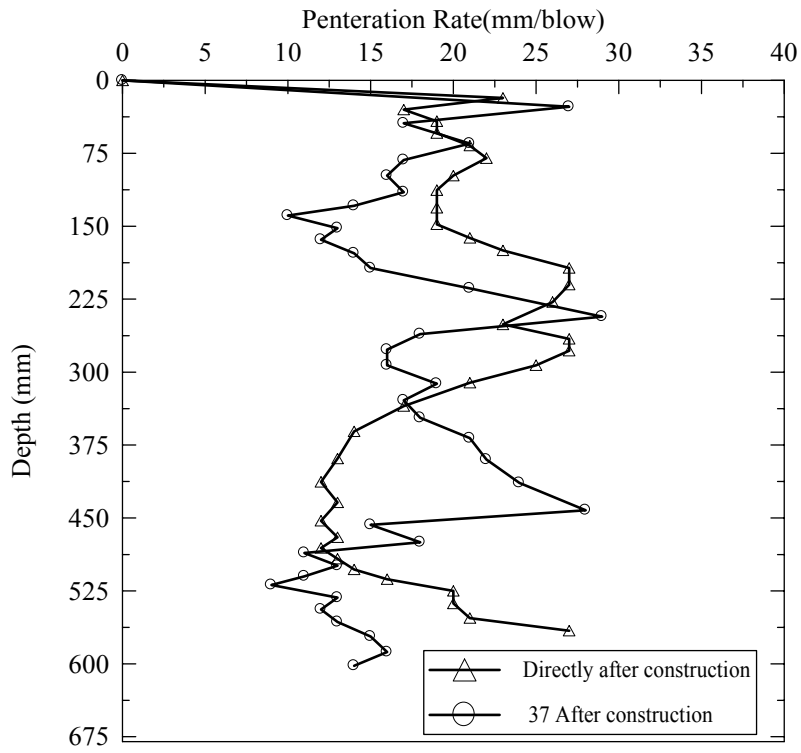


Figure 4.9 DCP-PR with time for lime treated soil section

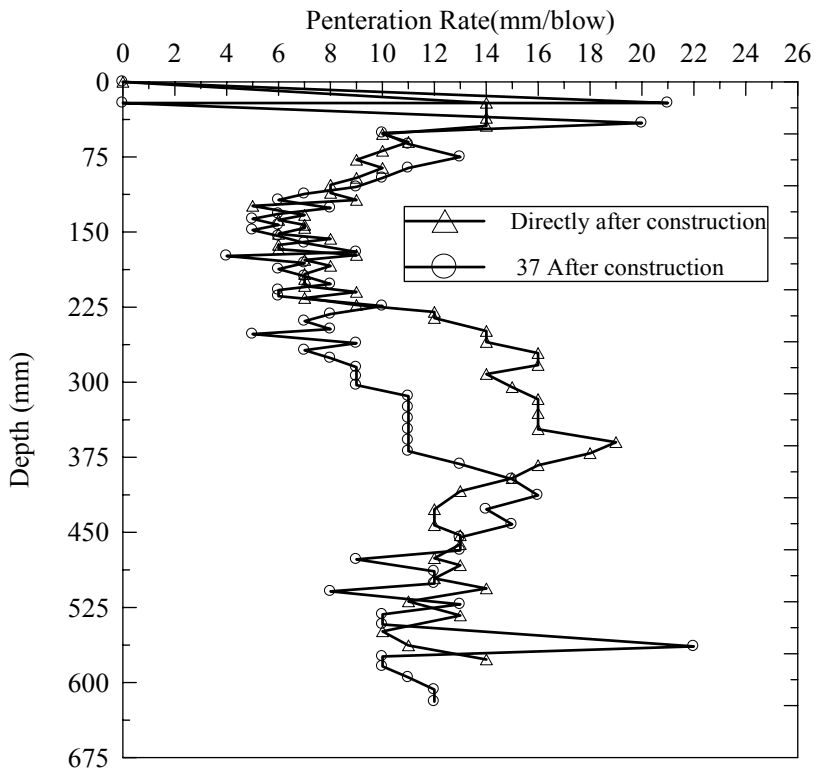


Figure 4.10 DCP-PR with time for Florolite section

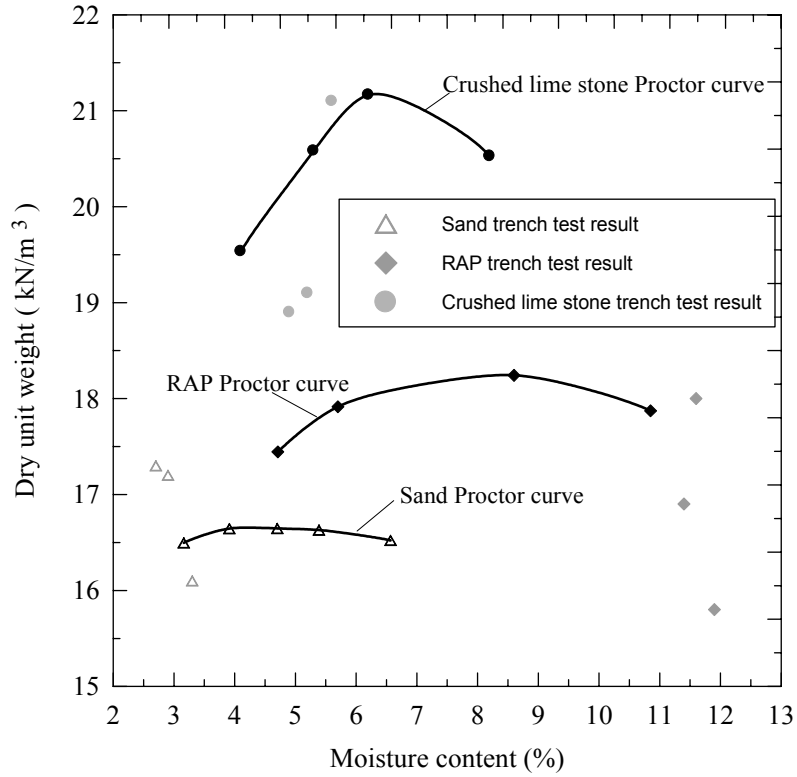


Figure 4.11 Trench test measurements with respect to Standard Proctor curves

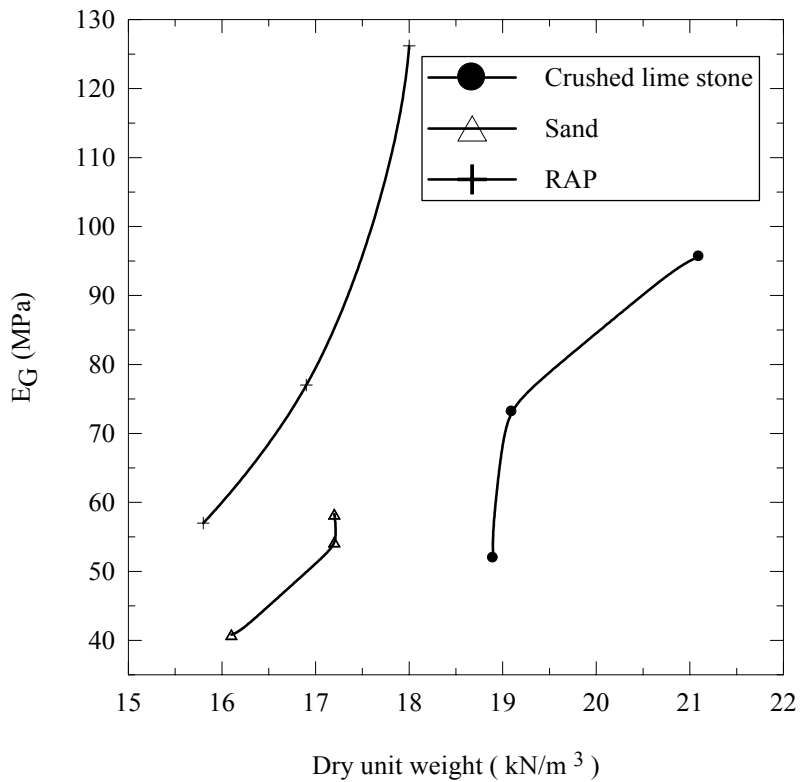


Figure 4.12 Geogauge modulus versus dry unit weight for different trenches

The variation of Geogauge modulus with dry unit weight for the three trenches constructed at the ALF site is presented in Figure 4.12. This figure shows that both the dry unit weight and Geogauge modulus increased with increasing the compactive effort as expected. Figure 4.13 shows the LFWD modulus variation with dry unit weight for the three trenches constructed at the ALF site. As for Geogauge, both the unit weight and LFWD modulus increased with increasing the compactive effort.

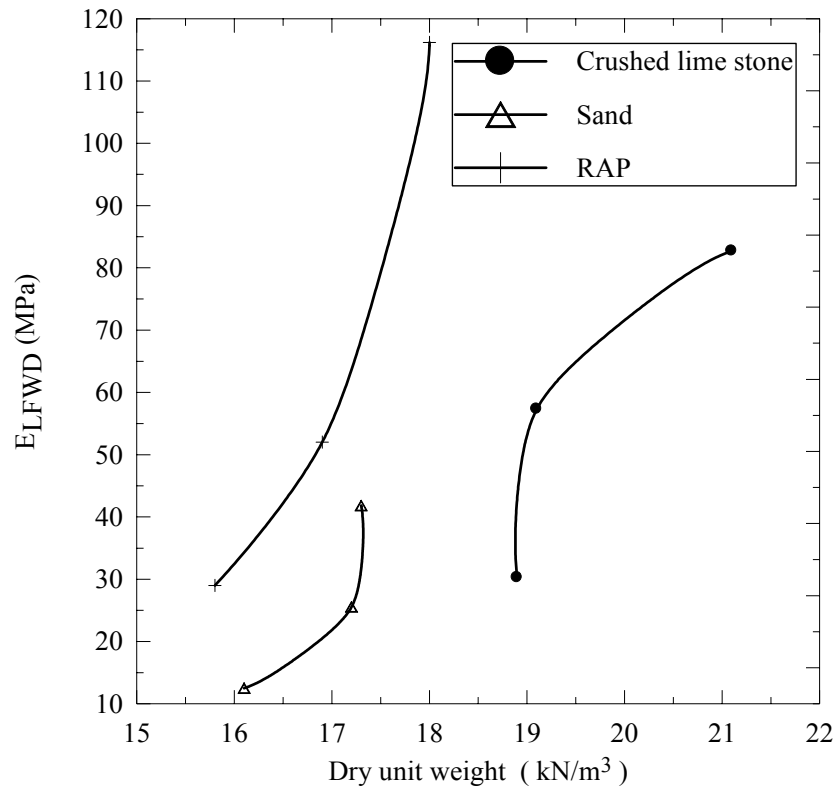


Figure 4.13 LFWD modulus versus dry unit weight for different trenches

These figures shows that both the LFWD and Geogauge stiffness moduli increased in same trend without any difference, which confirms the fact the stiffness increased with the increase in the dry unit weight in these tests. In addition, the results suggest that the stiffness moduli have relation with dry unit weight at the same moisture content, such that stiffness moduli increases with increasing dry density at the same

moisture content; however, this relation depends primarily on the tested material and its behavior.

The variation in DCP-PR profiles with depth for the different section in the three trenches is illustrated in Figures 4.14 through 4.16. In each figure the DCP-PR profile for. The highly and lightly compacted sections are plotted. It can be seen that the trench sections compaction effort, which indicates that the penetration ratio for a certain material is affected by the effort the material was compacted with; therefore, it can be related to the dry unit weight of this material. The DCP profiles for heavily compacted sections for all three trenches indicate that there is a sudden increase in DCP-PR value at depths greater than thickness of constructed trenches (3 ft), which indicates that the DCP was able to detect the existing weak natural soil layer underlying the constructed trenches.

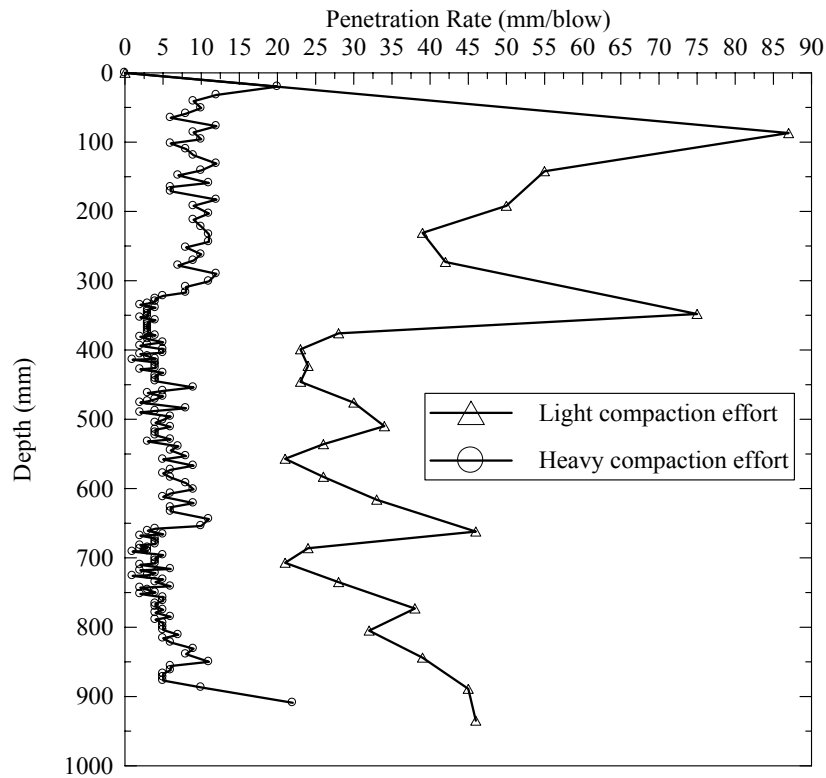


Figure 4.14 DCP-PR profiles for crushed lime stone trench sections

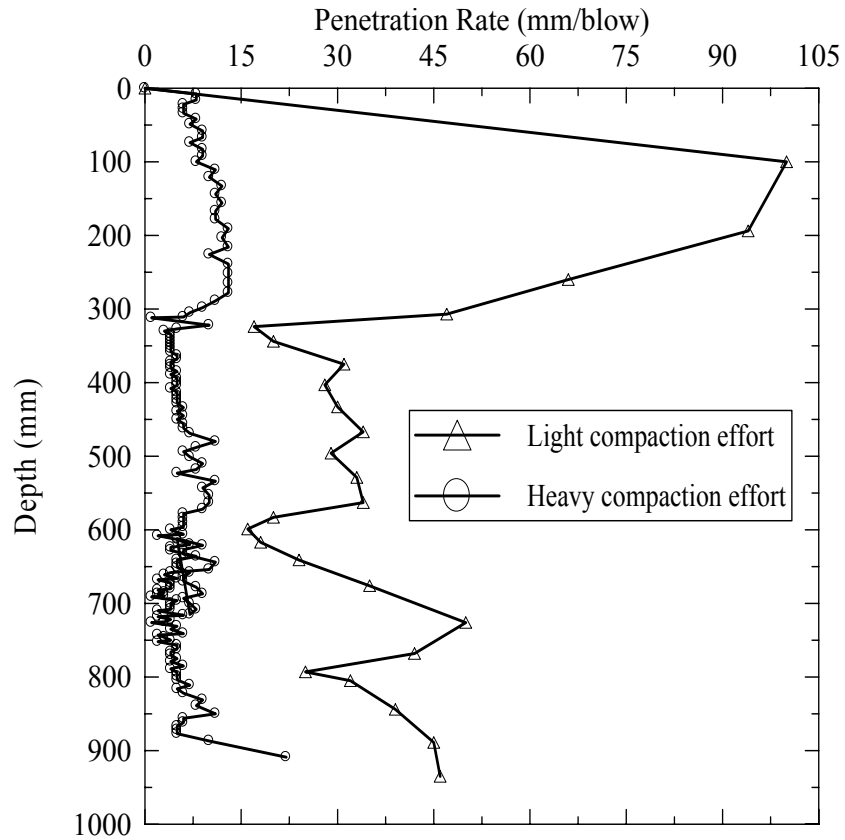


Figure 4.15 DCP-PR profiles For RAP trench sections

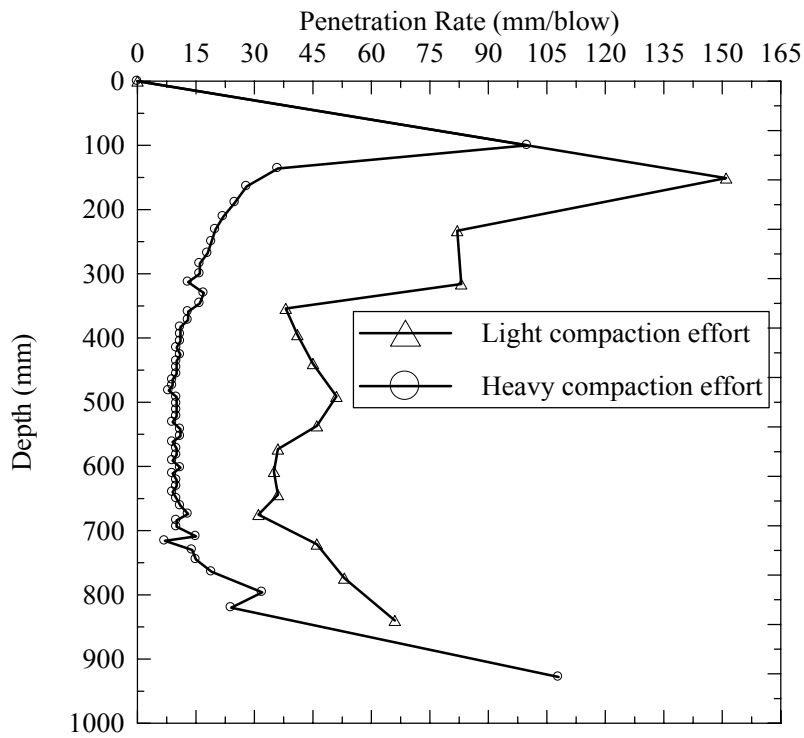


Figure 4.16 DCP-PR profiles for sand trench sections

Referring to Figure 4.16, it can be noted that the DCP profile for lightly compacted section had a sudden increase at depth of 300 mm (1 ft), which coincides with thickness of the first layer. These results do not only indicate that DCP-PR can be used as an indication of strength of material, but also demonstrates the ability of the DCP device to detect the thickness of the tested layer. Although the three layers in each trench section were evenly compacted; however, it was obvious that the DCP-PR values for the second and third layer for the three trenches were lower than that for the upper layer, which indicates the effect of confinement due to the overlaying layer for granular soils.

## **CHAPTER FIVE**

### **PARAMETRIC STUDY**

A series of tests were performed in two test boxes located at the LTRC Geosynthetic Engineering Research Lab (GERL) for the parametric study. The parametric study objective was to determine the influence zone of the Geogauge and LFWD.

#### **5.1 Experiment Setup**

The two test boxes in which the tests were conducted were 900 mm (36 inch) wide, 1824 mm (72 inch) long, and 900 mm (36 inch) deep (see Figure 5.1). A clay layer was placed and compacted at the bottom of the first box, while a Florolite layer was placed and compacted in the other box. A dynamic compactor was used in this compaction.

#### **5.2 Test Procedure**

For each experiment, a plastic cylindrical mold with 300 mm (12 inch) diameter was first placed at the center of the box. Then a 300 mm (12 inch) wide and 225 to 300 mm (9 to 12 inch) thick layer of the soil that will be tested was placed around this mold and compacted with a dynamic compactor. After that the plastic cylindrical mold was removed, which resulted in a cylindrical mold with a 300 mm (12 in.) diameter and 225 to 300 mm (9 to 12 inch) deep confined with an energy absorbing layer consisting of the tested soil (see Figure 5.2). This procedure was done to have a similar soil boundary condition effects.

To evaluate the influence depth, the tested material was placed in the cylindrical mold and compacted in 30 to 75 mm (1 to 3 inch) thick layers up to a 300 mm (12 inch)



Figure 5.1 Test box in which the experiments were conducted



Figure 5.2 The constructed mold within soil in test box

thickness. Each layer was well compacted with a standard hammer. Upon completion of compaction of each layer, Geogauge and LFWD measurements were made at the center of the compacted soil. It should be noted that in order to define clearly the zone of influence for the LFWD and Geogauge, stiff soil was build on top of soft soil, and soft soil was build on top of stiff soil in these experiments. For example, that Florolite was placed on top of the softer clay layer, while clay soil and sand were placed separately on top of the stiff Florolite layer.

### **5.3 Test Materials**

The experiments in this parametric study were conducted on the ALF clayey silt soil in addition to the sand and Florolite that were used in constructing the ALF trench backfill, which was described earlier in chapter 3.

### **5.4 Test Results**

The results of the tests conducted on Florolite, clayey silt soil, and sand to investigate the influence depth of Geogauge and LFWD are presented in Figures 5.3 through 5.7. In these figures the average Geogauge and LFWD moduli for the compacted soil layer are plotted against the thickness of this layer.

For tests conducted in the first box, where the stiff Florolite was build on top of the softer clay soil. The Geogauge and LFWD subsequent measurements increase with increasing depth, as shown in Figures 5.3 and 5.4, and gradually stabilizes at certain depth that corresponds to the influence depth of the investigated device. Figures 5.3 and 5.4 indicate that influence depth for the Geogauge and LFWD 190 mm (7.5 inch), and 267 mm (10.5 inch), respectively.

On the other hand, for tests conducted in the second box, in which ALF clayey silt soil and sand were built on top Florolite stiff layer, both the Geogauge and LFWD

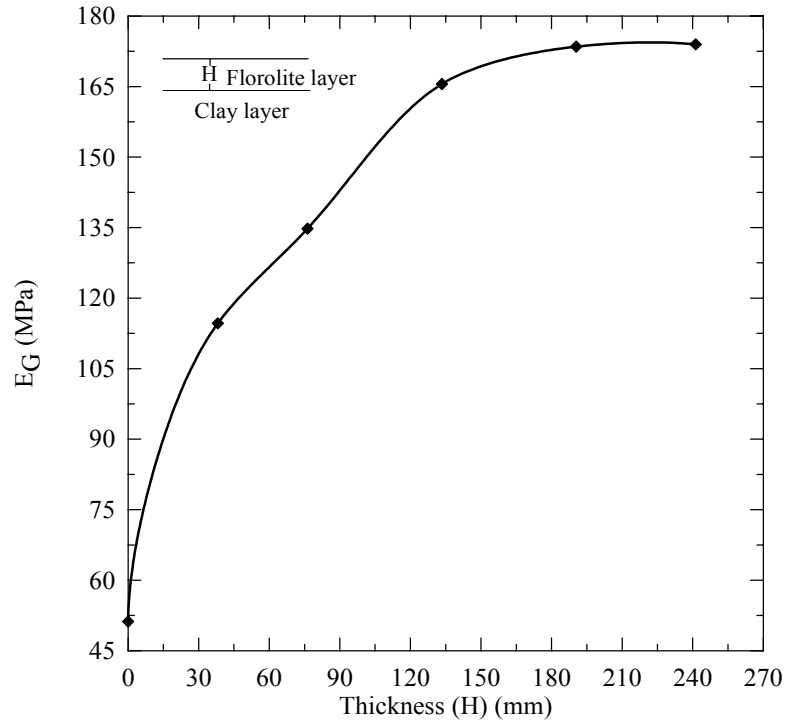


Figure 5.3 Geogauge stiffness modulus curve for Florolite layer vs. thickness

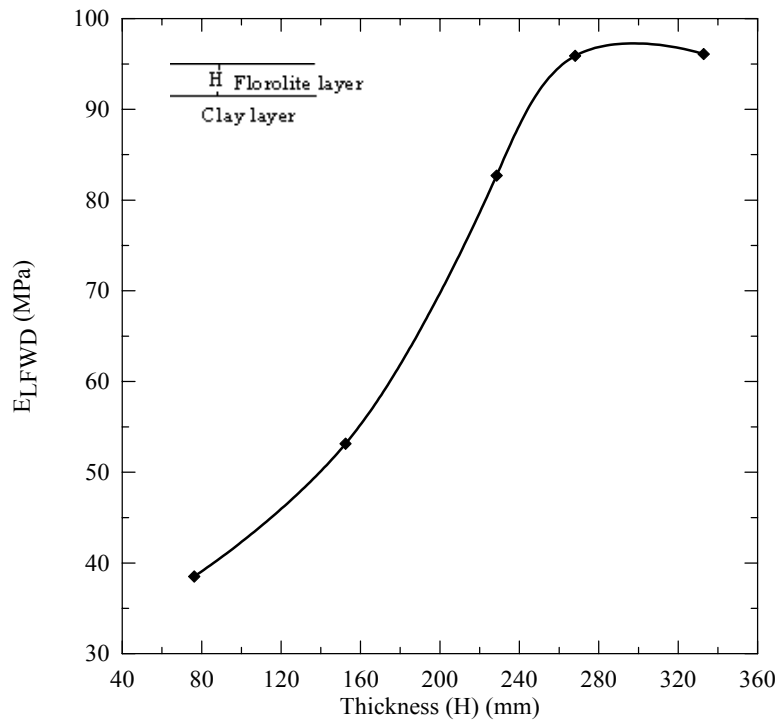


Figure 5.4 LFW D stiffness modulus curve for Florolite layer vs. thickness

stiffness moduli values decreased with increasing thickness till approached an asymptote at certain thickness which corresponds to the influence depth of these devices, as shown in Figure 5.5 through 5.7. For the Geogauge, this thickness was about 206 mm (8.1 inch) for the sand and the ALF soil. For the LFWD, the thickness at which the stiffness modulus curve stabilized was about 280 mm (11 inch).

The results of these test indicate, that in general, the influence depth for Geogauge ranges between 190 and 200 mm (7.5 and 8 inch), while it ranges between 267 and 280 mm (10.5 and 11 inch) for the LFWD. This result suggests that the influence zone of each device depends on the stiffness of the tested layer, such that the influence depth decreases with increasing this stiffness.

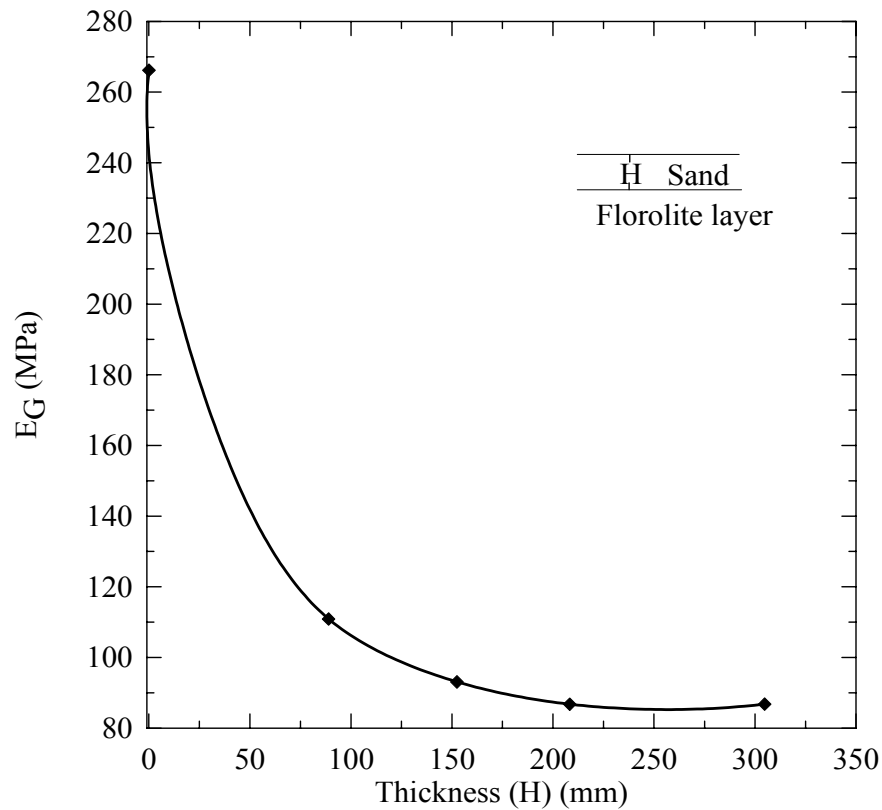


Figure 5.5 Geogauge stiffness modulus curve for sand layer vs. thickness

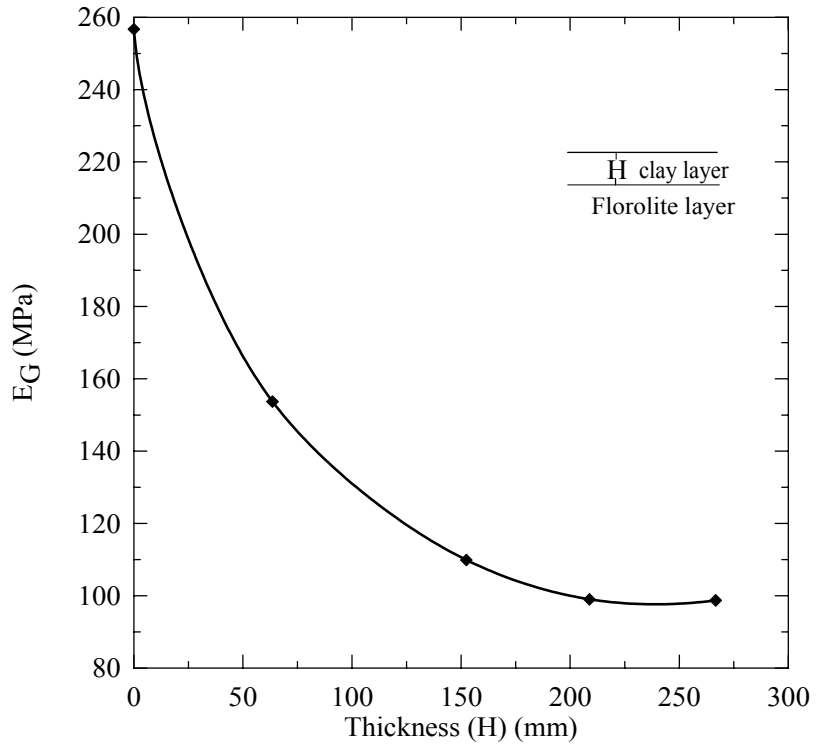


Figure 5.6 Geogauge stiffness modulus curve for clay layer vs. thickness

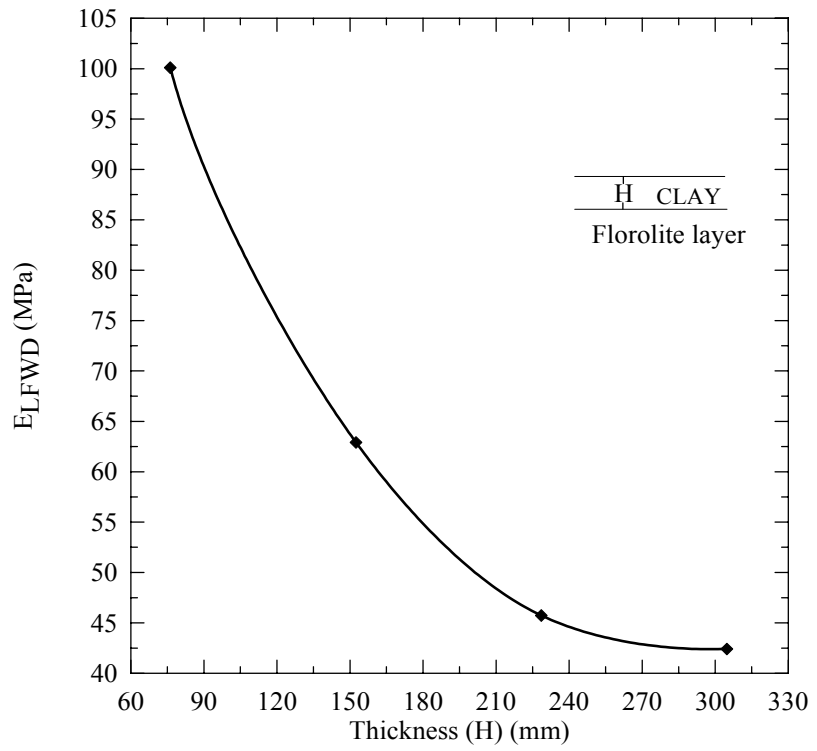


Figure 5.7 LFW D stiffness modulus curve for clay layer vs. thickness

## CHAPTER SIX

### EVALUATION OF GEOGAUGE, DCP, AND LFWD IN-SITU MEASUREMENTS

In this chapter the repeatability of Geogauge and LFWD devices is studied. In addition a comprehensive statistical analysis is conducted to correlate the measurements of the three devices (Geogauge, LFWD, and DCP) with measurements of two other well established in-situ devices; the PLT and the FWD. The Geogauge, LFWD, and DCP measurements are also correlated to the CBR tests conducted in the laboratory on the same material tested in the field. The correlations between the different measurements are developed based on routine regression analysis using the Statistical Analysis System (SAS) program.

#### 6.1 Repeatability

To assess the performance of any in-situ test device, the repeatability of this device measurement has to be considered. In this section the repeatability of both the Geogauge and LFWD devices are studied. As mentioned earlier, the Geogauge and LFWD values reported in this study for each test section represents the average of the five measurements taken at different spots within this test section. The repeatability of both devices is evaluated using the coefficient of variation,  $C_v$ , of the five measurements taken at each test section.

##### 6.1.1 Geogauge Stiffness Device

The coefficients of variation,  $C_v$ , for the Geogauge measurements of all tested sections (presented in the previous chapter) ranged from 0.37% to 11.39%, with most of the  $C_v$  values between 1% to 7%. The repeatability of the Geogauge was also evaluated in

the field tests conducted as part of FHWA study (SPR-2(212)) for the validation of Humboldt's suggested seating procedure for the Geogauge. These tests were conducted on cement stabilized soil section (2) in the ALF site after 60 days of construction. In these tests, three operators performed the tests using three different Geogauge devices that were verified using the procedure suggested in the Humboldt's manual for using the Geogauge. Tests were conducted at three different locations within the cement stabilized soil section (2) (Figure 6.1). Each of the three operators performed 6 sequential Geogauge measurements within the boundaries of each location for three times; hence, a total of 54 measurements were taken at each location.

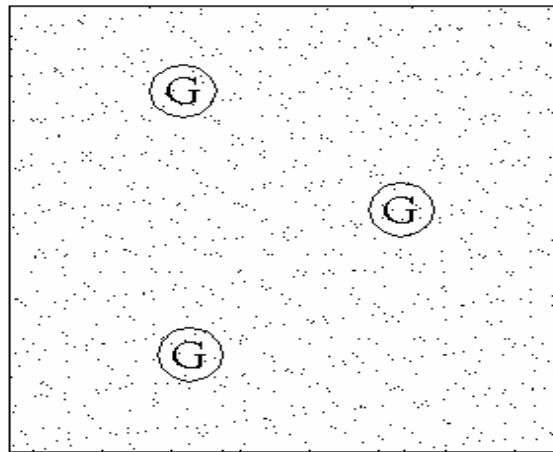


Figure 6.1 Layout of Geogauge measurements for seating-validation test

The mean stiffness, standard deviation and coefficient of variation were calculated for all measurements made from all Geogauges and all operators for each test location. The coefficient of variation for measurements made by all Geogauges ranged from 6.1% to 9.5%. In their report Humboldt's (2002) indicated that the precision demonstrated for these tests, using the suggested seating procedure, appears to be as good as or better than most geotechnical field measurements.

### 6.1.2 LFWD

The statistical analysis shows that the coefficients of variation,  $C_v$ , for LFWD measurements for the tested sections presented in the previous Chapter ranged from 2.1% to 28.1%, with most of the  $C_v$  values between 4.5% and 17.5%. Figure 6.2 shows the variation of the  $C_v$  with its corresponding average LFWD stiffness moduli. It can be noticed that there is a general trend for the points in this figure, such that the  $C_v$  value decreases with the increasing in the stiffness moduli. This observation was also noted during LFWD field tests, such that it was difficult to conduct the LFWD test on very weak material. On the other hand, the LFWD performance was enhanced for more compacted and stiff materials. Fleming (2001) has reached similar findings. The results of his study suggested that field tests conducted with LFWD and FWD had a greater variation on subgrade materials when compared to those conducted on stiffer sub-base and base course materials.

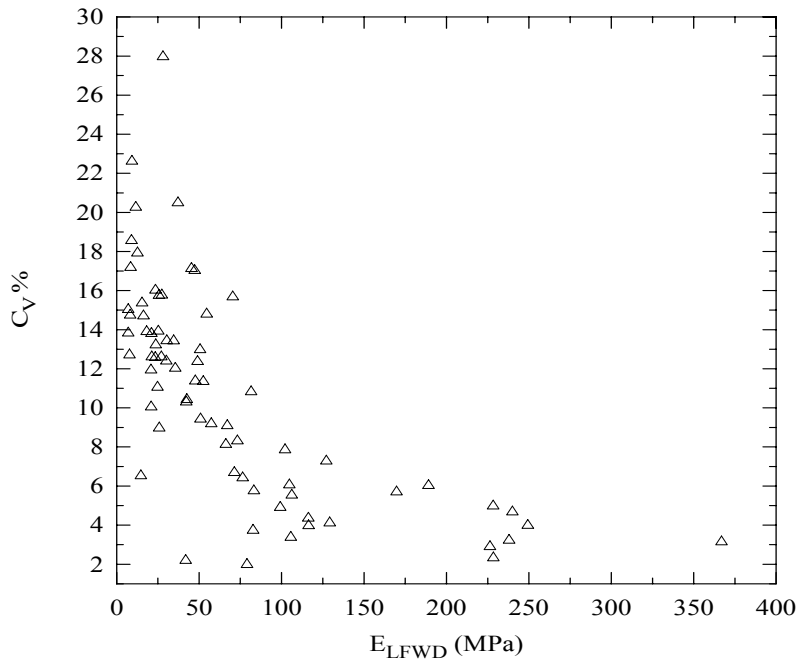


Figure 6.2  $C_v$  variation with LFWD modulus

## 6.2 Moduli from Plate Load Test

As in the case for other stress-strain tests, different elasticity moduli can be obtained from the plate load tests. Soil elasticity moduli can be defined as: (1) the initial tangent modulus; (2) the tangent modulus at a given stress level; (3) reloading and unloading modulus and; (4) the secant modulus at a given stress level. In this study, the initial tangent modulus was determined for all plate load tests. To determine the initial modulus ( $E_{PLT(i)}$ ) a line was drawn tangent to the initial segment of the stress-strain curve, and then an arbitrary point was chosen on this line, and stress and deflection corresponding to this point was used to determine the initial modulus. Figure 6.3 describes the deflection and stress used for determining  $E_{PLT(i)}$  from  $\delta_1$  and  $p$ . Another modulus was also determined for all plate load tests, which is similar to the reloading elastic modulus ( $E_{PLT(R2)}$ ) defined by the German code. This modulus was determined using the deflection under the second loading cycle of the plate, and the applied load by the end of that cycle ( $\delta_2$  and  $p$  in Figure 6.3).

## 6.3 Modulus and Zone of Influence of Different Devices

Since the field tests were performed on multi-layered systems, the influence zone of some tests may reached the underlying layers depending on the thickness of the tested layer. Therefore, the moduli obtained from different test devices does not reflect the true moduli for the tested layer, but rather reflect the composite modulus, which will result in erroneous results when comparing the moduli measured by these devices. There are many factors that affect the influence zone of each test; which include the stiffness of the tested layers, the magnitude and the way the stress is applied, the mode operation of each test, and the diameter of plate used in each test. To this problem the influence zone of each device was determined experimentally, and based on this, a multi-layered system

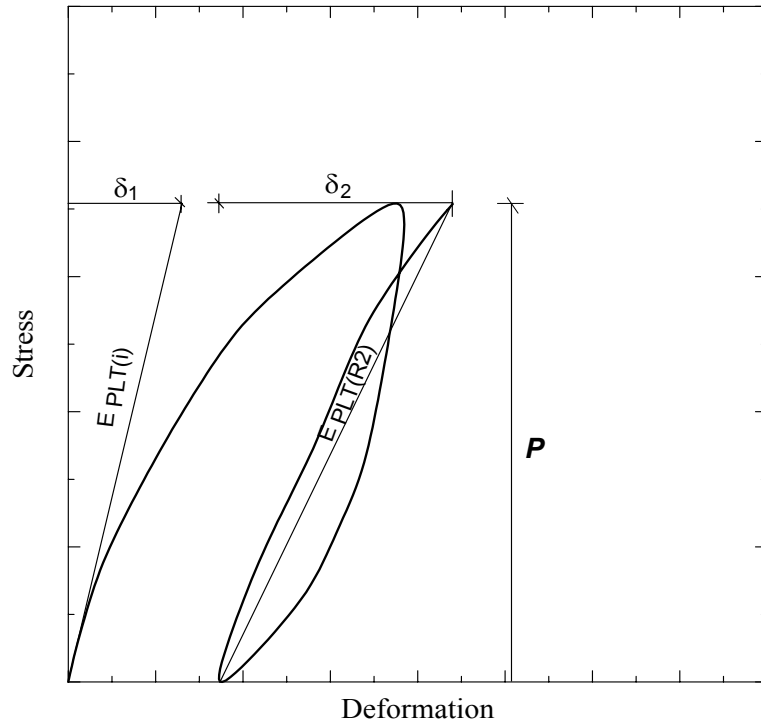


Figure 6.3 Definition of modulus from PLT

solution, usually used in pavement design, are performed to back calculate the moduli for the tested layers that have a thickness less than the influence depth of the test device.

For both Geogauge and LFWD a parametric study, which was presented in the previous chapter, was conducted in the test boxes in order to define the influence zone of these two test devices. The results of these experiments indicated that the influence zone for the Geogauge ranged between 190 mm and 200 mm (7.5 inch and 8 inch), which is less than thickness of the tested layer for all sections. On the other hand, the average influence depth of LFWD was between 267 mm and 290 mm (10.5 inch and 11 inch). For that the modulus LFWD modulus had to be back-calculated for tests with the tested layer thickness less than the determined influence depth. Similar study on plate load tests

showed that the depth of influence is approximately two times the plate diameter (Horhota, 1996). Therefore, a multi-layered systems solution was used to back calculate the PLT moduli.

### 6.3.1 Burmister Solution for Two Layer Systems

Burmister two-layer solution can be used to back-calculate the modulus for tests that have an influence zone greater than the thickness of the tested layer. In this solution, the total surface deflection for a two layer system can be obtained using equation 6.1 (Yoder and Witczak, 1975).

$$\delta = 1.18 \frac{pR}{E_2} F \quad (6.1)$$

Where

$\delta$  : total surface deflection of the circular plate with radius  $R$

$p$ : stress applied on the circular plate

$E_2$ : modulus of elasticity for the subgrade

$F$ : is a dimensionless factor depending on the ratio of the moduli of the subgrade ( $E_2$ ) and the tested (first) layer ( $E_1$ ), as well as to the thickness of the tested layer. This factor can be obtained using a design chart for vertical surface deflection (Yoder and Witczak, 1975).

Knowing the total deflection and the corresponding stress, and assuming that  $E_1/E_2$  ratio for the plate load test is the same as for the of  $E_1/E_2$  ratio for the FWD test,  $E_1$  can be back-calculated from the calculated  $E_2$ .

However, the main problem in this solution is its assumption that the tested material in each layer has Poisson's ratio of 0.5, which is different from Poisson's ratio for tested material which ranges between (0.25- 0.4).

### 6.3.2 Odmarks Method

Boussinesq's equations are used to determine stresses, strains and deflection in homogeneous, isotropic, and elastic (half space) media due to a point load. These equations were modified through mathematical integration to approximate the effects of a circular distributed load on a pavement surface. These modified equations for stresses, and displacement below the center of a circular loading plate are given in equations 6.2 and 6.3 (FHWA, 1994).

$$\sigma_z = \sigma_0 \left[ 1 - \frac{1}{\left( 1 + \left[ \frac{R}{Z} \right]^{\frac{2}{3}} \right)} \right] \quad (6.2)$$

$$\delta_z = \frac{(1+\nu)\sigma_0 R}{E} \left( \frac{1}{\sqrt{1 + \left[ \frac{Z}{R} \right]^2}} + (1-2\nu) \left( \sqrt{1 + \left[ \frac{Z}{R} \right]^2} - \left[ \frac{Z}{R} \right] \right) \right) \quad (6.3)$$

Where

$\sigma_z$  : Vertical stress at depth  $Z$  (MPa).

$\sigma_0$  : Stress at surface (MPa).

$Z$ : Depth below pavement surface (mm).

$\delta_z$  : Deflection at depth  $Z$  (mm).

However, these equations were developed for one layer systems. In order to apply them to multi-layer systems, the Method Equivalent Thickness (MET) which developed by Odemark (1949) can be used. In this method, a system consisting of layers with different stiffness is first transformed to an equivalent system where all the layers have

the same stiffness, such that the equations above can be used to predict the stresses and deflections in the layered system. For example, consider a two layered system with  $E_1$ , the stiffness modulus of the first layer, and  $E_2$ , the stiffness modulus of the second layer, when calculating the compression above the interface of the layers the system is treated as a half space with stiffness modulus value equal  $E_1$ . However, when calculating stresses and deflections at or below the interface, the layer above the interface is transformed, using the following equation, into an equivalent layer with stiffness modulus  $E_2$  (FHWA, 1994):

$$h_e = f \times h_1 \times \sqrt[3]{\frac{E_1}{E_2}} \quad (6.4)$$

Where

$h_e$ : the equivalent thickness of layer one

$h_1$ : thickness of layer one

$E_1$  and  $E_2$ : stiffness modulus of layer one and two, respectively.

$f$ : an adjustment factor, taken to be 0.9 for two layer system, and 1.0 for a multi layer system.

The MET method is used in this study to back-calculate the initial and the deformation modulus obtained from PLT tests conducted on multi layer systems. This method was also used to back-calculate the LFWD modulus when the tested layer had a thickness of 280 mm (11 inch) or less. Since the FWD is capable of testing multi-layer systems due to the presence of several geophone sensors, it was assumed in this back calculation process that the  $\frac{E_1}{E_2}$  ratio for FWD is the same as the  $\frac{E_1}{E_2}$  ratio for both the

PLT and LFWD.

Table 6.1 presents a summary of the results of Geogauge, DCP, LFWD, FWD, and PLT tests for all test sections that will be used in the proceeding regression analysis. A summary of all the CBR tests that were conducted in the laboratory and the corresponding Geogauge and LFWD modulus measurement taken in the field, is also presented in Table 6.2.

#### 6.4 Regression Analysis

The Statistical Analysis System (SAS) program is used to perform a comprehensive regression analysis on data presented in Tables 6.2 and 6.3, to find the best correlation between Geogauge, LFWD, and DCP measurements with FWD back-calculated resilient modulus,  $M_{FWD}$ , PLT initial and reloading moduli, and CBR value.

The objective of this regression analysis is to determine the parameters in the least square error models, which is used to predict the  $M_{FWD}$ , PLT moduli, and CBR value from Geogauge, LFWD, and DCP measurements, with their corresponding coefficient of determination,  $R^2$ , and standard error. Linear and non-linear regression models are examined in this analysis. In the linear regression models, the dependent variable is assumed to be a linear function of one or more independent variables plus an error introduced to account for all other factors, a typical form of a regression linear model is as follow:

$$Y_i = \beta_0 + \beta_1 x_{i1} + \dots + \beta_k x_{ik} \quad (6.5)$$

Where  $Y_i$  is the dependent variable, and  $x_{i1}, \dots, x_{ik}$  are the independent or explanatory variables, and  $\beta_0$  is the disturbance or error term.

Table 6.1 Summary for all Test Results

Section	Station	E <sub>P<sub>L</sub>T (i)</sub> (MPa)	E <sub>P<sub>L</sub>T (R2)</sub> (MPa)	E <sub>L<sub>F</sub>W<sub>D</sub></sub> (MPa)	E <sub>G</sub> (MPa)	DCP-PR (mm/blow)	M <sub>F<sub>W</sub>D</sub> (MPa)
US 190	12+530	174.18	144.83	153.44	128.50	5.5	169.50
	12+650	148.51	128.37	151.37	119.60	7.5	145.00
	15+800	162.3	162.3	291.87	155.90	4.8	173.00
LA 182	47+10(untreated)	25.00	22.1	37.10	54.56	53.80	--
	47+10(treated)	24.44	28.71	28.04	63.90	36.00	--
	173+68	609	611.37	865.0	238.15	3.27	828.94
	319+00	122.2	93.25	56.0	113.55	12.8	72.35
	319+10	--	--	50.9	99.68	14.25	69.45
	503+90	--	--	70.64	105.31	12.52	111.33
	504+00	--	--	71.56	107.64	12.22	122.22
US 61	504+10	128.39	113.52	78.17	111.33	10.00	133.90
	1 passes	--	--	46.54	69.39	14.50	84.30
	4 passes	61.39	59.47	69.26	80.05	10.25	92.50
ALF Site	Soil cement (1-6)*	155.13	145.6	99.15	136.54	7.56	132.91
	Soil cement (1-13)	--	--	102.07	137.90	8.14	138.97
	Soil cement (1-23)	--	--	116.39	146.14	7.81	139.11
	Soil cement (1-37)	98.90	99.67	127.1	118.58	8.73	118.44
	Soil cement (2-3)	250.3	259.63	228.48	194.40	5.69	186.72
	Soil cement (0-20)	--	--	184.2	186.87	6.00	213.31
	Soil cement (2-37)	170.62	155.80	169.72	150.86	6.89	180.24
	Soil lime (3)**	50.13	54.21	83.15	113.86	15.42	72.90
	Soil lime (20)	--	--	42.44	82.80	17.70	58.16
	Soil lime (37)	45.0	50.66	54.50	99.42	16.63	55.40
	Flororite(5)	202.19	185.04	249.44	394.23	5.52	238.53
	Flororite (22)	--	--	224.92	335.35	5.91	234.33
	lime stone	97.67	93.87	81.47	91.78	12.10	--
	clayey silt	54.91	41.96	35.5	77.78	29.00	34.50
	CLS-light***	3.85	24.45	30.25	51.93	37.8	38.9
	CLS-moderate	29.02	35.17	57.28	73.06	23.1	56.88
	CLS-heavy	77.38	96.90	82.69	95.59	9.8	92.3
	RAP-light	5.08	18.00	29.00	57.00	30.30	36.54
	RAP-moderate	16.93	31.43	52.00	77.00	16.13	78.02
	RAP-Heavy	101.57	105.23	116.24	126.21	9.97	138.57
Sand-light	13.30	15.38	12.50	40.80	66.67	30.725	
Sand-moderate	---	--	25.55	54.25	23.4	58.26	
Sand-heavy	36.93	40.03	41.83	58.28	18.80	76.47	

Soil cement (1-3)\*: cement treated soil section (1), tested after 3 days of construction.

Soil lime (3) \*\*: lime treated soil section tested after 3 days of construction.

CLS-Light\*\*\*: Crushed Lime stone trench backfill, light compacted section.

Table 6.2 Summary of CBR test results

Section	Station	CBR	E <sub>LFWD</sub>	E <sub>G</sub>	DCP
LA 182	319+10	13.80	50.9	99.68	14.25
LA 182	47+10(untreated)	1.10	37.1	54.56	53.8
LA 182	47+10(treated)	0.80	28.04	63.9	36
US 190	12+650	78.96	151.379	119.6	7.5
US 61	4 passes	12.4	69.26	80.05	10.25
ALF Site	Soil cement (2-3)	8.30	42.09	91.01	15.4
	lime treated-same day	7.2	19.5	83.3	21.36
	Soil cement (2-10)	135.40	174.5	184.11	6.31
	Soil cement (2-37)	129.20	169.72	150.86	6.89
	clayey silt	5.25	35.5	77.78	29
	CLS-light	12.20	30.25	51.93	37.8
	CLS-moderate	15.22	57.28	73.06	23.1
	CLS-heavy	50.64	82.69	95.59	9.8
	RAP-light	3.59	29	57	30.3
	RAP-moderate	27.80	52	77	16.13
	RAP-heavy	54.44	116.24	126.21	9.97
	Sand-light	5.82	12.5	40.8	66.67
	Sand-moderate	13.54	25.55	54.25	23.4
	Sand-heavy	14.12	41.83	58.28	18.8

On the other hand, a regression model is called nonlinear, if the derivatives of the model with respect to the model parameters depend on more than one parameter. A regression model is not necessarily nonlinear if the graphed regression trend is curved.

It should be noted that the measurements obtained using the reference tests (PLT, FWD, and CBR) were always used as the independent variable in the regression model obtained, while the measurement of the devices under investigation (GeoGauge, LFWD, and DCP) were used as the dependent variable.

In this study the coefficient of determination,  $R^2$ , the standard error, and the significance level is reported for each regression model developed. The coefficient of determination,  $R^2$ , represents the proportion of variation in the dependant variable that is

accounted by the regression model and has values from 0 to 1. If it is equal to one, the entire observed points lie on the suggested least square line, which means a perfect correlation exists. Significance level is the result of the statistic test with null hypothesis  $\beta_1 = 0$ ; it is expressed in percent. The greater the significance level the more supportive the model to alternative hypothesis ( $\beta_1 \neq 0$ ), which indicates that a relation does exist between the dependent and independent variable. Finally, the standard error is the square root of the mean square errors (MSE).

#### **6.4.1 Geogauge Modulus Correlations**

According to the Geogauge manufacturer (Humboldt), the Geogauge device may lose accuracy when measuring stiffness greater than 23 MN/m (Chen et al., 2000). Therefore, it is not recommended to use Geogauge stiffness measurements that are greater than 23 MN/m. In this regression analysis, only Geogauge measurements that are less than 23 MN/m were used. The results of the regression analysis for the Geogauge are as follow:

##### **6.4.1.1 Geogauge versus FWD**

The results of the regression analysis that was conducted to determine the best correlation between the FWD back-calculated resilient moduli,  $M_{FWD}$ , and the Geogauge stiffness modulus,  $E_G$ , yielded the regression model presented in equation 6.5. It should be noted that the SAS output for this analysis is provided in Appendix B.

$$M_{FWD} = -20.07 + 1.17 (E_G) \quad \text{for } 40.8 \text{ MPa} < E_G < 194.4 \text{ MPa} \quad (6.5)$$

With  $R^2=0.81$ , significance level  $< 99.9\%$ , and standard error=22.42. Figure 6.4 illustrates the results of the regression analysis.

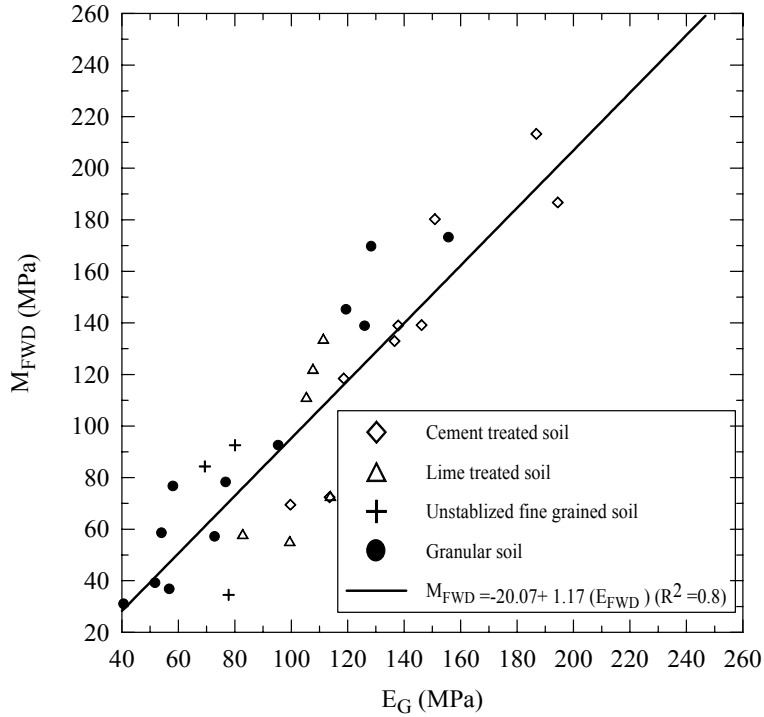


Figure 6.4  $M_{FWD}$  vs.  $E_G$

#### 6.4.1.2 Geogauge versus PLT

The Geogauge modulus,  $E_G$ , was correlated to the initial and reloading moduli, that were determined for PLT data,  $E_{PLT(i)}$  and  $E_{PLT(R2)}$ , respectively. The following regression models were obtained:

$$E_{PLT(i)} = -75.58 + 1.52 (E_G) \quad \text{for } 40.8 \text{ MPa} < E_G < 194.4 \text{ MPa} \quad (6.7)$$

With  $R^2 = 0.87$ , significance level  $< 99.9\%$ , and standard error = 24.35.

And

$$E_{PLT(R2)} = -65.37 + 1.50 (E_G) \quad \text{for } 40.8 \text{ MPa} < E_G < 194.4 \text{ MPa} \quad (6.8)$$

With  $R^2 = 0.90$ , significance level  $< 99.9\%$ , and standard error = 19.64. The results of the regression analysis are shown in Figures 6.5 and 6.6.

#### 6.4.1.3 Geogauge versus CBR

A correlation between the Geogauge stiffness modulus and CBR data presented in Table 6.3 was also developed. Based on the results of the regression analysis, the model shown in Equation 6.9 was determined.

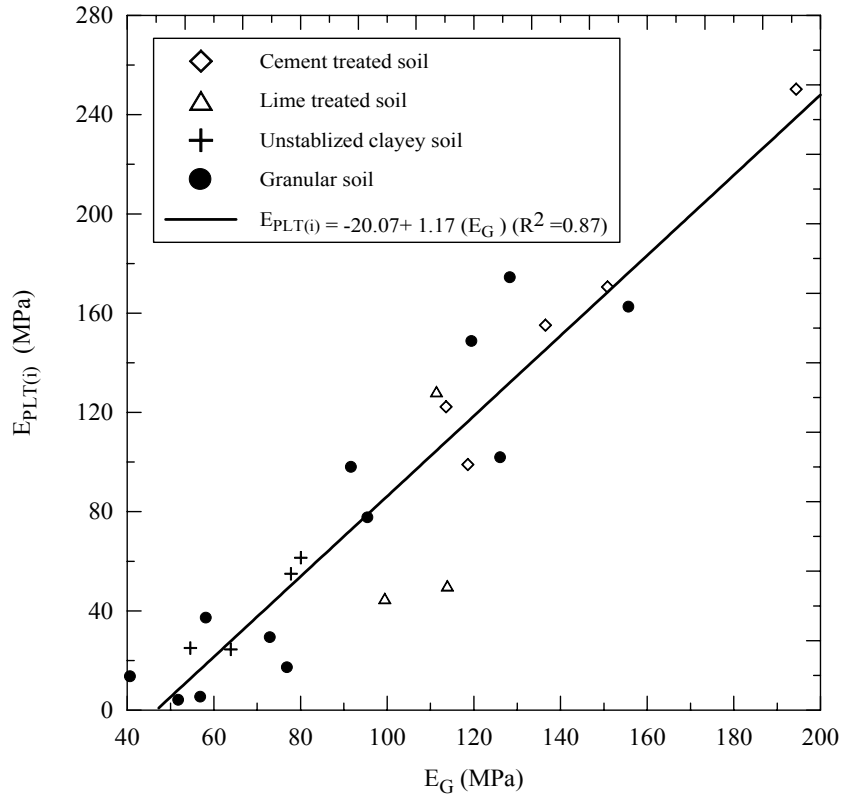


Figure 6.5  $E_{PLT(i)}$  vs.  $E_G$

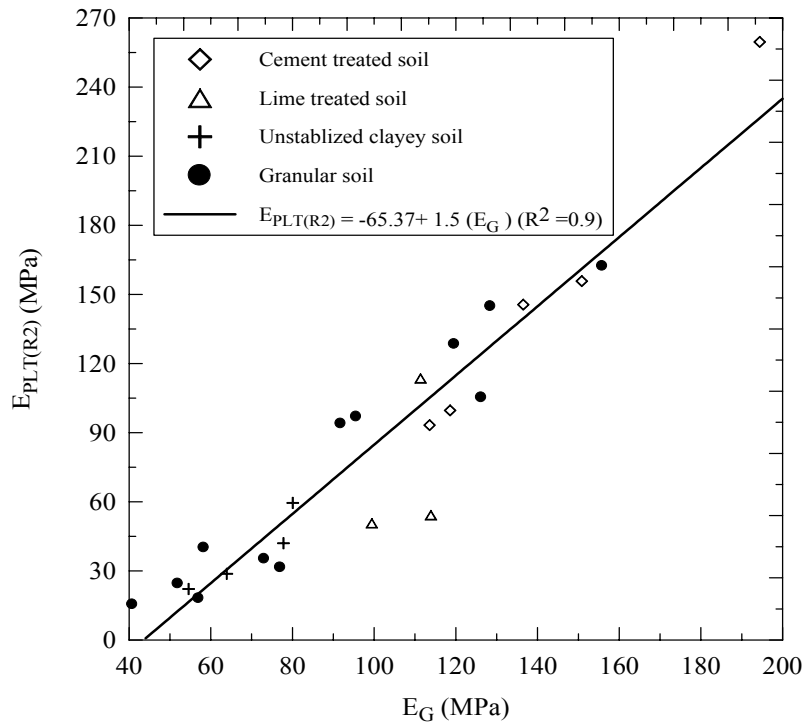


Figure 6.6  $E_{PLT(R2)}$  vs.  $E_G$

$$\text{CBR} = 0.00392 (E_G)^2 - 5.75 \quad \text{for } 40.8 \text{ MPa} < E_G < 184.11 \text{ MPa} \quad (6.9)$$

With  $R^2 = 0.84$ , significance level  $< 99.9\%$ , and standard error = 14.44. Figure 6.7 illustrates the results of the regression analysis.

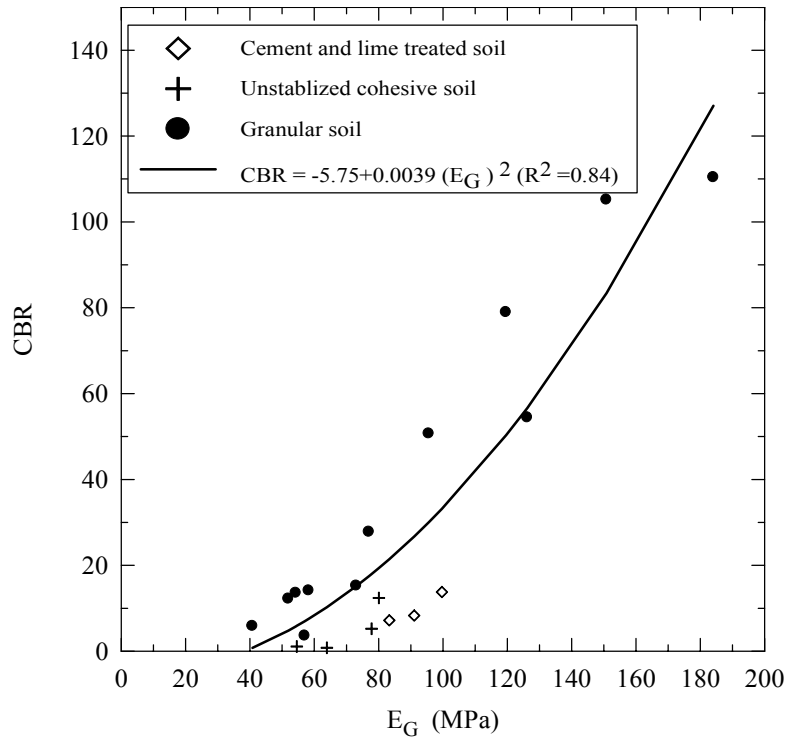


Figure 6.7 CBR vs.  $E_G$

## 6.4.2 LFWD Modulus Correlations

### 6.4.2.1 LFWD versus FWD

The results of the regression analysis have shown that the best model to predict the FWD back-calculated resilient moduli,  $M_{FWD}$ , in (MPa) from the LFWD modulus,  $E_{LFWD}$ , in (MPa) is as follows:

$$M_{FWD} = 0.97 (E_{LFWD}) \quad \text{for } 12.5 \text{ MPa} < E_{LFWD} < 865 \text{ MPa} \quad (6.10)$$

With  $R^2 = 0.94$ , significance level  $< 99.9\%$ , and standard error = 33.1. The results of the FWD-LFWD correlation are presented in Figure 6.8. A comparison of the suggested FWD-LFWD prediction model to that proposed by Fleming (2000) is shown in Figure 6.9. It can be seen that the suggested model is compatible to that by Fleming (2000).

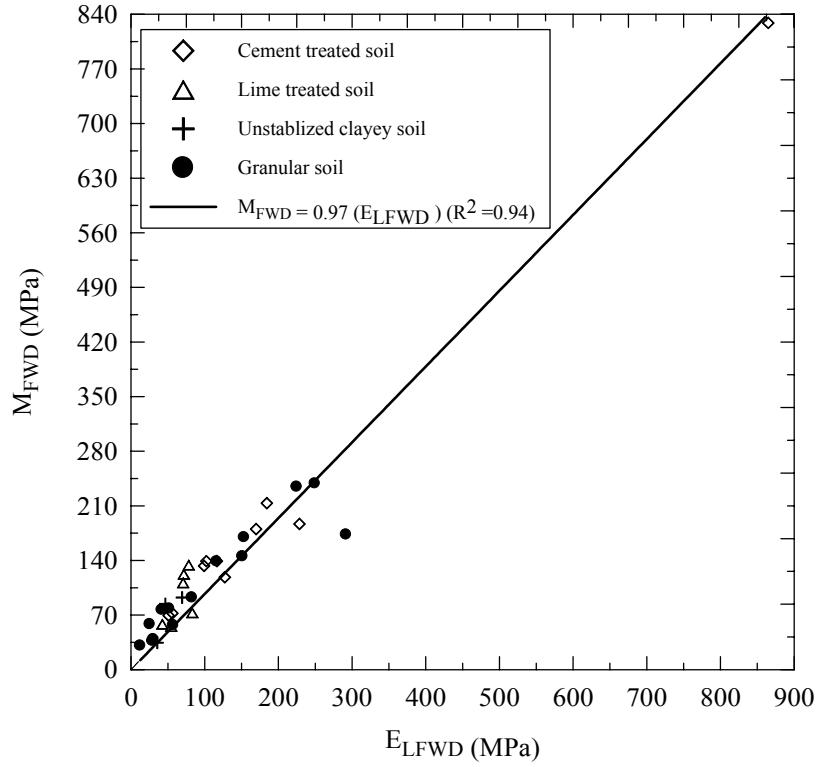


Figure 6.8  $M_{FWD}$  vs.  $E_{LFWD}$

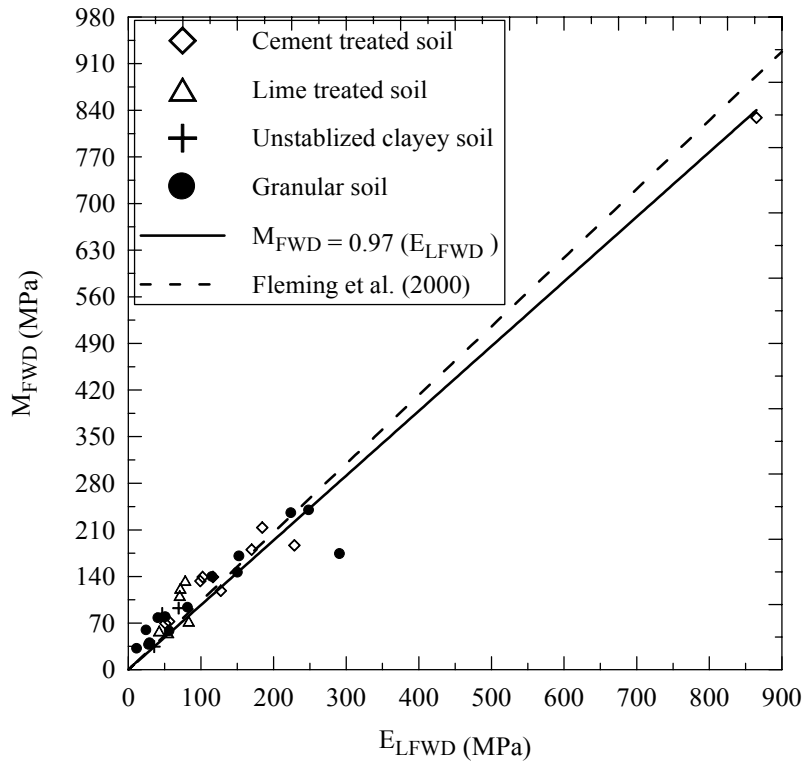


Figure 6.9  $M_{FWD}$  vs.  $E_{LFWD}$  correlation, comparison to Fleming et al. (2000)

#### 6.4.2.2 LFWD versus PLT

The elastic modulus obtained from LFWD,  $E_{LFWD}$ , was also correlated to  $E_{PLT(i)}$  and  $E_{PLT(R2)}$ . The obtained regression models were as follows:

$$E_{PLT(i)} = 22 + 0.7 (E_{LFWD}) \quad \text{for } 12.5 \text{ MPa} < E_{LFWD} < 865 \text{ MPa} \quad (6.11)$$

With  $R^2 = 0.92$ , significance level  $< 99.9\%$ , and standard error = 36.38.

And

$$E_{PLT(R2)} = 20.9 + 0.69 (E_{LFWD}) \quad \text{for } 12.5 \text{ MPa} < E_{LFWD} < 865 \text{ MPa} \quad (6.12)$$

With  $R^2 = 0.94$ , significance level  $< 99.9\%$ , and standard error = 29.8. These regression models are illustrated in Figures 6.10 and 6.11.

#### 6.4.2.3 LFWD versus CBR

The regression analysis, which was performed to find the best correlation between the CBR values and  $E_{LFWD}$ , yielded the following regression model:

$$\text{CBR} = -14.0 + 0.66 (E_{LFWD}) \quad \text{for } 12.5 \text{ MPa} < \text{LFWD} < 174.5 \text{ MPa} \quad (6.13)$$

With  $R^2 = 0.83$ , significance level  $< 99.9\%$ , and standard error = 9.1. Figure 6.12 illustrates the results of this correlation.

#### 6.4.3 DCP Correlations

Most of the previous attempts that have been made to find a correlation between the elastic modulus and DCP-PR, directly or indirectly, were based on non-linear models. Therefore a nonlinear regression analysis has been used here to correlate the DCP-PR with the modulus measured by other in-situ devices (i.e. PLT and FWD). In all of these correlations, the DCP-PR measurement that was taken on the base section at highway LA 182 was not used. This was done since this value was far from all the other test measurements as Figure 6.13 shows. In addition to that the DCP-PR measurement was based on only one DCP test.

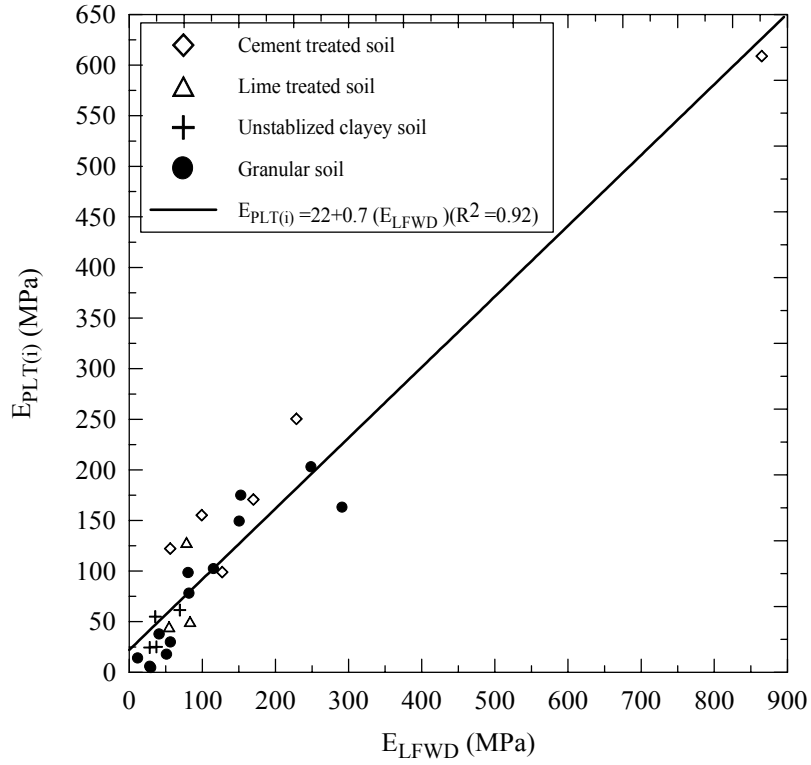


Figure 6.10 E<sub>PLT(i)</sub> vs. E<sub>LFWD</sub>

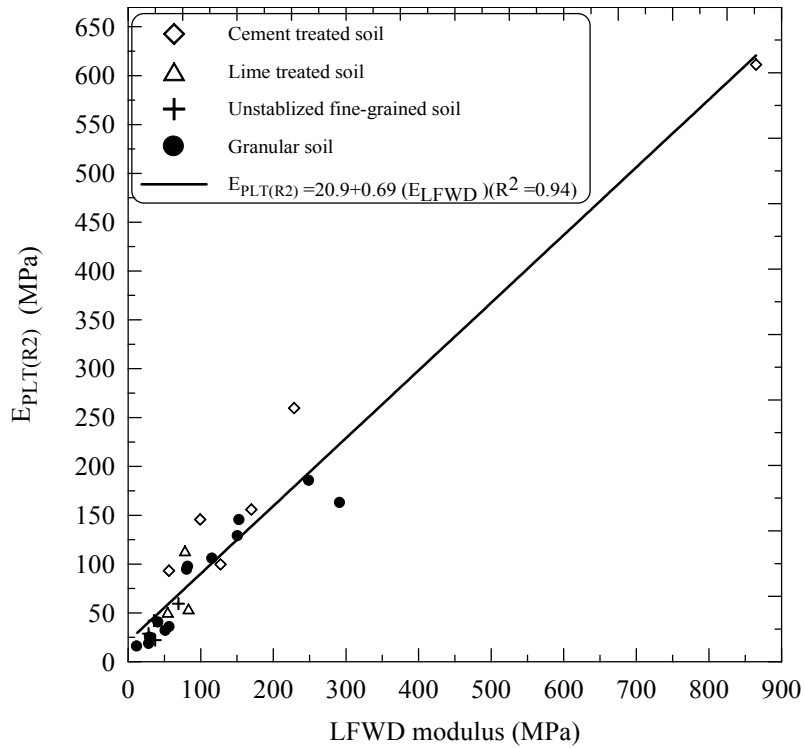


Figure 6.11 E<sub>PLT(R2)</sub> vs. E<sub>LFWD</sub>

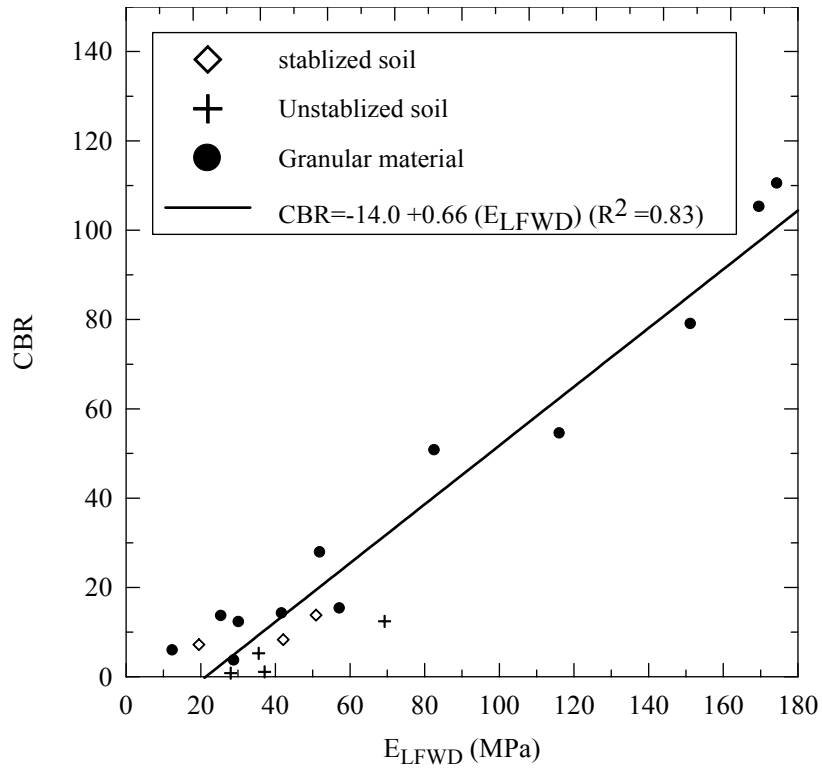


Figure 6.12 CBR vs. E<sub>LFWD</sub>

#### 6.4.3.1 DCP versus FWD

The regression analysis, which was conducted to find the best correlation between the M<sub>FWD</sub> in (MPa) and the DCP-PR in (mm/blow), yielded a non-linear regression model presented in equations 6.14.

$$\ln(\text{FWD}) = 2.35 + \frac{5.21}{\ln(\text{PR})} \quad (4.81 < \text{PR} < 66.67) \quad (6.14)$$

With R<sup>2</sup>=0.91, significance level < 99.9%, and standard error= 0.2. Both regression models are presented in Figure 6.13.

Comparison was made between the DCP-FWD correlation obtained in this study and those suggested by Chen et al. (2001) using equation 2.14 (Webster et al., 1992) to compute CBR and then use equation (2.15) to compute FWD modulus, as shown in Figure 6.13. The figure shows also a comparison to the correlation suggested by Chen et

al. (1999). It should be noted here that Chen et al. (1999) correlation was suggested only for the range of  $10 < PR < 60$  mm/blow. It can be seen from Figure 6.13, that the proposed equation in this study has a better correlation with the measured data than that suggested by Chen et al. (1999) and Chen et al (2001).

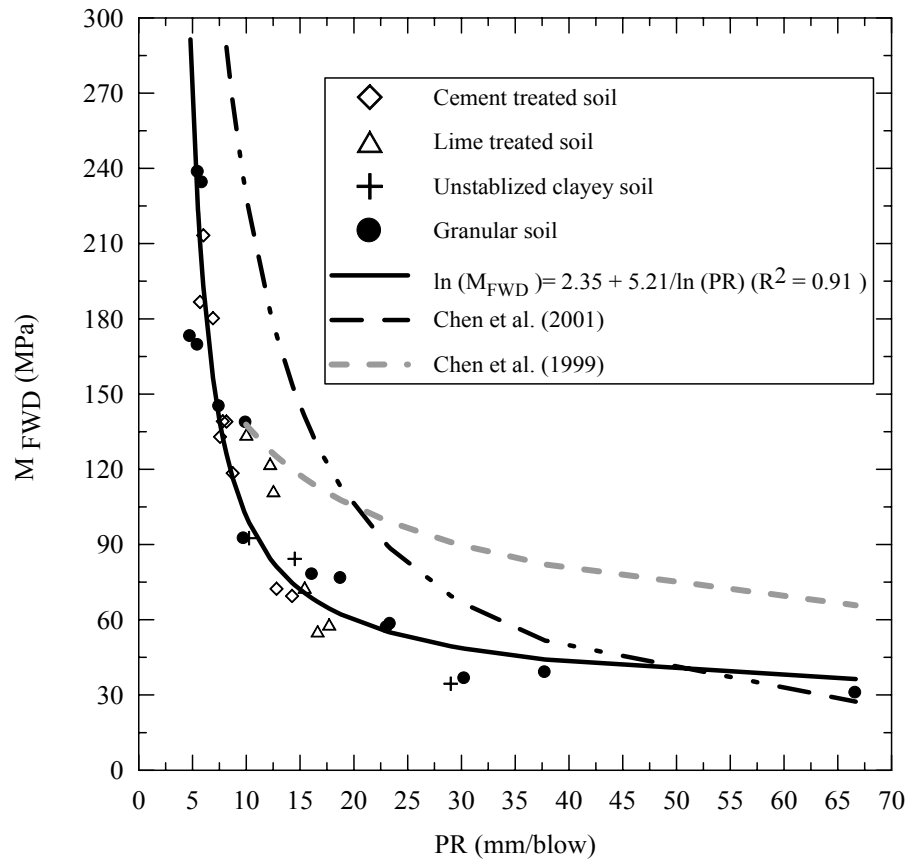


Figure 6.13  $M_{FWD}$  vs. DCP-PR

#### 6.4.3.2 DCP versus PLT

Correlation was made between the DCP-PR (mm/blow) and both the  $E_{PLT(i)}$  and  $E_{PLT(R2)}$  in (MPa). The results of the regression analysis yielded the following non-linear regression models:

$$E_{PLT(i)} = \frac{17421.2}{(PR)^{2.05} + 62.53} - 5.71 \quad (4.81 < PR < 66.67) \quad (6.15)$$

With  $R^2 = 0.94$ , significance level  $< 99.9\%$ , and standard error = 31.02.

$$\text{And } E_{\text{PLT}(R2)} = \frac{5142.61}{(\text{PR})^{1.57} - 14.8} - 3.49 \quad (4.81 < \text{PR} < 66.67) \quad (6.16)$$

With  $R^2 = 0.95$ , Significance level  $< 99.9\%$ , and standard error = 27.66. The results of these correlations are illustrated in Figures 6.14 and 6.15. Comparison between the DCP- $E_{\text{PLT}}$  relations proposed in equations 6.15 and 6.16 with the work done by Konard and Lachance (2000) is also presented in Figures 6.14 and 6.15. These figures show that the correlations suggested by Konard and Lachance (2000) are very close to those suggested in this study at DCP-PR values less than 10 mm/blow.

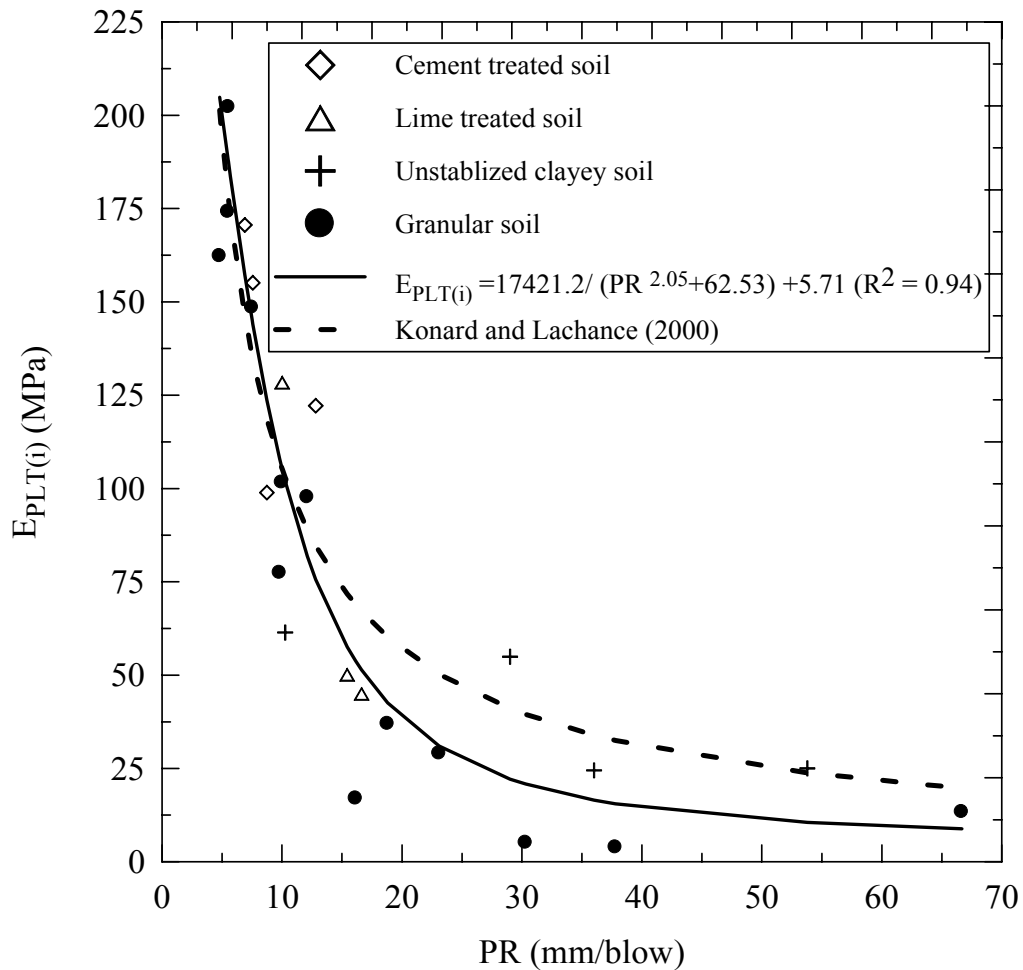


Figure 6.14  $E_{\text{PLT}(i)}$  vs. DCP-PR

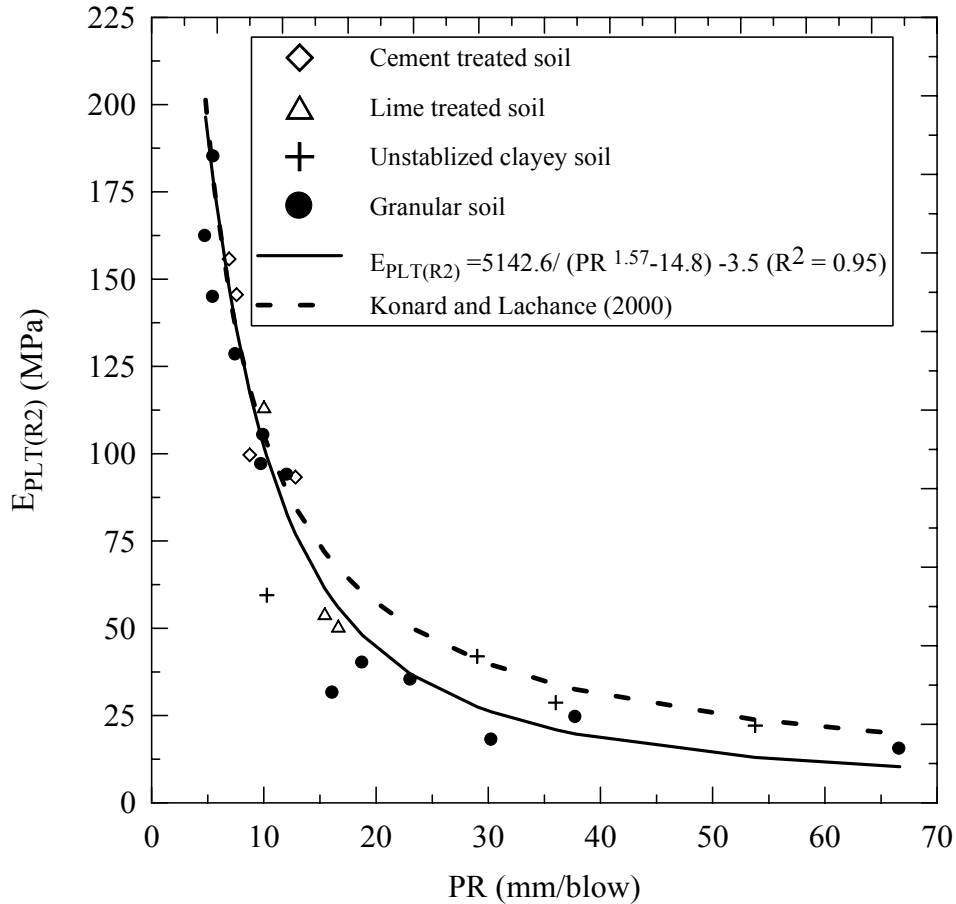


Figure 6.15  $E_{PLT(R2)}$  vs. DCP-PR

#### 6.4.3.3 DCP versus CBR

Regression analysis was performed to correlate the laboratory CBR and the DCP-PR. The following non-linear regression model was obtained:

$$CBR = 2559.44 / (-7.35 + PR^{1.84}) + 1.04 \quad \text{for } 6.31 < PR < 66.67 \text{ mm/blow} \quad (6.18)$$

With  $R^2 = 0.93$ , significance level  $< 99.9\%$ , and standard error  $= 9.6$ . The results are presented in Figure 6.16. Figure 6.16 also compares the DCP- CBR relation suggested in Equation 6.12 to the work done by Webster et al. (1992). As shown in the figure, correlations suggested by Webster et al. (1992) is similar with the one proposed in this study, at high PR values; however the variation between the two models increases as the PR value decreases

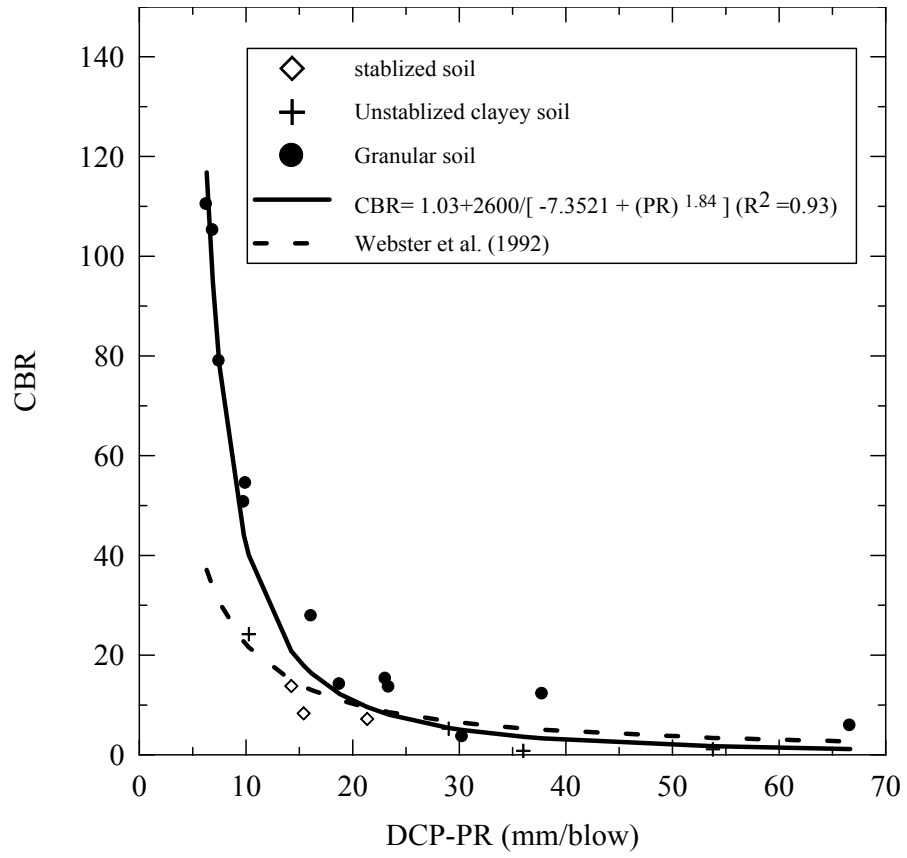


Figure 6.16 CBR vs. DCP-PR

## CHAPTER SEVEN

### CONCLUSIONS AND RECOMMENDATIONS

#### 7.1 Conclusions

The objective of this study is to evaluate the potential use of non-destructive testing devices such as Geogauge, DCP, and LFWD to measure the stiffness/strength parameters of highway materials and embankment soils during and after construction. To assess this a series of field tests were conducted on selected pavement projects under construction and test sections. The field testing program included conducting tests using the investigated devices, in addition to some standard tests, which included the static Plate Load Test (PLT), Falling Weight Deflectometer (FWD), and California Bearing Ratio (CBR) tests. Statistical analysis was conducted to correlate moduli obtained using these devices and the moduli obtained by PLT and FWD tests and with the CBR values obtained in the laboratory.

The results of the statistical analysis show that good correlation do exist between the devices under evaluation (Geogauge DCP, and LFWD) and the standard tests (FWD, PLT, and CBR). The relations obtained from statistical analysis, were linear for some models and non-linear for others. All regression models had an adjusted  $R^2$ , and a significance level greater than 0.8, and 99.9%, respectively. The result of this study suggests that Geogauge, DCP, and LFWD can be reliably used to predict the moduli obtained from PLT, FWD, and CBR values, and hence can be used to evaluate the stiffness/strength parameters of different pavement layers and embankment.

Some of the statistical relations obtained were also compared to some work done by other researchers. The results of comparison showed that the LFWD-FWD relation

proposed in this study is similar to that suggested by Fleming et al. (2000). In addition the proposed DCP-PLT relations were compatible with the relation suggested by Konard and Lachance (2000).

The repeatability of Geogauge and LFWD were tested using the coefficient of variation ( $C_V$ ) of their measurements at each test section. The results showed that the LFWD had a higher  $C_V$  than the Geogauge, which indicates that the later device have a better repeatability. It is suggested that the future research should study the repeatability of LFWD; since the results in this study suggests that repeatability of the LFWD was clearly enhanced when the tested section consisted of stiff well compacted material.

The results of the DCP tests indicate that this device can be used to evaluate the strength/stiffness properties of different pavement layers and embankments. In addition this device demonstrated the ability to determine the thickness of the tested layer, and to detect the existence weak points within compacted sections. It was also noted that when testing granular soils, the effect of vertical confinement is predominant on the DCP test results; therefore it is recommended that future study should investigate the use of DCP to evaluate compacted granular soil layers.

A parametric study was also conducted using the test boxes located in the LTRC-GERL lab to evaluate the influence depth of both the Geogauge and LFWD and the relation between Geogauge stiffness and dry density. The results of this study showed that the Geogauge influence depth ranges from 180 mm to 190 mm (7.5 inch to 8 inch), while the influence depth for the LFWD ranges from 267 mm to 280 mm (10.5 inch to 11 inch). These results supports the suggestion of using both devices for  $Q_C/Q_A$  procedure during construction of pavement layers, since these layers are constructed usually in lifts

with thickness ranging between 150 mm to 300 mm (6 inch to 12 inch).

Finally, the results of this study can be employed to develop new mechanistic  $Q_C/Q_A$  procedures for construction of pavement layers and embankment. In these procedures, the acceptance criteria should be based on the stiffness measurements that can be obtained using the Geogauge, LFWD, or DCP accompanied with moisture content measurement.

## **7.2 Recommendations**

- The Geogauge correlations developed in this study were developed for moduli values less than 200 MPa. It is recommended that Geogauge accuracy at moduli values greater than 200 MPa should be studied, and based on that, Geogauge correlation for these moduli values can be determined.
- Future research should investigate the use of the Geogauge to evaluate lime and cement treated compacted soils, and the effects of shrinkage cracks on its measurement.
- It is recommended that future research should thoroughly investigate the moisture content effect on Geogauge measurement.
- It is recommended that further field tests should be conducted to revalidate the relations proposed in this study. These tests should include different types of materials with a wide stiffness moduli range.
- Since different in-situ devices provides stiffness measurement at different stress and strain levels, therefore it is recommended that future research should study the correlation between the tests measurement taking in consideration the rate of moduli variation with strain and stress. This can be done using finite element analysis.

## REFERENCES

- AASHTO. *Guide for Design of Pavement Structures*. AASHTO, Washington, D.C., 1993.
- Aitchison, A. W., and Bishop, A. W., “Relationship of Moisture Stress and Effective Stress Function In Unsaturated Soils”, Proceeding, Conference Pore Pressure And Suction In Soils, Butterworths, London, 1960, pp.47-85.
- American Society of Testing and Materials (1998). D1883–94, Standard Test Method for CBR (California Bearing Ratio) of Laboratory-Compacted Soils. *Annual Book of ASTM Standards*, Vol. 04.08, pp. 159-167.
- American Society of Testing and Materials (1998). D1195-93, “Standard Test Method for Repetitive Static Plate Load Tests of Soils and Flexible Pavement Components , for use in Evaluation and Design of Airport and Highway Pavements”. *Annual Book of ASTM Standards*, Vol. 04.08, pp. 110-113.
- Bishop, A.W., Alpan, I., Blight, G.E. and Donald, I.B (1960). Factors controlling the strength of partly saturated cohesive soils. In *Proc., Research Conference on Shear Strength of Cohesive Soils*, ASCE, University of Colorado, Boulder, pp. 503-532.
- Burnham, T. (1996) “Application of the Dynamic Cone Penetrometer to Mn/DOT’s Pavement Assessment Procedures,” Revised raft Report. Office of Minnesota Road Research.
- Chaddock, B.C.J. and Brown, A.J. (1995), "In Situ Tests for Road Foundation Assessment." Proceedings UNBAR4 Symposium, Nottingham, UK.
- Chen, Dar-Hao, Bilyeu, J., and He, R. (1999) “Comparison of Resilient Moduli Between Field and Laboratory Testing: A Case Study,” Paper number 990591. 78<sup>th</sup> Annual Transportation Research Board Meeting. Washington D.C., January 10-14, 1999.
- Chen, D. H., Wu, W., He, R., Bilyeu, J., and Arrelano, M., (2000) “Evaluation of In-Situ Resilient Modulus Testing Techniques” Texas DOTD Report, Austin, TX.
- Chen, D. H., Wang, J. N., Bilyeu, J. (2001) “Application of the DCP in Evaluation of Base and Subgrade Layers” 80<sup>th</sup> Annual Meeting of the Transportation Research Board, January 2001, Washington, D.C.
- Chen, J. , Hossain, M., LaTorella, T. (1999) “Use of Falling Weight Deflectometer and Dynamic Cone Penetrometer in Pavement Evaluation,” 78<sup>th</sup> Annual Transportation Research Board Meeting. Washington D.C.

Cho, G. C. and Santamarina, J. S. (2001) "Unsaturated Particulate Materials- Particle Level Studies", *Journal of Geotechnical and Geoenvironmental Engineering*, Vol. 127, No. 1.

Dynatest Engineering, *Dynatest 8000 FWD Test System owner's Manual*, 1995.

Ellis, R; Bloomquist, D; Patel, M; Velcu, B. (2001) "Development of Compaction Quality Control Guidelines That Account For Variability in Pavement Embankments in Florida", UF 4504-710-12,; Final Report

Fiedler, S., Nelson, C., Berkman, F., and DiMillio, A. (1998) "Soil Stiffness Gauge for Soil Compaction Control", *Public Road, FHWA*, Vol. 61, No. 4.

Fleming, P.R., Rogers, C.D.F., and Frost, M.W. (1988) "Performance Parameters and Target Values for Construction of UK Road Foundations." *Proceedings of the Fifth International Conference on Bearing Capacity of Roads and Airfields*, Vol. 3, Trondheim, Norway.

Fleming, P.R. (1998) "Recycled Bituminous Planings as Unbound Granular Materials for Road Foundations in the UK." *Proceedings of the Fifth International Conference on Bearing Capacity of Roads and Airfields*, Vol. 3, Trondheim, Norway, 1998.

Fleming, P.R., Frost, M. W., Rogers, C.D.F (2000) "A Comparison of Devices for Measuring Stiffness In- situ." *Proceedings of the Fifth International Conference on Unbound Aggregate In Roads*, Nottingham, United Kingdom, 2000.

Fleming, P.R , (2001) "Field Measurement Of Stiffness Modulus For Pavement Foundations" *Transportation Research Record* 1755, Submitted to the 2001 Annual Meeting of the Transportation Research Board for Presentation and Publication, pp 69-77.

Fredlund, D. G. and Rahardjo, H., 1993, *Soil Mechanics for Unsaturated Soils*, John Wiley and Sons, Inc., New York, NY.

Gurp, C.; Groenendijk, J.; and Beuving, E., (2000) "Experience with Various Types of Foundation Tests" *Proceedings of the Fifth International Conference on Unbound Aggregate In Roads*, Nottingham, United Kingdom.

Harrison J.A. (1986) "Correlation of CBR and Dynamic Cone Penetrometer Strength Measurement of Soils" *Australian Road Research*, June 1986, Vol. 16, No.2 pp130-136.

Horhota, D. (1996) " Evaluation Of the Spectral Analysis of Surface Waves (SAWS) Test Method For Florida Department Of Transportation (FDOT) Applications" dissertation presented to the University of Florida.

Heukelom, W. and Klomp, A.J.G. (1962) "Dynamic Testing as Means of Controlling

Pavements During and After Construction,” Proceedings of the First International Conference on Structural Design of Asphalt Pavement, University of Michigan, 1962.

Holtz, R.D., and Kovacs, W.D. (1981), *An Introduction to Geotechnical Engineering*, Prentice-Hall, Englewood Cliffs, New Jersey.

Kamiura, M.; Sekine, E.; Abe, N.; and Meruyama, T. (2000), “Stiffness Evaluation of the Subgrade and Granular Aggregate Using the Portable FWD”. Proceedings of the Fifth International Conference on Unbound Aggregate In Roads, Nottingham, United Kingdom, 2000.

K. M. Chua, and R. L. Lytton (1981), “Dynamic Analysis Using the Portable Dynamic Cone Penetrometer”, Transportation Research 1192, TRB, National Research Council, Washington, DC.

Konard, J-M.; and Lachance, D. (2000), Mechanical Properties of Unbound Aggregates from DCP and Plate Load Tests” Proceedings of the Fifth International Conference on Unbound Aggregate In Roads, Nottingham, United Kingdom, 2000.

Kleyn, E. G. 1975, “The Use of the Dynamic Cone Penetrometer (DCP). Report 2/74. Transvaal Roads Department, Pretoria.

Livneh, M., (1989) “Validation of Correlations Between a Number of Penetration Tests and In Situ California Bearing Ratio Tests,” TRR 1219.

Livneh, M., and I. Ishai. Pavement and Material Evaluation by a Dynamic Cone Penetrometer (1987), *Proc., Sixth International Conference on the Structural Design of Asphalt Pavement*, Vol. 1, Ann Arbor, Michigan , pp. 665-674.

Livneh, M., Ishai, I., and Livneh, N. (1995) “Effect of Vertical Confinement on Dynamic Cone Penetrometer Strength Values in Pavement and Subgrade Evaluations” TRR 1473. pp. 1-8.

Livneh, M; Goldberg, Y. (2001), “Quality Assessment During Road Formation and Foundation Construction: Use of Falling-Weight Deflectometer And Light Drop Weight”, *Transportation Research Record 1755*, Submitted to the 2001 Annual Meeting of the Transportation Research Board for Presentation and Publication, pp 69-77.

Louisiana Office of State Climatology rainfall record for Baton Rouge station (2003), <http://www.losc.lsu.edu/stations.php?Id=btr>.

Pinard, M.I. "Innovative Compaction Techniques for Improving the Bearing Capacity of Roads and Airfields. 1998, “Proceedings of the Fifth International Conference on Bearing Capacity of Roads and Airfields, Vol. 3, Trondheim, Norway.

Lenke, L., McKeen, R., and Grush, M. (2003) "Laboratory Evaluation of the GeoGauge for Compaction Control", Submitted to the 82 th Annual Meeting of the Transportation Research Board for Presentation and Publication. Washinton D.C.

Mitchell, J. K. (1993). *Fundamentals of Soil Behavior*, Second Edition, Wiley-Interscience, pp. 161-170.

Nunn, M.E., Brown, A., Weston, D., and Nicholls, J.C. (1997), "Design of Long Life Flexible Pavements for Heavy Traffic." TRL Report 250, Transport Research Laboratory, Crowthorne, Bershire, UK.

Odemark (1949), "Investigations as to the Elastic Properties of Soils and Design of Pavements according to the Theory of Elasticity" Statens Väginstytut, Mitteilung No. 77, Stockholm.

Petersen, L.; Peterson, R.; and Nelson, C. (2002)" Comparison of Quasi-Static Plate Load Tests with the Humboldt GeoGauge" CNA Consulting Engineers Report.

Pen, C. K. (1990), "An Assessment of the Available Methods of Analysis for Estimating the Elastic Moduli of road pavements", Proc. 3 rd Int. Conf. on Bearing Capacity of Roads and Airfields, Trondheim.

Rogers, C.D.F ;Fleming, P.R.; and Frost, M. W., (2000) " Stiffness Behavior of Trial Road Foundations" Proceedings of the Fifth International Conference on Unbound Aggregate In Roads, Nottingham, United Kingdom.

Rodriguez, A. R., Castillo, H.D, Sowers, G. F. (1988), *Soil Mechanics in Highway Engineering*, Germany, pp. 448-451.

Sawanguriya, A.; Edil, T.; Bosscher, P. (2002a), "Laboratory Evaluation of The Soil Stiffness Gauge (SSG)", 81 th Annual Meeting of the Transportation Research Board, January 2002, Washington, D.C.

Sawanguriya, A.; Edil, T.; Bosscher, P. (2002b), "Comparison Of Moduli Obtained From The Soil Stiffness Gauge With Moduli From Other Tests", 81 th Annual Meeting of the Transportation Research Board, January 2002, Washington, D.C.

Seed, H.B., and Chan, C.K. (1959), "Structure and Strength Characteristics of Compacted Clays, *Journal of the SoilMechanics and Foundations Division*, American Society of Civil Engineers, Vol. 85, No. SM5, pp. 87-128.

Siekmeier, J.A., Young, Duane, and Beberg, D. (2000) "Comparison of the Dynamic Cone Penetrometer With Other Tests During subgrade and Granular Base Characterization in Minnesota, Nondestructive Testing of Pavements and Backcalculation of Moduli: Third Volume, ASTM STP 1375, p175-188. S.D. Tayabji and E.O. Lukanen, Eds., American Society for Testing and Materials.

Thom, NH, (1993), "A review of European Pavement design", Proc. Euroflex, Libson, pp. 229-77.

Webster S.L., Grau, R.H., and Williams, R.P. (1992) "Description and Application of Dual Mass Dynamic Cone Penetrometer," U.S. Army Engineer Waterways Experiment Station, Instruction Report, No. GL-92-3.

Wu, S.; Gray, D. H.; and Richart, F. E., Jr. (1984) "Capillary effects on dynamic modulus of sands and silts" J. Geotech Engrg. Div., ASCE, 110(9), 1188-1203.

U.S. Department of Transportation FHWA (1994), "Pavement Deflection Analysis Participant Workbook", NHI Course No. 13127.

Yoder, E. J. and M. W. Witczak (1975), *Principles of Pavement Design*, 2<sup>nd</sup> ed., John Wiley & Sons, New York.

Zaghloul, S.M. and Saeed, N.S. (1996) "The Use of the Falling Weight Deflectometer in Asphalt Pavement Quality Control, Quality Management of Hot-Mix Asphalt." ASTM STP 1299, D.S. Decker, Ed., American Society for Testing and Materials, West Conshohocken, PA.

**APPENDIX A**  
**GEOGAUGE OPERATION PROCEDURE**

Humboldt suggested the following operation procedure for good geogauge measurements:

**1-Verify and prepare Geogauge Operation,**

- Clean the ring shaped foot prior to testing.
- At the beginning of each testing day verify the gauge's operation per Humboldt's procedure.
- If gauge meets verification values, proceed to site.
- If the gauge does not meet verification values, do not use gauge until after calibration and then repeat verification procedure.

**2. Geogauge Seating procedure:**

**2.1 Preparation**

If the surface of the ground is dry and loose, use a straight edge to scrape away loose surface material until cohesive or compacted material is exposed from the test location.

Based on the tested material conduct tests with placement of geogauge on the surface with or without sand coupling layer;

**2.2 Direct placement of geogauge on the surface without sand coupling layer use the following procedure:**

- Assure that the ring foot is clean and free of soil and other debris.

Assure that the external case of GeoGauge does not come into contact with a trenchwall, pipe or any other object.

- Place GeoGauge on the prepared surface without any downward force on the gauge.
- Placing hands of side only, rotate GeoGauge by hand about 1/2 turn without exerting any downward force. An eyeball estimation of degree of rotation is adequate.

On removal of the gauge inspect footprint. Accept the measurement if 80% or more of the footprint is clearly visible.

If the above validation criteria is not acceptable, place the geogauge on the surface with sand coupling layer

### **2.3 Placement of Geogauge on the surface without sand coupling layer**

- Scrape the footprint away.
- Place moist mortar sand onto the prepared soil surface. Firmly pat the sand flat by hand until a uniform thickness of approximately 1/4" and a diameter of approximately 6" are achieved. No pieces of aggregate or other ground materials should protrude above the top of the completed sand-coupling layer.
- Place the gauge on the prepared surface with sand coupling layer without any downward force on the gauge.
- Placing hands on the side only, rotate the gauge by hand no more than a 1/4 turn without exerting any downward force. An eyeball estimation of degree of rotation is adequate.
- On removal of the gauge inspect footprint. Accept the measurement if 80% or more of the footprint is clearly visible.
- If the adequate seating cannot be established at this location, go to next location.
- Complete seating trials on 6 or more locations for which adequate seating is obtained either by direct placement of the gauge on the surface or by the use of a sand coupling

layer.

- If more than 1 out of 6 (i.e., >17%) sample locations requires a sand-coupling layer for acceptable seating; use a sand-coupling layer for all stiffness measurements on site.
- If only 1 out of 6 or less of the sample locations required a sand coupling layer for adequate seating, apply GeoGauge directly to the ground without a sand coupling layer for all individual stiffness measurements.

Note that the coupling layer consists of mortar sand per AASHTO M 44-99 or ASTM C144-02 with 10 to 20% gravimetric.

## APPENDIX B

### SAS OUTPUT

#### SAS output for regression analysis done to correlate $E_G$ and $M_{FWD}$

The SAS System 08:54 wednesday, April 5, 2003

The REG Procedure  
Model: MODEL1  
Dependent Variable: MFWD

#### Analysis of Variance

Source	DF	Sum of Squares	Mean Square	F Value	Pr > F
Model	1	60119	60119	118.49	<.0001
Error	28	14206	507.35897		
Corrected Total	29	74325			

Root MSE	22.52463	R-Square	0.8089
Dependent Mean	103.69583	Adj R-Sq	0.8020
Coeff Var	21.72183		

#### Parameter Estimates

Variable	DF	Parameter Estimate	Standard Error	t Value	Pr >  t
Intercept	1	-20.07961	12.09152	-1.66	.01079
EG	1	1.17130	0.10760	1	<.0001

## VITA

Munir Nazzal was born on January 18<sup>th</sup>, 1980 in Jerusalem, Palestine, to Dr. Darwish Nazzal and Ibtisam Nazzal. He finished his high school from Friends Schools, Ramallah, Palestine, in June 1997. He received his Bachelor degree in civil engineering from Birzeit University, Birzeit, Palestine, in February 2002. He came to United States in the summer of 2002 to pursue his master's degree in civil engineering at Louisiana State University, Baton Rouge, Louisiana. He is anticipated to fulfill the requirements for the master's degree in civil engineering in December 2003.